**FACULTY
OF MATHEMATICS
AND PHYSICS**
Charles University

DOCTORAL THESIS

Jana Doubravová

Automatic and semi-automatic processing of seismograms from local networks WEBNET and REYKJANET

Department of Geophysics

Supervisor of the doctoral thesis: Ing. Josef Horálek, CSc.

Study programme: Physics

Study branch: Physics of the Earth and Planets

Prague 2020

I declare that I carried out this doctoral thesis independently, and only with the cited sources, literature and other professional sources. It has not been used to obtain another or the same degree.

I understand that my work relates to the rights and obligations under the Act No. 121/2000 Sb., the Copyright Act, as amended, in particular the fact that the Charles University has the right to conclude a license agreement on the use of this work as a school work pursuant to Section 60 subsection 1 of the Copyright Act.

In . . . . date . . . .
                                                                                    Author's signature

First, I'd like to thank to my supervisor Josef Horálek for all his care, patience and helpful advice through the whole PhD study. He was the first opponent and the first careful reader of all the texts and his thoughtful comments contributed substantially to a smooth review process of the two presented papers. Then, I'd like to express gratitude to Jan Wiszniowski (IGF PAN Warsaw) for his outstanding help with the artificial neural networks by providing years of his experience that enabled to learn from his past research and achieve superb results.

I also appreciate all the routine work of my colleagues from the Department of Seismology of the Institute of Geophysics CAS. The presented work would be impossible without a contribution of the *skilled interpreters* and *precise manual processing* which both in practice usually mean the work of Alena Boušková and Zuzana Procházková. Also the excellent condition of seismic stations which was asured by Jakub Klicpera and Josef Kotek, formerly also by Petr Jedlička and Jiří Soukup was essential. Finally, the data conditioning, collection and back-up made by Bohuslav Růžek must not be forgotten.

Next, my special thanks go to all the people from the IG CAS that helped me in the personal or scientific level and together with the people from the Department of Geophysics of the Charles University introduced me to that charming world of Geophysics and Seismology.

Last, but not least, I thank to all my loved ones for emotional support which was often more important than scientific discussions.

Title: Automatic and semi-automatic processing of seismograms from local networks WEBNET and REYKJANET

Author: Jana Doubravová

Department: Department of Geophysics

Supervisor: Ing. Josef Horálek, CSc., Department of Seismology, Institute of Geophysics, CAS

Abstract: The automatic processing of seismic data is inevitable step in all seismological research. The quality of the pre-processing of recordings affects the whole subsequent work. Well-performed pre-processing leads to much more effective use of man-power and also computational power in following processing and interpretation of observed data. The main result of the presented thesis is a detector of seismic events based on the use of artificial neural networks, namely a newly defined architecture of the Single Layer Recurrent Neural Network (SLRNN). The neural network of this type enabled to use the detector trained on seismograms of West Bohemia/Vogtland (Czechia) local seismic network WEBNET to seismicity recorded on Reykjanes Peninsula (Iceland) by the REYKJANET local seismic network. A considerable reduction of amount of input data owing to reliable event detection is a key for both effective manual and sophisticated automatic primary processing leading to high quality scientific investigations. Furthermore, I present an interactive software Seismon_WB used for routine manual seismic data processing, because the automatic processing especially for utilization of artificial neural network using supervised learning is closely connected to the manual processing. The artificial neural network training needs examples of waveforms based on verified manual processing and, the other way round, the results of automatic procedures must be then manually verified by the skilled expert.

Název práce: Automatické a poloautomatické zpracování seismogramů z lokálních sítí WEBNET a REYKJANET

Autor: Jana Doubravová

Katedra: Katedra Geofyziky

Vedoucí disertační práce: Ing. Josef Horálek, CSc., Geofyzikální ústav Akademie věd, v.v.i.

Abstrakt: Autrmatické zpracování seismických dat je nevyhnutelným krokem v seismologickém výzkumu. Kvalita předzpracování seismických záznamů ovlivňuje veškeré následné zpracování. Dobře fungující předzpracování dat umožňuje efektivně využít lidské síly i výpočetní výkon při dalším zpracování a intepretaci seismických pozorování. Hlavním výsledkem mé dizertační práce je detektor seismických jevů, který využívá umělou neuronovou sítě s nově zavedenou architekturou nazvanou Single Layer Recurrent Neural Network SLRNN (jednovrstvá rekurentní neuronová síť). Neuronové sítě umožnily aplikovat detektor trénovaný na záznamech ze sítě WEBNET v Západních Čechách/Vogtlandu na seismicitu měřenou sítí REYKJANET na Islandu (poloostrov Reykjanes). Značné snížení objemu dat s použitím spolehlivého detektoru užitečných seismických jevů je klíčovým prvkem pro efektivní manuální zpraconání stejně jako pro sofistikované automatické zpracování dat, které umožňují kvalitní vědecký výzkum. Dále prezentuji interaktivní softwarový balík Seismon_WB, který slouží pro rutinní manuální zpracování seismických dat, protože automatické zpracování zvláště při použití umělých neuronovýh sítí využívajících učení s učitelem je úzce spjato s manuálním zpracováním. Umělá neuronová síť potřebuje pro trénink příklady záznamů založené na precizním manuálním zpracování a naopak pro vyhodnocení automatického zpracování je potřeba manuálního posouzení zkušeným odborníkem.

Klíčová slova: Zpracování seismických dat, Detekce seismických jevů, Umělá neuronová síť, Západní Čechy/Vogtland, Poloostrov Reykjanes, Zemětřesné roje

Contents

Chapter 1

Introduction

Automatic processing of seismic data is nowadays a crucial point in seismology. The number of stations operated in global, regional and local seismic networks or deployed in various temporal field experiments has been growing and the stations are mostly running with continuous digital recording. In the last thirty years, observational seismology has undergone a radical progress from autonomous stations equipped with frequency narrow-band seismographs to the networked digital broadband stations with constant Internet access. The seismic processing developed from fairly limited manual procedures (visual event detection and manual readings of travel times and selected amplitudes of detected events) allowed by the analog seismograms on a photographic paper, into near-real time automatic or semi-automatic data processing enabled by the digital seismic data streamed on-line. In the era of the analog recordings only seismograms of prominent events could be analyzed in more details, quantitative processing of seismograms was practically impossible; accordingly there were only sporadic demands on more advanced databases. Digital seismic observations, which started to be increasingly used at the turn of 80's and 90's of the twentieth century, meant a significant milestone in seismology. The main progress was the possibility of quantitative analyses of event waveforms or complete seismograms using advanced processing methods. This together with a progress in data acquisition systems and data transmission technologies led to a development and growth of seismic networks, particularly of local ones consisting of larger number of stations operated with higher sampling rate, usually of 125 or 250 Hz. Especially, continuously recording dense seismic networks produce a huge amount of data. The WEBNET and REYKJANET networks operated in West Bohemia earthquake-swarm region and in South-West Iceland (Chapter 3), producing currently about 2 GB/day and 1.3 GB/day, are a typical example of that. Data from seismic networks should be quickly accessible and processed as quickly as possible, particularly in case of prominent seismic events or increased earthquake activity. However, it cannot be achieved without up-to-date data transfer, advanced databases, and high level of automated/semi-automated data processing.

First of all, there has been a need to reduce the amount of recorded data so that only target seismic events (e.g., local earthquakes) would be processed. In the initial stage of digital seismic observations the seismic stations were operated in a trigger

mode. That means event detection was carried out in real time. Only triggered events were recorded and remaining information was irretrievably lost (due to absence of the sufficient capacity memory storage at that time). The triggering algorithms all relied on some version of STA/LTA (Short-Time-Average over Long-Time-Average). However, the STA/LTA triggering algorithms required precise tuning of the parameters to obtain optimal detection performance for a given task and local conditions. In order to achieve good sensitivity of the triggered recording there has been large number of false records due to disturbances, that had to be excluded from further processing (usually manually); on the other hand some weaker events immediately following stronger ones were undetected due to the raised LTA.

Availability of the high capacity memory storage and computational performance of the relatively cheap computers enabled to meet the growing demands of seismologists for continuous seismograms. Consequently, the recording turned to continual regime which made significant progress in observational seismology allowing to record and preserve whole seismograms including very weak events, long-period waves and seismic noise. However, the changeover to continual recordings resulted in an urgent need for automatic pre-processing of continual records. First of all, a reliable automatic event detection was necessary. Besides, a suitable database for efficient data management was required.

Although automatic processing of records enables near-real time computation of all basic parameters of an earthquake the manual processing is still considered as a true reference. The automatic algorithms often fail in case of multiple and overlapping events, or any case of complicated waveforms. In case of earthquake swarms, the prevailing type of seismic activity in our target areas of West Bohemia/Vogtland and South-West Iceland, the overlapping events are very common. Therefore the automatically processed data are continuously under supervision of an expert. The supervision is usually achieved by some interactive software with GUI (Graphical User Interface).

My doctoral thesis concerns automated processing of data from local seismic networks WEBNET and REYKJANET which have been operated in earthquake-swarm areas of West Bohemia and South-West Iceland by the Institute of Geophysics (IG) and Institute of Rock Structure and Mechanics (IRSM) of CAS. I have mainly focused on the development of a reliable detection method of local earthquakes using machine learning based on artificial neural networks (ANN). I trained the ANN for the West Bohemia/Vogtland swarm-like events and put the ANN detector into practice for processing of continual recordings from the WEBNET and REYKJANET networks. Furthermore, I have developed the Seismon_WB program package for seismic data processing of the WEBNET and REYKJANET networks. The software enables manual work together with automatic routines and their interconnection and combination supplemented by a communication with the database as an integral part of the program. Seismon_WB is used as a primary tool for visual interactive processing of continual seismograms and displaying the results. Its concept arose from the necessity to replace an obsolete program Seisbase (Fischer and Hampl [1997]) formerly used for processing the WEBNET data, which enabled to work with triggered recordings only. Both these topics solved in my doctoral thesis are not only of

crucial importance for automatic or semi-automatic data processing from networks in question but they are also applicable to other local seismic networks.

Chapter 2

Motivation

Although earthquakes and also earthquake swarms were intensively studied over many decades the possibilities of recording, processing and interpreting the data are increasing rapidly with the well-known increase of computational power obeying the Moor's law. This together with growing data storage capacity has lead to great progress in observation seismology in recent years, which is more and more focused on detailed investigations of the earthquake-source processes and the Earth's crust/lithosphere structure using broadband recordings from dense seismic networks. Original continuous recordings are stored on special data archive servers preserving all data including ambient seismic noise and unnecessary disturbing or noise signals to be available for re-processing and re-interpretation, when needed. The demand for thorough processing of huge amount of data from local seismic networks WEBNET and REYKJANET results from our ambition to explain the primary causes leading to earthquake swarms in areas with completely different tectonic setting as West Bohemia/Vogtland and the Reykjanes Peninsula in South-West Iceland.

The West Bohemia/Vogtland seismogenic region is situated in the western part of the Bohemian Massif, geographically in the border area between Czechia and Saxony (Vogtland is a southern part of Saxony). It is a unique European intra-continental area affected by Quaternary volcanism that exhibits simultaneous activity of various geodynamic processes. Seismic activity is manifested by repeated occurrence of earthquake swarms, but the mainshock-aftershock sequences may rarely occur. Persistent swarm-like seismicity clusters in a number of small epicentral zones that are scattered in the area of about 40x60 km (see grey dots in Fig.3.2). Larger swarms ($\sim M_L > 2.5$) cluster predominantly in the focal zone Nový Kostel which dominates the recent seismicity of the whole region. The swarms usually consist of several thousands of weak earthquakes and their duration is from several days to few months. Notable earthquake swarms in the last four decades occurred in 1985/86 (with the strongest event of magnitude M_{Lmax}=4.6), 1997 (M_{Lmax}=2.9), 2000 (M_{Lmax}=3.3), 2008 (M_{Lmax}=3.8), 2011 (M_{Lmax}=3.7), 2017 (M_{Lmax}=3.2) and 2018 (M_{Lmax}=3.8); an exceptional M_{Lmax}=4.4 non-swarm activity occurred in 2014. The depths of foci in the whole area range from 5 to 20 km (e.g. Horálek and Fischer [2010]) but depths between 7 and 12 km are typical of earthquake swarms and mainshock-aftershock sequences (Čermáková and Horálek [2015], Jakoubková et al. [2018]). The region is

well known by its fluid activity that is probably closely connected with the local swarm-like seismicity (e.g. Horálek and Fischer [2008], Fischer et al. [2017]). For summarizing information about the area in question refer to Fischer et al. [2014].

Reykjanes Peninsula is the onshore continuation of the mid-Atlantic Ridge that separates two major lithospheric plates, the Eurasian Plate to the east and the North American Plate to the west. The plate boundary on the Reykjanes Peninsula is formed by pronounced en-echelon stepping rift segments and extends from the southwest to the east and forms a pronounced oblique rift along the whole peninsula in length of about 65 km (Sæmundsson and Einarsson [2014]). The plate motion rate on the Reykjanes Peninsula is about 20 mm/yr in E–W direction and about 5 mm/yr perpendicular to it (Geirsson et al. [2010]). The plate boundary is flanked by a deformation zone of about 30 km width where strain is built up by the plate movements (Einarsson [2008]). The Reykjanes Peninsula is a highly complex geophysical structure with the interaction between volcanic and tectonic activity (Sæmundsson and Einarsson [2014]), most of the Reykjanes Peninsula surface is covered by lava. The Reykjanes Peninsula is one of the most seismically active parts of Iceland, especially at the micro-earthquake level. Swarm-like sequences and solitary events scattered along the plate boundary, both with magnitudes mostly of $M_L < 3$, represent a major part of seismicity on the peninsula. Large swarms took place there in 2000 with the strongest event of magnitude $M_{Wmax} = 5.9$, in 2003 with $M_{Wmax} = 5.3$ and in 2013 with $M_{Wmax} = 5.0$ (Jakobsdóttir et al. [2002], Jakobsdóttir [2008], Einarsson [2014]). Since the installation of REYKJANET network, few micro-swarms ($M < 3$) and four medium swarms with magnitudes $M_W = 3.9$ (in May 2015), $M_W = 4.1$ (in July 2017), $M_W = 3.7$ (in December 2019) and $M_W = 4.3$ (in January 2020) occurred on the Reykjanes Peninsula; the last mentioned related to a striking uplift of Mt. Thorbjörn possibly associated with magma accumulation beneath the volcano. Prevailing depths of the foci on the Reykjanes Peninsula are between 2 and 5 km which is much shallower compared to the focal depths in West Bohemia/Vogtland.

Both West Bohemia and Reykjanes Peninsula earthquake swarms usually contain from thousands to tens of thousands events ($M_L > 0$) which are necessary to be processed to get insight into triggering mechanisms and driving forces of earthquake swarms. Manual processing of continual seismograms from the WEBNET (24 stations) and REYKJANET (15 stations) networks is extremely time-consuming, and therefore it is possible to process manually only stronger events. Consequently many weaker events being recorded with a sufficient signal-to-noise ratio remain untouched. The automatic processing is the only way to achieve as low completeness magnitude as possible which is essential for deeper insight into nature of earthquake swarms. Nevertheless, the manual processing is considered as the true reference which is in case of complicated events incomparably better. This doctoral thesis presents the methods and tools I developed for automatic or semi-automatic data processing from the WEBNET and REYKJANET and other local seismic networks.

Chapter 3

Local seismic networks WEBNET and REYKJANET

Continuous data produced by local seismic network WEBNET and later on also REYKJANET were the main motivation for whole this thesis. WEBNET local seismic network deployed in West Bohemia earthquake-swarm region (latitude $\approx 49.8°$ N to $50.7°$ N, longitude $\approx 12°$ E to $13°$ E) has a history of 30 years of monitoring microseismicity, while REYKJANET operated on the Reykjanes Peninsula (SW Iceland, latitude $\approx 63.8°$ N to $64.1°$ N, longitude $\approx 21.5°$ W to $22.3°$ W) dates back to 2013 only. Both networks are nowadays similar in many aspects. They have the same instrumental equipment, sampling frequency or spatial extent and there are plans to achieve full data streaming of all their stations through the Internet. The WEBNET network has generally lower noise than REYKJANET due to installation in deep vaults and compact bedrock (compare the waveforms in Fig. 3.1). The stations of REYKJANET are sited on the basement mainly formed by lava fields which is typical for the Reykjanes Peninsula. A rough estimate of the background noise level is $90\,\mathrm{nm/s}$ for REYKJANET and $20\,\mathrm{nm/s}$ for WEBNET, and despite the shallower depth of South-West Icelandic hypocenters there is typically higher signal-to-noise ratio (SNR) for WEBNET recordings.
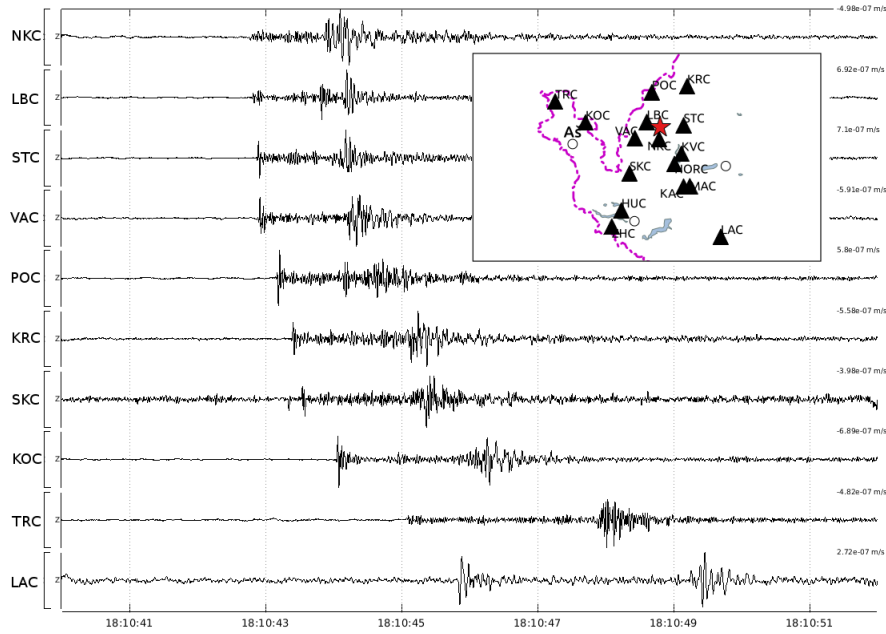
(a) Origin time: December 1, 2018, 18:10:40.916 UTC, depth $d = 9.2\,\mathrm{km}$
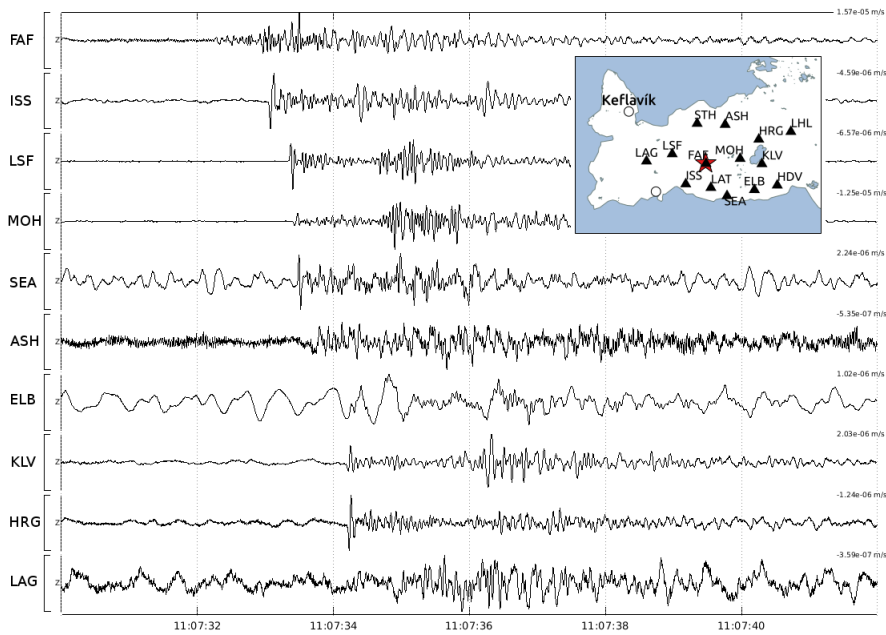
(b) Origin time: July 26, 2017, 11:07:31.554 UTC, depth $d = 2.5\,\mathrm{km}$

Figure 3.1: Waveform examples for (a) WEBNET and (b) REYKJANET events with local magnitude $M_L = 0.5$ (epicenter denotes red asterisks in the insets) were located in the center of the seismic networks at depths characteristic of West Bohemia/Vogtland and the Reykjanes Peninsula. Only vertical components of the ground-motion velocity filtered by bandpass of 1–40 Hz at 10 stations with the best SNR are depicted. All traces are scaled according to the maximum of absolute value of displayed waveform. It is apparent that the noise is generally lower at the WEBNET stations and that the seismograms from the REYKJANET stations are more complex with longer codas which makes their interpretation more demanding.

9

3.1 WEBNET

Seismicity in the West Bohemia/Vogtland region has been monitored by the WEB-NET network since 1991 (Institute of Geophysics [1991], Horálek et al. [2000a], Fischer et al. [2010a]) starting with four stations - NKC, KOC, KRC and LAC, complemented with SKC in 1994. These core stations enabled to locate local events in the region concerned. The WEBNET network was gradually extended, consisting of seven stations in 1997 (Horálek et al. [2000b]), nine in 2000 (Horálek et al. [2000a]), twenty-two in 2008 (12 on-line and 10 off-line, Fischer et al. [2010b]) up to present configuration of 24 stations (Institute of Geophysics [1991]) covering an area of about $900\,\mathrm{km}^2$ (Fig. 3.2). The network layout ensures proper areal and azimuthal coverage of the focal area, particularly with respect to the main focal zone Nový Kostel.

The stations were equipped with several types of instruments which were upgraded in a few steps. At the early stage the stations were equipped with SM-3 or LE-3Dlite short-period sensors and PCM 5800 or Mars-88 data-acquisition systems (by Lennartz) with one-way (PCM 5800) and two-way (Mars-88) UHF telemetry transmitting data to a data center on the TV tower Zelená Hora near Cheb. All the stations were operated in triggered mode using fine-tuned STA/LTA algorithm. Initially, the data were recorded on magneto-optical disks that had to be periodically replaced. The data center on the Zelená Hora TV tower was connected to the Internet in 1999 and since then the data were temporarily buffered on hard disk and transmitted overnight via Internet (due to slow data transmission rate) to the processing laboratory in the IG in Prague. The WEBNET history up to beginning of 2000 is presented in Horálek et al. [2000a], the WEBNET stations operated in the time of the 1997 and 2000 swarms including their instrumentations are given in Horálek et al. [2000b] and Horálek and Šílený [2013].

The WEBNET network was importantly upgraded in 2002. The stations (except two outermost ones KOC and LAC) were equipped with the Janus-Trident data acquisition systems (by Nanometrics) and connected to the TV tower Zelená Hora using the Wave-LAN technology, hence the stations have had continuous Internet access. Besides, the central station NKC was supplemented by a broadband seismometer Guralp CMG-40T. All the stations have been connected to electrical grid; due to their priority and technical background they are called permanent or on-line stations. During 2003 and 2004 the WEBNET network has been extended with supplementary stations to provide the best possible areal and azimuthal coverage of the West Bohemia seismogenic region. The stations were equipped with the Lennartz LE-3Dlite sensors and GAIA digitizers (by VISTEC) working in autonomous triggered regime without a data transmission. They were powered by periodically exchanged batteries and are usually called autonomous or off-line stations. The WEBNET network and its state including basic parameters of the on-line and off-line stations in the time of the 2008 swarm are given in more details in Fischer et al. [2010b]). Continuous recording of data in WEBNET began in 2008 on the on-line stations equipped with the Nanometrics acquisition systems (Janus-Trident at that time) which enabled parallel continual and triggered recording. The continuous data were archived for later use, while the triggered waveform recordings were used in

sensor	lower corner frequency [Hz]	upper corner frequency [Hz]	sensor type
SM-3	0.5	-	passive electro-mechanical
LE-3Dlite	1	-	active electro-mechanical
CMG-40T	0.03	50	electronic feedback - force-balanced
CMG-3ESPC	0.03	100	electronic feedback - force-balanced

Table 3.1: Seismic sensors used in WEBNET and REYKJANET networks

the routine manual processing until 2014. The supplementary off-line stations were turned into continuously recording during 2013 by upgrade of GAIA digitizers. In 2015 were the WEBNET on-line stations fully upgraded with up-to-date broadband sensors Guralp CMG-3ESPC, which replaced obsolete SM-3 passive seismometers. The Centaur digitizers by Nanometrics offering SeedLink data streaming, and calibration and diagnostics of the sensors were installed at the same time. The off-line stations underwent a similar upgrade in 2019. Additionally, these stations have been connected to the Internet with mobile 4G communication and powered from batteries recharged by solar panels. At present, WEBNET consists of 24 broadband stations covering the area of about 40x25 km.

In the period 1992 to 2015 are seismograms from the on-line stations proportional to the ground velocity in a frequency band of 0.5–80 Hz except several stations with the LE-3Dlite sensors (particularly in the early stage of the WEBNET operation, see Horálek et al. [2000a,b], Fischer et al. [2010a]) having frequency band of 1–80 Hz. The same frequency response is valid for the off-line stations in the period 1994 to 2019 (equipped with the LE-3Dlite sensors/ Gaia recorders), see Tab.3.1 and 3.2. At present, all 24 WEBNET stations are broadband (on-line stations since 2015 and off-line stations since 2019) producing ground-velocity seismograms in the 0.03 to 80 Hz frequency band. The upper corner frequency is limited by the anti-aliasing filter of the digitizer and varies from 80 to 100 Hz (6 dB bandwidth) for the sampling frequency of 250 Hz depending on the digitizer. All the stations have been operated with sampling rate of 250 Hz since the beginning of the WEBNET observations. The current amount of data produced by WEBNET is around 2 GB/day.
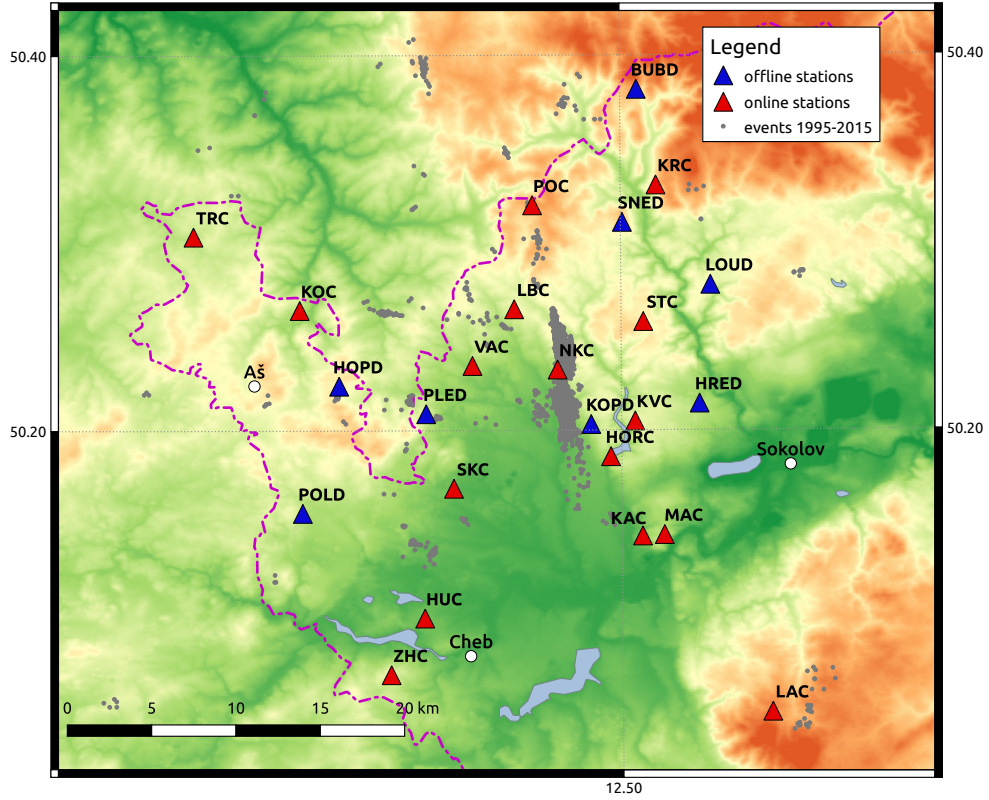
Figure 3.2: WEBNET network before upgrade in 2019. Red triangles denote on-line stations and blue triangles denote off-line stations. The light grey dots represent epicenters of earthquakes in the period 1995-2015

digitizer	manufacturer	upper cut-off [Hz]
GAIA	VISTEC	80
Trident	Nanometrics	100
Taurus	Nanometrics	100
Centaur	Nanometrics	90
Mars 88	Lennartz	80
PCM-5800	Lennartz	80

Table 3.2: Digitizers and their anti-aliasing upper cut-off frequencies for 6 dB bandwidth.

3.2 REYKJANET

The REYKJANET stations were deployed on the Reykjanes peninsula in 2013 (Horálek [2013]) by the Institute of Geophysics and the Institute of Rock Structure and Mechanisms of the Czech Academy of Sciences with know-how, technical and material support of the University of Uppsala, Icelandic Meteorological Office (IMO) and Iceland GeoSurvey (ÍSOR). The network consists of 15 stations covering an area of 40x25 km similarly to WEBNET (Fig.3.3). All the stations have been operated in off-line regime in continuous mode. Sensors are placed in special vaults on a concrete pillars connected to the bedrock. Originally, nine broadband stations were operated with Guralp CMG-40T seismometers and six short-period stations with Lennartz LE-3Dlite, which were replaced by Guralp CMG-40T in 2016; so, since 2016 all the REYKJANET stations have been broadband. The stations were equipped with low-power GAIA recorders having storage capacity about ten months (SD memory cards were used). State-of-health (SOH) of the stations was reported once in 48 hours via SMS. During 2019, the Guralp CMG-40T sensor with various sensitivities and upper corner frequency only 50 Hz were completely exchanged for Guralp CMG-3ESPC and the obsolete GAIA digitizers were replaced by Nanometrics Centaur recorders. At present, the WEBNET and REYKJANET stations have identical instrumentation. Until 2019, the frequency response was proportional to the ground velocity at frequencies of 0.03 to 50 Hz for the former broadband stations (Guralp CMG-40T/GAIA) and 1 to 80 Hz for short-period stations (Lennartz LE-3D/GAIA). The current broadband stations (Guralp CMG-3ESPC/Centaur) record undistorted ground velocity in the range from 0.03 to 90 Hz, see Tabs 3.1 and 3.2. The sampling rate of 250 Hz has been used since the beginning of the REYKJANET network. The stations have been operating in the off-line regime, so far. The data are regularly downloaded once in four months or upon request in case of some extraordinary seismic activity. Such incident happened at the beginning of 2020 when the seismic activity together with an uplift measured form GPS stations triggered an alert of possible magma intrusion under Mt. Thorbjörn volcano. Anyway, the accessibility of REYKJANET stations is strongly dependent on the harsh weather conditions and despite the urgent need some stations remained unaccessible for few more weeks. However, during 2020 the stations will be experimentally connected to 4G-LTE mobile network to stream the measured data in real time. Probably not all sites will be covered by mobile signal because some of the stations are installed in deserted places of lava fields far from the main road and farm houses. The amount of data produced by REYKJANET is around 1.3 GB/day. The stations are powered by batteries which are recharged from solar panels combined with wind turbines.
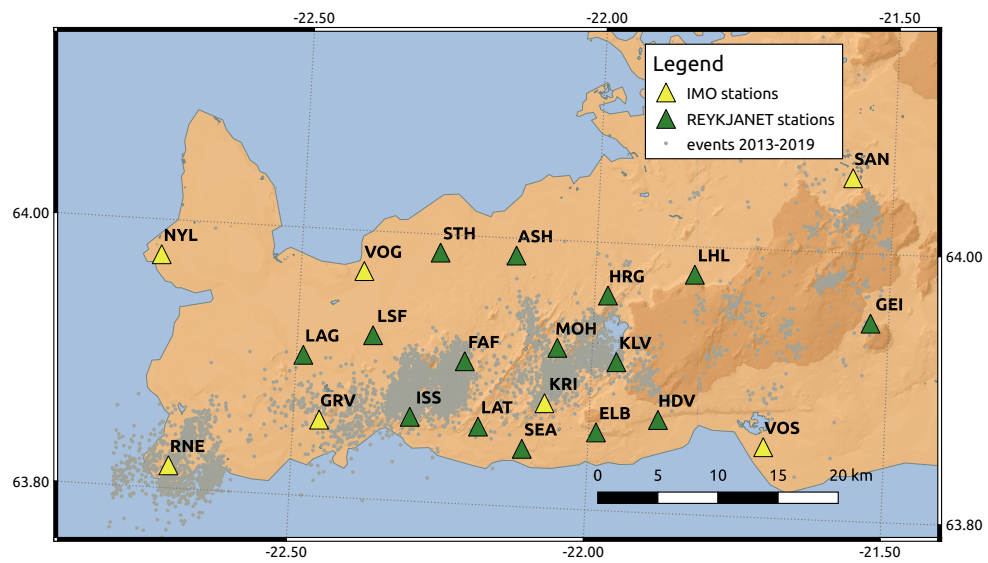
Figure 3.3: Green triangles are the locations of REYKJANET network stations. Yellow triangles are stations operated by IMO. One can see that REYKJANET network is denser in the area of Reykjanes peninsula. The light grey dots mark the epicenters of earthquakes according to IMO catalog (local magnitude $M_L > 0.5$) in the period 2013-2019.

Chapter 4

The data processing chain

Output data of the WEBNET and REYKJANET stations are in miniSEED format, which is an international standard format for the seismological data exchange (for more information on the Standard for the Exchange of Earthquake Data - SEED - and miniSEED format see Ahern et al. [2009] and Ringler and Evans [2015]). The Centaur digitizers at the on-line stations serve as individual SeedLink servers (all the WEBNET stations, and selected REYKJANET stations in the near feature). SeedLink is a TCP/IP based protocol for robust transmission of packets in miniSEED format. The SeedLink client requests data from a SeedLink server and the server starts streaming data packets to the client. Besides SeedLink, the data at the individual stations are backed up on a high-capacity removable SD memory cards and CF internal storage in the digitizers.

Once the data of the on-line stations are recorded and transfered to a data center they are multiple times copied and checked using several different servers to prevent data loss.

A simple scheme of the data flow for WEBNET and REYKJANET data is in Fig.4.1. The raw seismogram files and - if available - also SOH (State-of-Health) files in miniSEED format from the on-line stations are primarily collected at the data collection server. The data collection server is a SeedLink client which requests the data streams from the individual SeedLink servers at the stations (by *slarchive* program by IRIS consortium) and it is also a SeedLink server that provides all the data to other SeedLink clients (*ringserver* program provided by IRIS is used). In fact, there are two such servers collecting the data in parallel, first one is in the data center at the IG and the second one is at TV tower Zelená Hora.

Next, the data archive server collects the on-line data streams and stores all continual recordings in miniSEED files each containing one-day seismogram (since 2012 when the continuous miniSEED recording started).

The data from the off-line stations which are collected irregularly are saved on this server as well (former autonomous WEBNET stations and all REYKJANET stations up to now).

The different naming conventions, directory structures or record lengths are converted on the archive server to homogeneously archived 24-hours long record files. Older data in GSE2.0 format are also stored here. The data archive is thoroughly
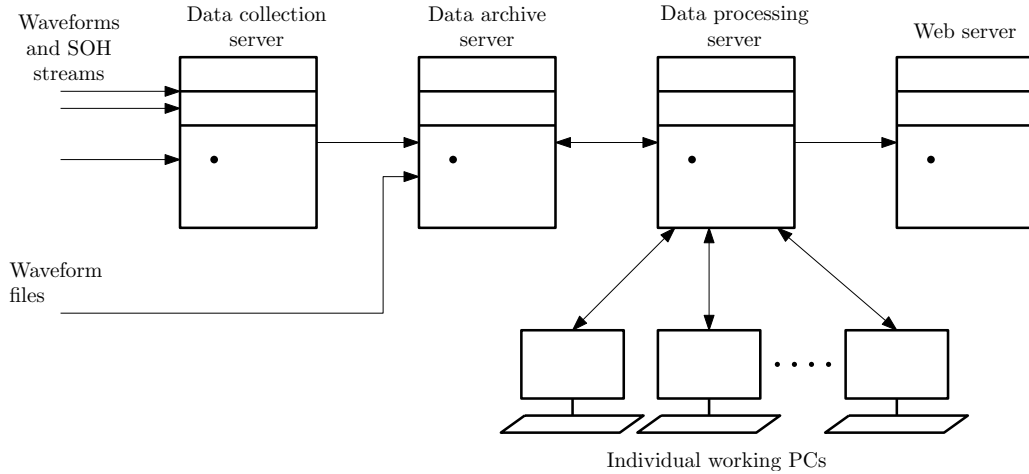
Figure 4.1: Data processing scheme and the data flow from the first SeedLink client to the presentation of the results on the web site. The main processing work is performed on the data processing server and/or individual workstations.

backed up to an external data storage.

Data processing server provides local copies of the waveforms, usually one hour long because smaller files are easier to handle since they demand much less memory to be processed. The individual users work with these files from their personal computers and also all automatic processing routines take place on the data processing server. This server also performs data quality check and basic automatic pre-processing. The results of analyses either manual or automatic are stored in a database on the data processing server which is then again backed up on the data archive server every day.

4.1 Station condition and data quality check

The automatic processing of seismic events is accompanied by continuous data availability and data quality check. In case of any irregularity, the technical support must be notified about that. The automatic procedure therefore checks for the presence of recording files from all the on-line stations (only WEBNET stations up to now) and also the SOH (State-of-Health) files are collected and tracked. We observe mainly power-supply voltage, GPS status and mass position of sensors (in Volts). These are the main indicators of the station conditions. For example, irregular discharging of the backup battery indicates a power-supply failure, when the number of satellites is zero, the GPS antenna might be broken. I developed a simple GUI (Graphical User Interface) program *SOH Monitor* which graphically represents the values obtained from SOH files in real time via SeedLink. The main window with a quick overview of station condition is in Fig.4.2. As the SOH files are preserved for one year, the user can plot the history of each SOH channel by clicking the cell and selecting desired dates. As an example, the history of input voltage is shown in Fig.4.3. Information about usage of data storage is not provided via SeedLink so we check the removable

	VEI	VM1	VM2	VM3	GAN	GNS	GST	LCQ	VEC	VDT
BUBD	no data	no data	no data	-0.144	no data	no data	no data	no data	no data	no data
HORC	13.504	0.397	-0.313	-0.799	0	no data	no data	90	148	22.94
HRC	no data	no data	no data	no data	no data	no data	no data	no data	no data	no data
JOC	11.457	-0.624	0.204	-0.286	0	14	0	90	216	18.00
KOC	13.463	-0.319	-0.817	0.344	0	10	2	100	142	20.19
KOPD	12.023	0.090	0.045	-0.080	0	12	0	90	204	17.31
KRC	12.938	-0.060	-0.031	0.271	0	10	2	100	176	17.69
KVC	13.611	0.076	0.164	0.067	0	10	2	100	169	17.94
LAC	13.032	-0.147	-0.001	-0.740	0	10	2	100	182	18.53
LBC	12.83	-0.332	0.358	0.456	0	10	2	100	174	17.50
LOUD	no data	no data	no data	no data	no data	no data	no data	no data	no data	no data
MAC	12.413	0.475	-0.439	-0.089	0	10	0	90	167	17.16
NKC	13.396	-0.352	0.008	-0.429	0	9	2	100	167	24.25
POC	13.369	0.242	0.835	0.417	0	10	2	100	177	19.03
POLD	no data	no data	no data	no data	no data	no data	no data	no data	no data	no data
SNED	no data	no data	no data	no data	no data	no data	no data	no data	no data	no data
SKC	12.952	-0.633	-0.215	-0.089	0	9	2	100	178	23.31
STC	13.53	0.689	0.037	-0.595	0	10	2	100	168	19.16
TRC	12.696	-0.468	-0.118	-0.740	0	9	2	100	179	18.66
VAC	13.45	0.514	-0.478	-0.138	0	10	2	100	174	22.59
ZHC	no data	no data	no data	no data	no data	no data	no data	no data	no data	no data

Figure 4.2: *SOH Monitor* main window. If the values are out of defined limits, the color is changed from green to orange or red (depending on how severe such deviation is). If the SOH data file is not refreshed, the color fades out. If there is no SOH file for current day, the field becomes yellow with 'no data' note.

SD card in everyday routine based on direct communication with the Centaur units at each station (using SSH - a remote administration protocol that allows to control a remote computer over the Internet). As a result a list of stations with percentage of disk usage is sent via email. For the diagnostic purposes we also monitor the traffic on the data-transfer links by the MRTG (Multi Router Traffic Grapher, free software available at `https://oss.oetiker.ch/mrtg/`). We can distinguish between fluctuations of data speed, which is usually a problem at the side of the Internet provider, and completely dead data link.
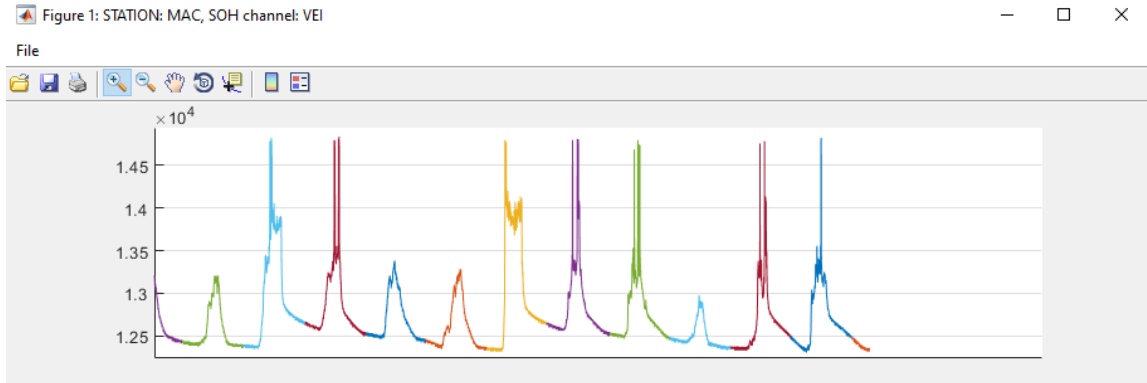
Figure 4.3: History of power-supply voltage (in millivolts) on WEBNET station MAC powered by solar panels. The charging during the days and discharging during the nights is clearly visible as well as differences between sunny and cloudy days.

4.2 Preliminary automatic analyses

The records from the WEBNET stations are automatically processed every 15 minutes at the data center (Fig. 4.1) to check the occurrence of a potentially felt local earthquake (above $M_L = 2$) for a quick response to the event for municipal authorities and media, if required. Every hour the record files are re-processed and the resulting events together with their basic parameters (hypocentral time, hypocenter locations and local-magnitude estimations) are saved to the database on the data processing server for further processing and on the web server for publication on the website. The preliminary automatic processing/re-processing is performed by code PePin developed especially for the WEBNET network by Fischer [2003] (see also Section 5.1). The reason for the double processing (each 15 minutes and each hour) is only practical. The shorter time segment the quicker response to the event but also increased probability that an event occurs at the boundary of two consecutive segments, so with respect to swarm-like character of the local seismicity the time-window of 15 minutes with one-minute overlap is used. It ensures detection of the event, however incompletely recorded event in one of the time windows may result in another detection of a fictitious event with wrong origin time and hypocenter location. It is then hard to automatically decide whether this is a false double event detection or a correct detection of two differently located events. Thus an event evaluation in the fifteen-minute window is used just as an informative alert of possibly socially important event. The location results as well as magnitude estimations obtained from one-hour window are therefore more reliable in exchange for a later response. They are saved to the database and presented automatically on the website.

Additionally, once a day the waveform files are searched for all possible events using SLRNN event detection algorithm (see Chapter 5). These event detections accompanied by automatic amplitude evaluation are used by the interpreters for manual seismic event processing.

18

Figure 4.4: A web page with automatic locations. The web page enables also to display manual locations and provides link to manual catalogs of events above $M_L = 0$. The manual catalogs are refreshed once a day.

4.3 Manual analyses

The manual seismogram processing of WEBNET and REYKJANET data is exclusively done with Seismon_WB software (more in Chap. 6). The individual researchers and interpreters with their own accounts and Seismon_WB installation on their personal computers work with record files and databases on the data processing server. The results are then stored in a shared database on the data processing server so they remain accessible for other users. Most of the intermediate or final results are labeled with the author who produced it, or with the name of the automatic method which was used, so it can be revised and inspected later.

The everyday routine of the interpreter is the detailed analysis of automatically detected events. For fine phase-onset picking the user can apply various tools like particle-motion plot, envelope or total vector amplitude. The polarity of the first motion and amplitude of the direct P-wave (possible data for source-mechanism estimation) and maximum amplitude of the S-phase (data for the magnitude estimation) are determined automatically, but the interpreter can change them, usually in case of overlapping events or extraordinary strong event. When the phase reading is finished, the interpreter calls location (NLLoc Lomax et al. [2000, 2009]). The resulting location is displayed together with a graphical representation of the residuals of the phase readings, so the interpreter can test the stability by excluding some stations or unreliable phase onset picks and repeat the action. If the result is reasonable, the location is saved to the database together with its parameters. The local magnitude is computed by NLLoc using the formula of Čermáková and Horálek [2015] for WEBNET and Jakoubková [2018] for REYKJANET. In case of significant event also source mechanism (moment tensor) is computed using amplitudes of direct P-waves and - if considered stable - saved to the database.

Each day the interpreter edits a text file on the data-processing server with the date up to which the WEBNET data are completely manually processed (for events with local magnitude $M_L > 0$). An automatic script then creates a text file with catalog of manually processed events exported from the Seismon database and publishes the new/updated file on the website. The text files are generated for each month of current year, while the catalogs of past years are saved in one file each. During earthquake swarms the magnitude threshold is temporarily raised, so first all events above $M_L = 1$ or $M_L = 0.5$ are processed in order to be quickly available and the weaker ones are examined later.

The catalogs for REYKJANET data are not published on the web, because the manual processing of REYKJANET data is not performed for all the observed period completely. Only selected episodes of increased seismicity on Reykjanes Peninsula are inspected.

```
Date of completeness:2020-02-13 00:00:00
Completeness magnitude:0
Origin time; longitude; latitude; depth; magnitude Ml
 2020-02-03 00:31:12; 12.4469; 50.2526; 7.8; 1.2
 2020-02-04 11:17:08; 12.6497; 50.0411; 7; 0.4
 2020-02-05 04:49:45; 12.3437; 50.1363; 11.6; 0
 2020-02-05 07:18:30; 12.3456; 50.1363; 11.7; 0.7
 2020-02-05 07:18:42; 12.3451; 50.1367; 11.8; 0.3
 2020-02-05 07:21:02; 12.3456; 50.1377; 11.8; 0
 2020-02-08 17:56:43; 12.444; 50.2526; 7.9; 0.1
 2020-02-08 17:56:43; 12.4459; 50.2533; 7.8; 0.1
 2020-02-12 23:54:37; 12.4523; 50.2551; 9.8; 0.1
```

Figure 4.5: Example of public WEBNET catalog for February 2020 complete for local magnitude $M_C = 0$ until February 13th.

Chapter 5

Automatic event detection

5.1 Event detection methods and machine learning in seismology

Seismic events, the useful part of seismic records for the most of seismological research, occur in just a small fraction of total recorded time even in episodic periods of increased seismic activity, for example, earthquake swarms. The target seismic events recorded on seismic stations may differ in few orders of amplitude and they may have fairly different shape and frequency content. Therefore, the classical STA/LTA (Short-Term Average over Long-Term Average) or other power-based detector detects also various disturbances and with the aim to detect even weak earthquakes it results in a high number of false detections. Well-performing detection algorithm minimizes false detections while preserving all important information, that is, all target seismic events. In our case we want to detect only local events with completeness magnitude as low as possible. Such reduction of data enables effective processing of events either manually or automatically.

Automatic processing of seismic events could be performed in different ways. The first approach accords with the steps of manual processing. Initially, an event must be detected, then the P- and S-phases are picked and the location of the event is computed using those picks (as in Sleeman and van Eck [1999]). In the second approach, a search is made for all possible P- and S-wave phases to combine them to satisfy the events, which are subsequently located (Le Bras et al. [1994], Dietz [2002], Fischer [2003]). During the third approach a search is made through all possible hypocenters and if a concurrence of theoretical data with observed data is detected the event is declared at tested hypocenter without phase onset picking (Withers et al. [1999], Kao and Shan [2004]). We apply the first processing scheme which begins with detecting an event. There are several methods of detection, which can be sorted into the time domain methods, the frequency domain methods, particle motion processing, and pattern matching (Withers et al. [1998]) or using a combination of these approaches.

All groups of detection can be achieved through the Artificial Neural Networks (ANN hereinafter) - machine learning algorithms inspired by the functionality of the

human brain.

ANN concept has been used in seismological applications mainly for classification or discrimination purposes (Dowla et al. [1990], Romeo [1994], Tiira [1996], Esposito et al. [2006], Kuyuk et al. [2011], Mousavi et al. [2016]), phase picking (Dai and MacBeth [1997], Wang and Teng [1997], Gentili and Michelini [2006], Gravirov et al. [2010], Ross et al. [2018]) or earthquake prediction (Panskkat and Adeli [2007], Morales-Esteban et al. [2013], Reyes et al. [2013]). Several neural network concepts have been used for seismic event detection.

ANNs were applied to detection in the time domain (Wang and Teng [1995, 1997], Gentili and Michelini [2006]), the frequency domain (Wang and Teng [1995], Tiira [1999]), as well as pattern matching (Madureira and Ruano [2009], Tiira [1999]). Mostly all of these methods are based on feed-forward multi-layer-perceptron (MLP) networks with one hidden layer, where the ANN is fed by moving window vectors. The output of MLP neural networks depends only on the vector currently present on the input, thus there is no memory and the time-series history can be prolonged only by longer time-window, i.e., more inputs at the cost of much higher computation load in training. Wang and Teng [1995] compared the detection performance of two ANN detectors with MLP architecture. The input of the first detector was fed by consecutive samples of STA/LTA of the whole full frequency band signal, while the input of the second one was samples of moving window spectra. The authors concluded that a spectral content must be considered for successful detection. Similarly, Madureira and Ruano [2009] designed an MLP network whose inputs are frequency samples in consecutive time windows. The work of Tiira [1999] uses MLP fed by STA/LTA of different lengths in seven frequency bands to detect teleseismic events. He also experimented with recurrent networks - Elman [1990] and Jordan [1986] networks - which enable to preserve the previous state and introduces a memory into the system, but both performed worse than MLP. Recurrent neural network was also applied by Wiszniowski et al. [2014] for detection of small local events by a Real Time Recurrent Network (Williams and Zipser [1989]). The detection capability of the neural network fed by STA/LTA ratios in narrow frequency bands and recurrent neurons with one step delay were compared to classical STA/LTA detector with filtration and proved to be better especially when signal to noise ratio was small. Nevertheless, the result showed the rapid forgetfulness of a recurrent network with single delay units, which limited the discrimination in the time domain. This concept was improved by a set of delay units with variable delays used in SLRNN neural network described here and in Doubravová et al. [2016] and Doubravová and Horálek [2019]. Recently even very deep neural networks have been successfully applied, namely Mousavi et al. [2018] combined convolutional and recurrent units in a deep network with 256 000 trainable parameters.

PePin (Fischer [2003]) which is used routinely to process the WEBNET data in near-real time applies polarization analysis to find candidate onsets of P- and S-wave phases which are then associated together to define events. A set of parameters must be tuned in order to achieve good reliability of the resulting events. The algorithm naturally fails to correctly associate phases in case of complex waveforms (e.g. multiple events) which results in omitting some of the events which can be

sometimes of not negligible magnitude. On the other hand, if an event is found and located by PePin, the location usually differs from the manual location by few hundreds of meters and the detection threshold for the WEBNET data is as low as $M_L = -1$.

5.2 SLRNN concept

5.2.1 Network architecture

The advantage of ANN detection methods is the ease of adjusting parameters of detection by training in the ANN. Consequently, a detailed description of what are common features for events, or on the other hand, what are the most significant differences between events and disturbances, are not required. The Single Layer Recurrent Neural Network (SLRNN) consists of a set of m artificial neurons. The i-th artificial neuron (Fig. 5.1) at moment t has an output value

$$V_i = g\left(\sum_{j=1}^{n} w_{ij} v_j\right) \tag{5.1}$$

where w_{ij} are weight coefficients of the neuron inputs, $v_j(t)$ are input values, $V_i(t)$ is an output value, and $g(.)$ an activation function. The activation function defines a neuron activation behavior depending on the neuron's weighted input. The activation function of the biological neuron is described as a Heaviside step function - the neuron is activated or not. In artificial neural networks using a gradient-based optimization a continuously differentiable approximation is used. In this case a widely used hyperbolic tangent is used (the neuron outputs are limited from -1 to 1).

The SLRNN is based on the Real Time Recurrent Network (RTRN, Williams and Zipser [1989]) and the Nonlinear Autoregressive Neural Network (NARX, Narendra and Parthasarathy [1991]). The structure of the Single Layer Recurrent Neural Network is shown in Fig. 5.2.

Each SLRNN neuron has the following inputs:
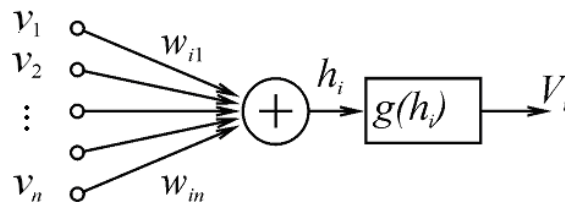
Figure 5.1: Single i-th neuron with n inputs (from v_1 to v_n), weight coefficients (from w_{i1} to w_{in}), adder with output $h_i = \sum w_{ij} v_j$, activation function $g(.)$ with output $V_i = g(h_i)$.
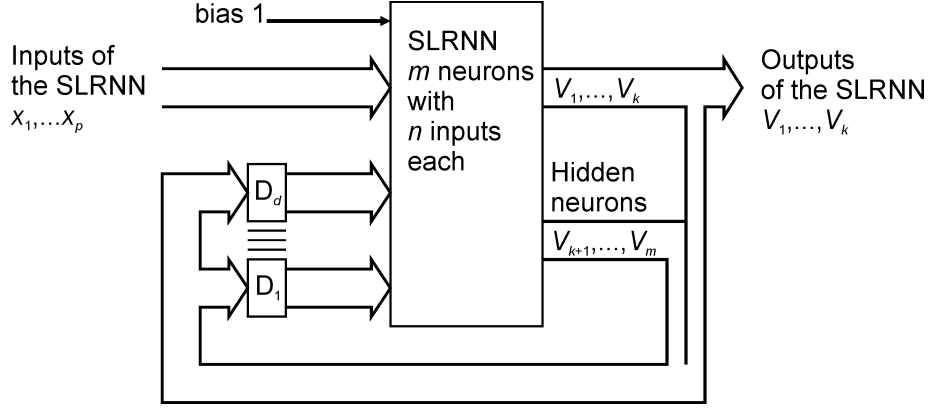
Figure 5.2: Schema of SLRNN: p inputs of the network $x_1, \ldots, x_p$; k outputs, which are output of neurons $V_1, \ldots, V_k$; and $m - k$ hidden neurons $V_{k+1}, \ldots, V_m$. Output of each neuron is connected to d inputs delayed by the corresponding (D_c) number of cycles, $c = 1, \ldots, d$. $D_1, \ldots, D_d$ are delay units.

$$
v_j(t) = \begin{cases}
V_K(t - D_c) & j = 1, \ldots, n_r; K = 1, \ldots, m; c = 1, \ldots, d & \text{recurrent inputs} \\
x_i(t) & j = n_r, \ldots, n - 1; i = 1, \ldots, p & \text{inputs of the SLRNN} \\
1 & j = n & \text{constant value 1, bias}
\end{cases}
$$
(5.2)

where m is the number of neurons, n is the number of inputs of each neuron ($n = p + n_r + 1$), p is the number of inputs of the SLRNN, $n_r = m \cdot d$ is the number of recurrent inputs, and d is the number of delay units D_c. As opposed to the RTRN, which has one step delay between output and input, the delay in the SLRNN is variable similar to the NARX. One output of neuron can be connected to many inputs of neurons with different delays. Consequently, there can be more recurrent inputs than neurons. An output of K-th neuron is delayed by D_1 to D_d steps and fed back as a part of the first n_r inputs of the neurons. The use of delays of more time steps allows remembering time relations longer compared to the RTRN (Wiszniowski et al. [2014]). Thus, the inputs from 1 to n_r are the recurrent ones, the inputs from $n_r + 1$ to $n - 1$ are those of the whole network, and the n-th input (also called bias) is connected to a constant value of 1. As opposed to the NARX, only a part of neural outputs (k) are outputs of the SLRNN. Other hidden neurons allow building self-adapted time relations not controlled by expected outputs.

5.2.2   Inputs of the network

The input data of the neural network must be preprocessed before it is used as SLRNN inputs (Fig. 5.4). Original data is three component seismic records (N, north-south; E, east-west; Z, vertical). First, the signals are filtered by a filter bank. It consists of nine half-octave IIR filters with the narrow frequency bands of 0.6–1 Hz, 1–1.6 Hz, 1.6–2.5 Hz, 2.5–4 Hz, 4–6.3 Hz, 6.3–10 Hz, 10–16 Hz, 16–25 Hz, 25–40 Hz, see Fig. 5.3. After filtration we compute a total horizontal component
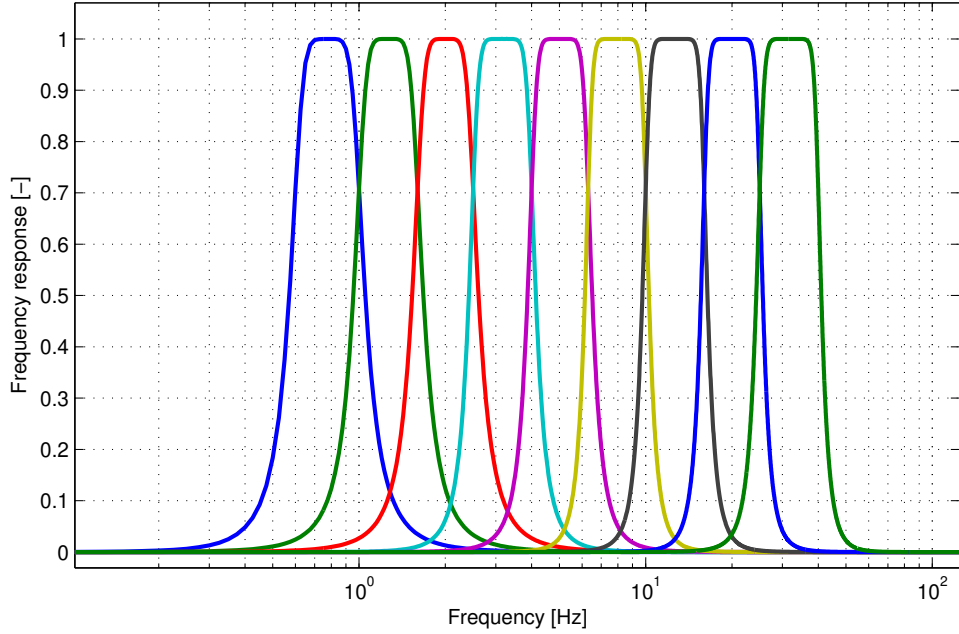
Figure 5.3: Filter bank frequency response. Each half-octave filter filters out a narrow frequency band from the input signal.
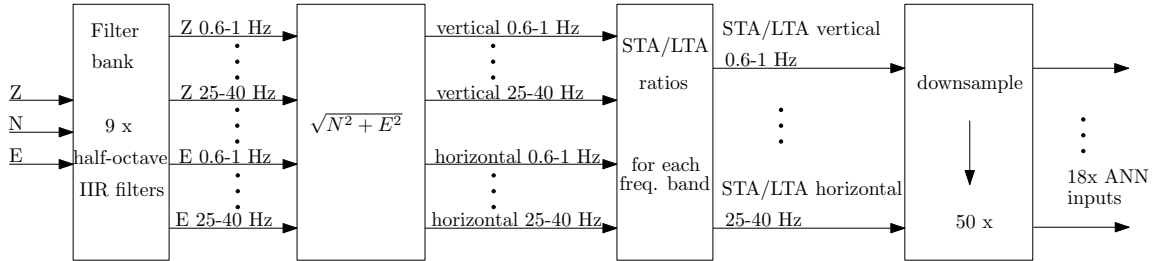
Figure 5.4: Processing scheme of the SLRNN input data. Three-component raw seismograms are processed into 18 SLRNN inputs.

$\sqrt{N^2 + E^2}$. Then, we calculate the STA/LTA ratios. The length of the short term average (STA) window is two times longer than the shortest period (defined by the higher corner frequency of each filter) and the long term average (LTA) window is ten times longer than the longest period (defined by the lower corner frequency of each filter). The original sampling rate is then decimated to 5 Hz, thus the SLRNN works in 0.2 s time steps. The time step 0.2 s of our SLRNN is a compromise between the acceptable computational load and a good separation of individual waves.

5.2.3 Configuration of the SLRNN for WEBNET

Our SLRNN, designed for detection of small natural earthquakes in WEBNET, consists of 8 neurons and 18 inputs (test for sufficient number of neurons is provided in Section 5.4.2). The feedback connections of the output of each neuron are delayed

by 1, 2, 4, and 8 time steps. Thus the neurons have 32 feedback inputs, 18 inputs of the network, and 1 bias input. The 18 inputs come from a filter bank of STA/LTA ratios. The filter bank is an array of narrow band-pass filters that separate the input signal into multiple components, each one carrying an isolated frequency band of the original signal (Fig. 5.3). The outputs of the first three neurons, which are also outputs of the SLRNN, correspond to: V_1 —detection of event, V_2 —detection of P wave onset (P onset hereafter), and V_3 —detection of S wave onset (S onset hereafter). This is achieved by adjusting the weights w_{ij} during the training process (in our case for 32 + 18 + 1= 51 inputs and 8 neurons it is 408 weights). After successful training, the V_1 output is used for event detection, while the rest of the outputs (outputs of the hidden neurons and phase detections) are used only as feedback. The detection outputs V_2 and V_3 cannot be used as pickers because of a long time step of the SLRNN being 0.2 s.

5.3 The training process

5.3.1 Training

A suitable training of an ANN is of key importance for proper performance of the ANN, so that training of our SLRNN network is one of the most exacting tasks and forms a significant part of my thesis.

We applied a supervised learning algorithm, which means that neuron weights w_{ij} (408 weights in our case) are adjusted in order to get the best possible fit of the real and required outputs of the SLRNN. It is achieved by minimizing the cost function of real and required outputs. Consequently, the required outputs of the network and the cost function E must be defined. The output of a well-trained network ought to fall below a certain threshold during the occurrences of seismic noise and disturbance, whereas it must significantly exceed the threshold during the seismic local event. In our case, the threshold was zero. However, the detection is not required to exceed the threshold at the beginning of the event. It can occur any time during the event. It is not even recommended to exceed the threshold at the beginning until, for example, secondary waves come. Otherwise, some disturbances similar in shape to the P waves might generate detection. Therefore, the required output is negative at the beginning of an event, whereas after the S onset the positive output is strongly enforced. The error between required and real output is weighted in order to ignore or emphasize the error. The cost function E for one waveform in the training set is defined as a sum of output errors in the form:

$$E = \sum_t \sum_{i=1}^{3} \eta_i(t) \left[\zeta_i(t) - o_i(t) \right]^2, \qquad (5.3)$$

where ζ_i is the expected output of i-th neuron, η_i is the learning-error weighting coefficient (learning coefficient hereafter) and o_i is the real output of the SLRNN ($i = 1, 2, 3$, corresponding to outputs V_1, V_2 and V_3). Time t is discrete in time steps of the SLRNN which is 0.2 s in our case. Both ζ and η depend on the P and

S phases of the seismic event. The learning coefficient defines how sensitive is the learning process of SLRNN to certain periods of the event waveform (Figs. 5.5 and 5.6). To improve generalization of the detection, we implemented the weight decay regularization method (Hinton [1989]) into SLRNN learning. Hinton showed that it is possible to improve generalization by adding a term that amounts to the sum of squares of the network weights to the cost function. Then the cost function is

$$E = \gamma \sum_t \sum_{i=1}^3 \eta_i(t) \left[\zeta_i(t) - o_i(t)\right]^2 + (1-\gamma) \sum_{i=1}^m \sum_{j=1}^n w_{ij}^2. \tag{5.4}$$

where the regularization parameter γ controls the extent to which the second penalty term influences the cost function. The minimization is based on a gradient of (5.4) according to the formula

$$\frac{\partial E}{\partial w_{pq}} = 2\gamma \sum_t \sum_{i=1}^3 \eta_i(t) \left[\zeta_i(t) - o_i(t)\right] \frac{\partial o_i(t)}{\partial w_{pq}} + 2(1-\gamma) w_{pq}. \tag{5.5}$$

Two methods most often used to compute the gradient of cost function of recurrent neural networks are the Real Time Learning algorithm (Williams and Zipser [1989]) used by Wiszniowski et al. [2014] and Back Propagation Through Time (BPTT) algorithm (Werbos [1990]). Regarding the SLRNN, we chose BPTT because it is faster and it is implemented in Matlab Neural Network Toolbox that we use. The definition of the expected outputs $\zeta_1(t), \zeta_2(t), \zeta_3(t)$ (Figs. 5.5b and 5.6b) and learning coefficients $\eta_1(t), \eta_2(t), \eta_3(t)$ (Figs. 5.5c and 5.6c) can be found in detail in Doubravová et al. [2016].

5.3.2 Training data

The SLRNN network was trained by applying the Levenberg–Marquardt BPTT algorithm to the WEBNET data. The training data was divided randomly into an actual training set (80% of data) and the validation set (20% of data). Each step of the training procedure reduces the cost function of the training set and in addition computes the cost function of the validation set, which is not used for training. As long as the cost function of the training set and cost function of the validation set decrease, training continues. When the cost function of the validation set starts to increase, the training stops. This prevents over-training the network when it would perfectly detect the training events but would not recognize other events well. Because of the strong nonlinearity of the cost function, the training was performed numerous times with different random initial neuron weights w_{ij}. The regularization parameter γ was set to 0.6. For training the SLRNN we used data from the earthquake swarms of 2008 and 2010. The 2008 data include thousands of local swarm events with manually picked P- and S-wave onsets which are consistent throughout the whole period. We chose randomly about one hundred events for each station with various magnitudes, locations or focal mechanisms. Additionally, a similar number of examples of disturbances and non-local events were needed. For this purpose we chose the 2010 data because it exhibited low local seismicity without earthquake
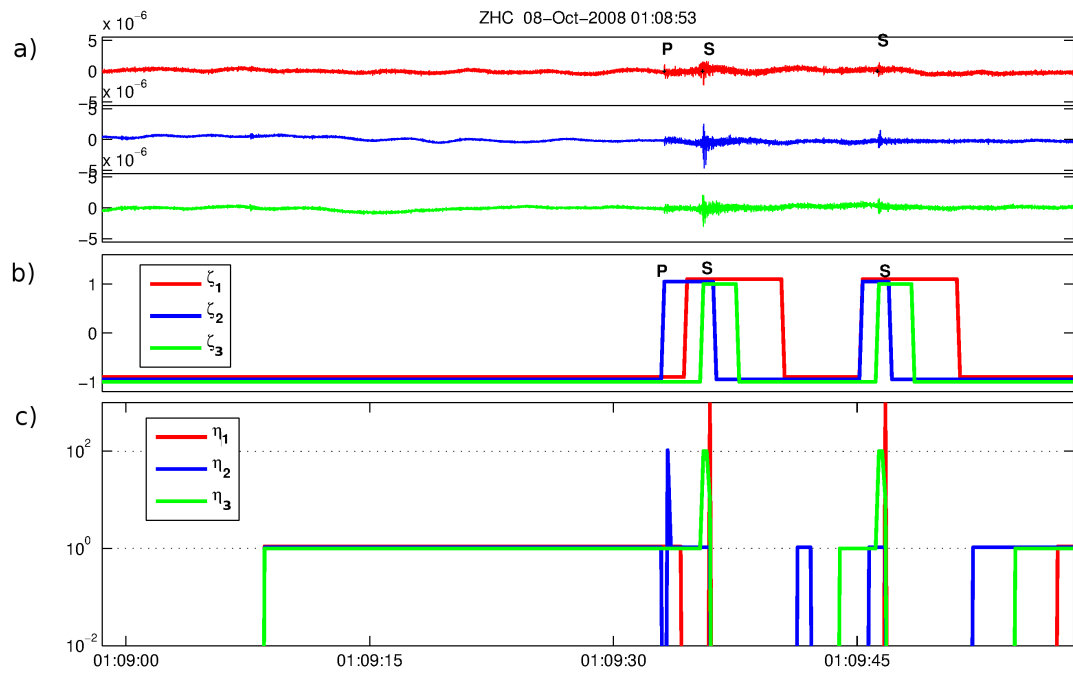
Figure 5.5: Example of SLRNN learning on the ZHC station from the 8 Oct 2008 event with P- and S-wave onset picks, and a later event with S pick only. a) the seismic signal with marked phases, red - Z component, blue - N component, green - E component, b) expected outputs of the SLRNN, red - event detection, blue - P wave detection, green - S wave detection, c) learning coefficient, red - event detection, blue - P wave detection, green - S wave detection.
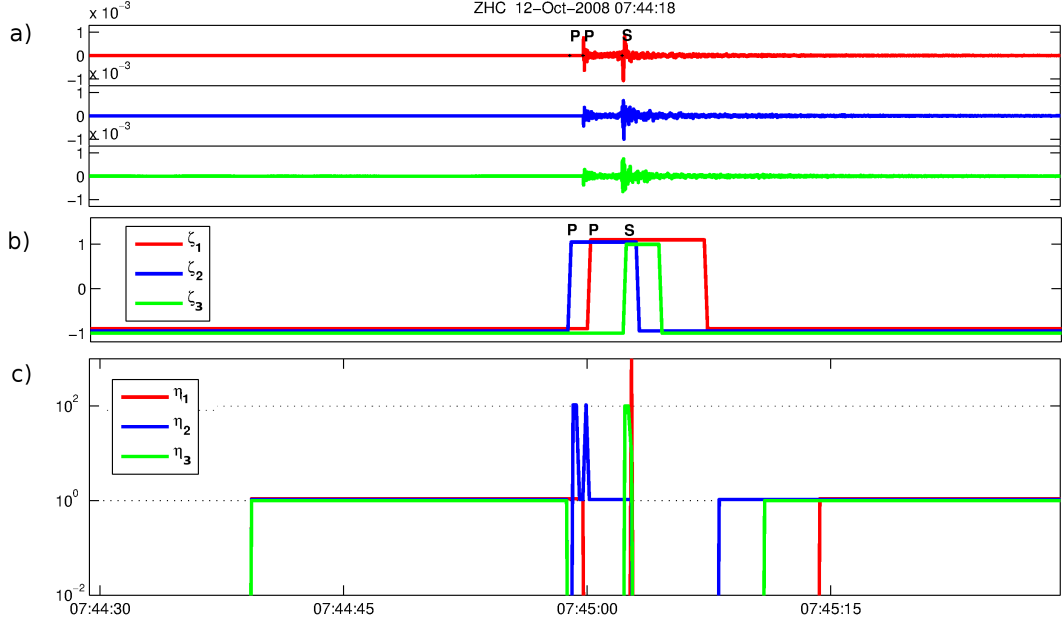
Figure 5.6: Example of SLRNN learning on the ZHC station from the 8 Oct 2008 event with P- and S-wave onset picks, preceded by small event with P pick only. (For further legend see Fig. 5.5)

swarms, so finding a variety of well recognized disturbances was easy. We used manually classified quarry blasts, regional or teleseismic events, disturbances by wind or storms and other unspecified disturbances. Major problems in our training process are lacking picks which may be due to higher noise masking onsets or to unclear P onsets on stations lying near nodal planes of a particular event, rarely due to a failure during the manual processing. When the P- and S-wave picks are missing, the SLRNN network is forced to learn that the signal is a disturbance, causing the training to act in just the opposite way. Additionally, during the evaluation of network performance on the test set many right detections not verified by manual picks (mostly very weak events preceding and following the properly picked event) are wrongly treated as false detections. To eliminate this problem it was necessary to re-process manually the set of the training events to complete the P- and S-wave onset picks even if their right position was not clear (considering that the step of our SLRNN is 50 samples, i.e., 0.2 s). Accordingly, we must have re-processed both the training and test sets several times. An example of an unpicked event is shown Fig. 5.7. At least three events were unpicked. They were detected by the SLRNN, which shows that the network can work trained by partly wrong data.
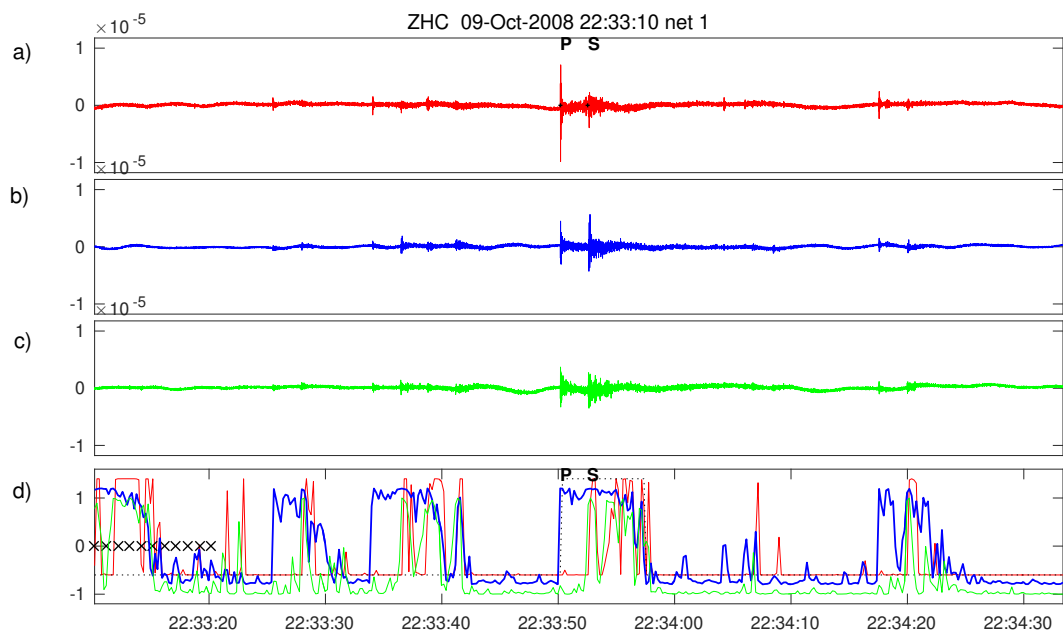
Figure 5.7: An example of one properly picked event and events not picked (before and after the picked event). Seismogram (the ground velocity in m/s) from station ZHC: (a) Z component with marked phases, (b) N component, (c) E component, (d) detection signals: red – event detection, blue – P wave detection, green – S wave detection.

5.4 Tests and evaluation of training

5.4.1 Statistical measures of the SLRNN performance

Although training the SLRNN minimizes the cost function E, the quality of detection depends on number of events detected and number of false detections, which are not wholly related to E. To assess the SLRNN performance we evaluate mainly three characteristics – specificity, sensitivity and receiver operating characteristic (Zweig and Campbell [1993]). All of them are obtained based on the values of:

- true positive (TP) – number of correctly detected events,

- false negative (FN) – number of undetected events,

- true negative (TN) – number of correct rejections,

- false positive (FP) – number of false detections.

The training set consists of seismograms with local seismic events and seismograms with any other signal regarded as a disturbance. In the case of the picked seismic events the number of true positives is incremented if the detection output of SLRNN is above zero ($V_1 > 0$) a few seconds after the P-wave onset (Fig.5.7), but if $V_1 < 0$ the number of false negatives is incremented. The event detections outside picked events are ignored because there may be some unpicked events (mostly very weak ones as in Fig.5.7) which are detected by the SLRNN. Regarding non-local earthquakes or disturbances the number of false positives is incremented if there is at least one point where detection output (V_1) was above zero. Otherwise, the number of true negative is incremented. The sensitivity, also designated as the true positive rate (TPR) or recall, is calculated according to the formula

$$TPR = \frac{TP}{TP + FN} \tag{5.6}$$

where $(TP+FN)$ is the sum of all detected and undetected events. The specificity (also designated as the true negative rate (TNR)) is calculated according to the formula

$$TNR = \frac{TN}{TN + FP}. \tag{5.7}$$

It is the ratio of true negatives to the total number of all disturbances ($TN+FP$). Ideally, the sensitivity $TPR = 1$, i.e., all local earthquakes are detected, similarly the specificity $TNR = 1$, i.e., all disturbances are rejected. Low TNR means that the SLRNN tends to produce an excess of false detections. Increasing the number of detections for small events is always associated with expanding the number of false detections. Therefore, slightly lower sensitivity could be acceptable together with a high specificity value.

A precision or positive predictive value (PPV) is defined as a ratio of truly identified events to all detections

$$PPV = \frac{TP}{TP + FP}. \tag{5.8}$$

The relation of the sensitivity and specificity is described by the receiver operating characteristic (ROC) that is usually depicted by the ROC diagram (Swets [1996]). When the sensitivity and specificity depends on the parameters of the detection algorithm used or on the parameters of training the neural network, the ROC-curves represent a relation between the sensitivity and the specificity for various values of parameters.

In an attempt to automatically compare manual catalog to detections provided by the SLRNN we faced a problem with many weak events being missing in the manual catalog correctly detected by the SLRNN. After all, the only reliable method to evaluate the correctness of each detection is to inspect it manually (Table 5.4 in Section 5.6.3). However, precise manual processing revealed also few weak events undetected by the SLRNN (usually with $-1 < M_L < -0.5$). Our goal is to get complete catalog down to $M_L = 0$ for WEBNET and $M_L = 0.3$ for REYKJANET. The smaller events will never be complete due to lower signal-to-noise ratio and are often unsuitable for further processing either. In practice, we need to reduce the amount of data for further processing as much as possible, in other words to remove redundant data from the continuous recordings. On the other hand, if the selected time segment with a seismic event is few samples longer or shorter then it does not make a difference. In case of overlapping events during the seismic swarm, we joined detections together and therefore simply counting a number of detections does not correspond to the number of detected events. In case of a very sensitive network with low threshold or little coinciding stations, many swarm events blur into long time segment; thus the useful information is preserved but the reduction of data is less effective.

5.4.2 Number of neurons

Estimating the number of neurons is always a difficult task. Generally, it is a parameter empirically set by the designer. On the one hand, it must be the lowest possible to have reasonable time for training and good generalization, but on the other hand, it must be high enough to satisfy the complexity of the problem. We tested 4,8,12,16 neurons which is in our case 140, 408, 804 and 1328 weights. The ROC characteristic in Fig. 5.8 shows that the detection is significantly inferior to four neurons. Increasing the number of neurons to 12 or 16 improved the detection only slightly while the training got significantly more time-consuming. As a result, the SLRNN with 8 neurons is suitable for detection of local swarm-like events in the WEBNET recordings.

5.4.3 Testing the training parameters

The most important point for training is the weighting coefficient η_1 just after the S-wave onset having the highest value in all weighting functions course (red curve
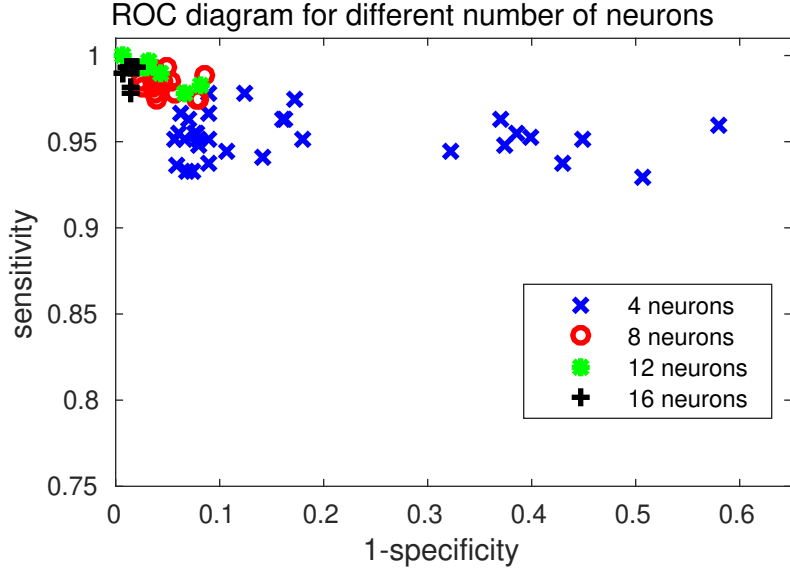
Figure 5.8: ROC diagram for different number of neurons—results of a few trails of training when all stations were trained together. Note that horizontal axis corresponds to $1 - TNR$ (specificity).

in Fig. 5.5 and 5.6). We call the value the Learning Importance Weight of Events (LIWE) more details on the definition can be found in Doubravová et al. [2016].

We evaluated the impact of the $LIWE$ value on the learning process. We tested the training of the SLRNN with $LIWE$ values of 1000, 500, 200, 100, 50, 20, and 10. The same set of the $LIWE$ values are also used in additional tests. The sensitivity of the SLRNN trained with $LIWE = 1000$ was high, but there were too many false detections and the specificity was low. Therefore smaller values of LIWE were tested, i.e., 500, 200, 100, 50, 20, and 10. The cost function is strongly nonlinear, having a number of local minima which results in some of them stopping the SLRNN learning, a tendency increases with the value of $LIWE$. Fig. 5.9 shows the sum of cost function values over the training set for 2000 trials of the training detection for station POC for the set of LIWE values. The POC station was chosen because it was one of stations showing the best detection results. When $LIWE$ was small (10–100), only 30–40% of training periods failed completely. In the case of big $LIWE$ (1000) more than 60–70% of periods of training failed.

The $LIWE$ value significantly affects the nonlinearity of training. The BPTT algorithm must be iterated more times or nonlinear optimization methods should be applied instead. To assess detector performance we examined the sensitivities and specificities. For $LIWE$ values we computed the sensitivities and specificities for 10 training results with the smallest cost function. The influence of the $LIWE$ value on sensitivity and specificity is presented in Fig. 5.10. For greater $LIWE$s the specificity decreases, which means that the number of wrong detections is growing. On the other hand, for smaller $LIWE$s the sensitivity decreases, so more events are not detected. This implies that the best $LIWE$ value is between of 50 and 200.
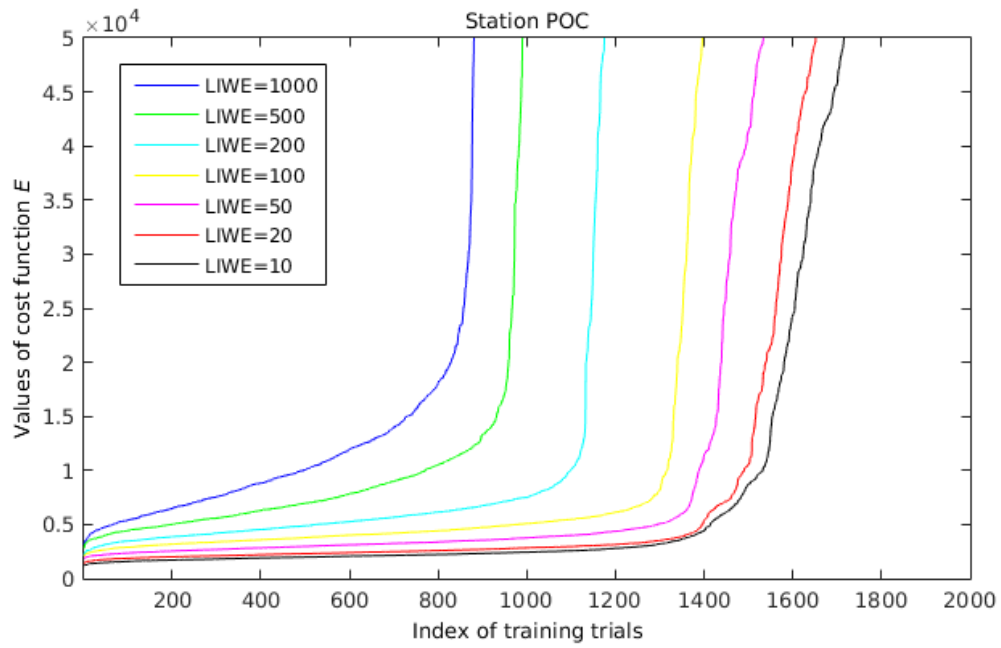
Figure 5.9: Sum of E-values over the training set for 2000 trials of training detection for one station POC for the individual $LIWE$ values. Each of 2000 training periods for each $LIWE$ finished at some of the local minimum of the cost function. For each trial the value of the cost function has been computed and results for each $LIWE$ were sorted from best to worst (from lowest E to highest E). The curves show how many trials failed. The number of successful training periods is higher for lower $LIWE$s.
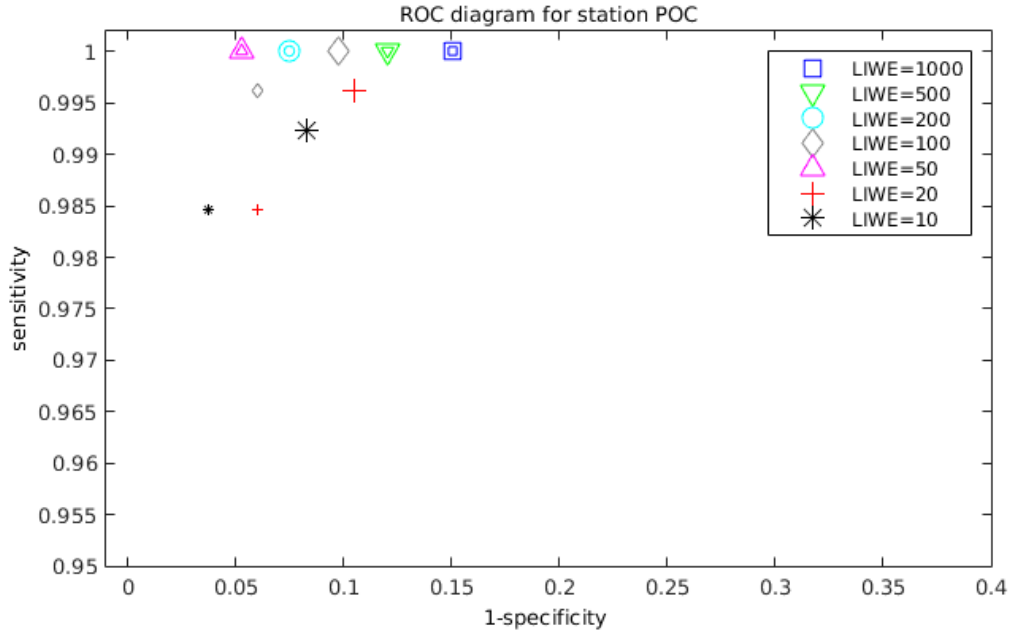
Figure 5.10: The ROC diagram for the POC station the set of *LIWE*s (given in upper-right corner) for station POC. To reduce number of points in the ROC diagrams, only two of the ten sensitivities (TPRs) and specificities (TNRs) are presented. Both TPR and TNR are required to be the highest possible (equal 1), thus our figures show the result with maxima of TPR·TNR (smaller symbols), and maxima of TNR for the best TPR (bigger symbols).

5.4.4 Individual versus joint training

The detection ability of our SLRNN was tested in two ways. First, the network was trained and used individually for each station. The results for all the WEBNET stations, which were trained individually with $LIWE = 100$ are shown in the ROC diagram (Fig. 5.11a). Second, the network was trained for all stations together. The result is shown in Fig. 5.11, where sensitivity is computed individually for each station. There are large differences between stations. The ROCs show that some stations like POC and LBC have 100% sensitivity and high specificity >90%, whereas some other stations like KAC, ZHC, NKCN have 99.5% sensitivity and smaller specificity. Results of training all stations together are similar; stations POC, LBC, and NKCN are the best, whereas stations KAC, and ZHC are significantly worse. The difference between joint and individual training at NKCN is probably caused by the lack of many picks at this station. The reason is that the former station NKC, which was located at the same site as NKCN (parallel operation), was routinely used for event location until recently. That is why a number of smaller events have not been picked on NKCN, but NKC was operated in the triggered mode, so the data from this station is not used for training the SLRNN.

The test showed that some stations always detect events as being worse than the others, so we compared it to signal-to-noise ratios (SNR) on individual WEBNET
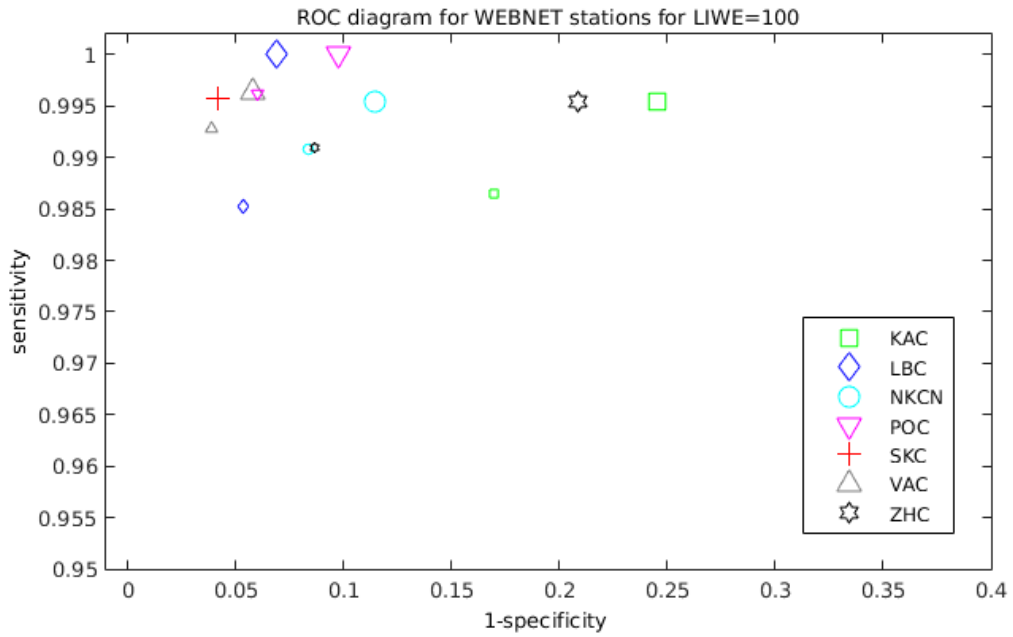
(a) Each station trained individually.
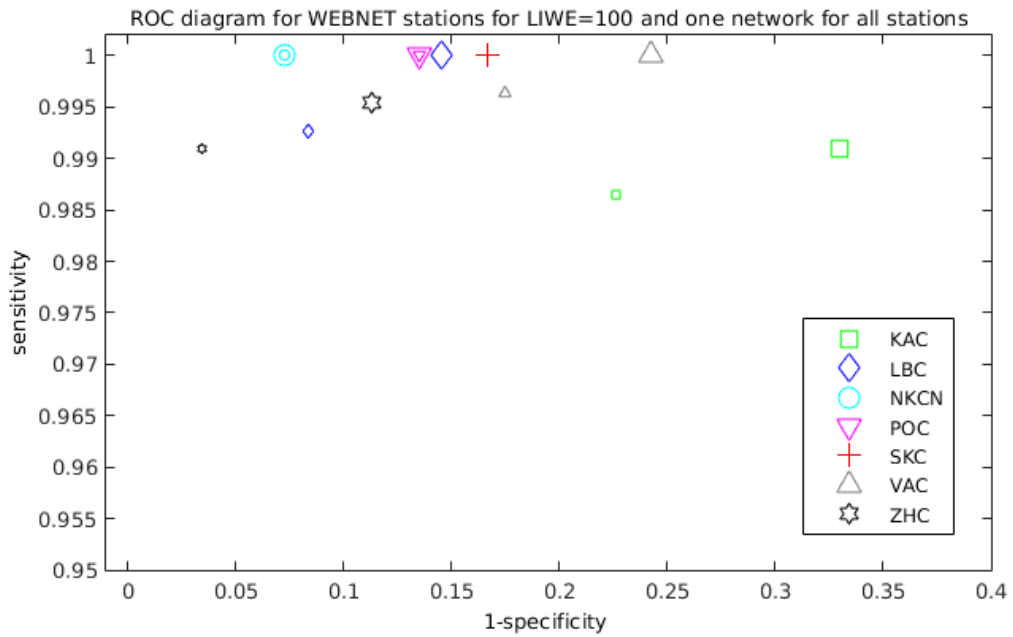
(b) All stations trained together

Figure 5.11: ROC diagrams for individual and joint training - maxima of TPR·TNR (bigger symbols), and maxima of TNR for the best TPR (smaller symbols). Individual training stations KAC and ZHC reveal the worst results. The joint training improved results in some cases, e.g., NKCN and ZHC.

stations. We processed five local events with local magnitude of $M_L \approx 1$ so as to have reasonable signal power and spectral content. Although events with lower magnitudes may be contaminated by noise, they have higher-frequency content than that of larger events. Events with higher magnitudes have lower prevailing frequencies. We computed fast Fourier transform (FFT) spectra of noise just before the event and the spectra of the event. The signal and noise spectra of five events were averaged and the resulting SNRs were smoothened by moving average (window length 5 Hz). To eliminate the signal decay due to different hypocentral distances, the SNR for the individual stations is corrected by factor R corresponding to the hypocentral distance in km.

$$SNR = 20 \cdot \log \frac{S(f)}{N(f)} R \tag{5.9}$$

The resultant SNRs are depicted in Fig. 5.12. It is obvious from this fact that the SNR pattern of the three components is consistent. We thus assume it is mostly a question of the site effects. Stations ZHC and KAC having the lowest SNR between 1.0 and 80 Hz also indicate the worst ROC. A lower SNR on these stations may be due to a shallower installation of sensors when contrasted with other stations; additionally, the ZHC station is situated close to a TV tower and also a larger town Cheb, so the higher noise cannot be avoided. I would like to emphasize that the signal-to-noise ratio at frequencies between 5 and 40 Hz are of crucial importance for a detection performance of our SLRNN, particularly for detection of weak local events.

5.4.5   False detections

We tested the performance of our trained SLRNN using data from earthquake swarm 2011 for the POC station. We chose station POC since it was used to test $LIWE$ values during the training process. The results showed a large number of "false" detections (a few hundred depending on the SLRNN realization). After an experienced interpreter inspected the 2011 waveforms and catalogs, we found that there were a number of unpicked smaller events. So we checked carefully only 5 hrs of the swarm-activity recording. In this way six originally picked events with magnitudes between $M_L = 0.6$ and $M_L = 0.9$ were supplemented with 154 new events having magnitudes $M_L = -0.3$ to $M_L = 0.6$. The next test at the same time period showed a huge improvement; many false detections switched to true ones but still some remained (from tens to a hundred). After the interpreter's inspection we found that some of these events are visible in the seismogram but definitely impossible to be picked. Besides, many other of detected events might be buried under noise. I wish to note that neural networks with very low false positives often have a tendency to increase the false negative. Generally, the ANN networks with the lowest number of false detections generally do not detect some of the events.

(a) E component

(b) N component

(c) Z component
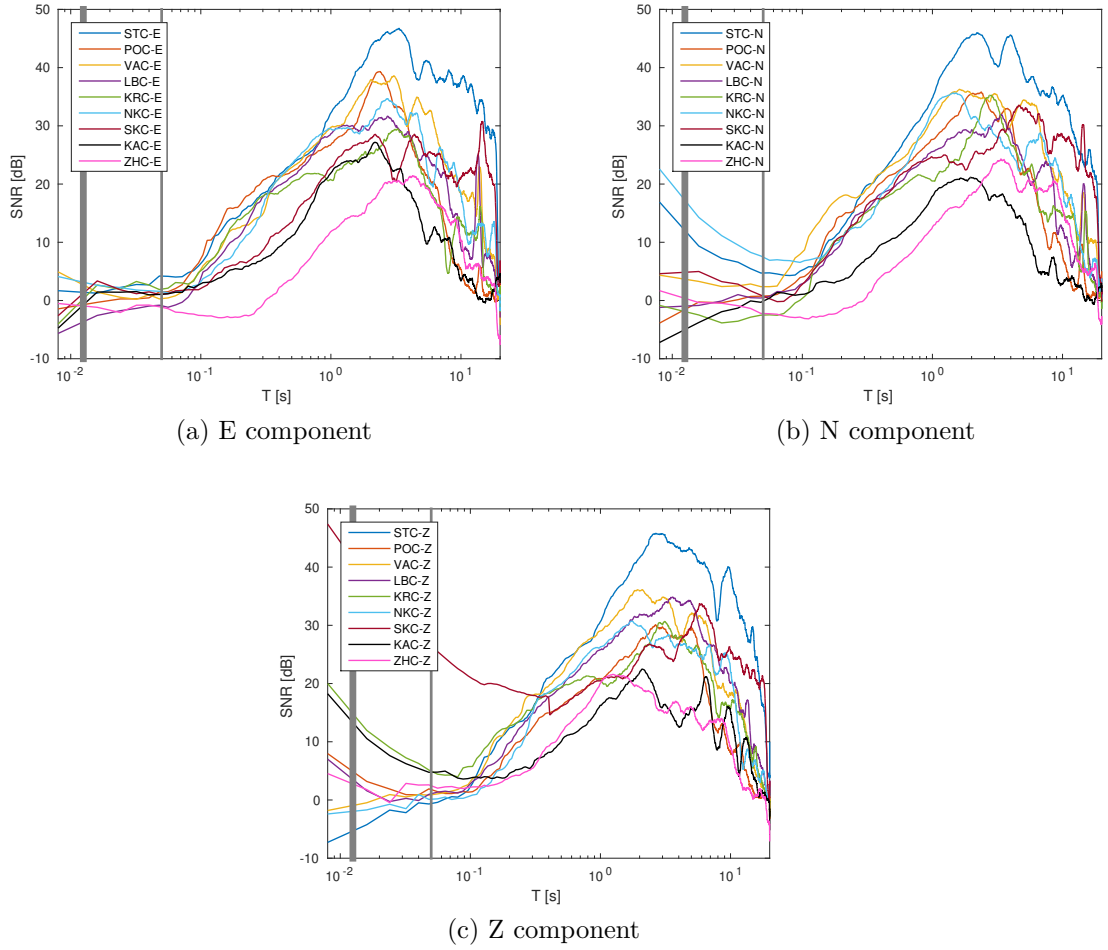
Figure 5.12: SNR for all stations used for events with local magnitude $M_L \approx 1$ corrected by the distance factor R. The thicker vertical line at $0.0125\,\text{s}$ ($80\,\text{Hz}$) corresponds to the corner frequency of the anti-aliasing filter in recording units, and the thinner one at $0.05\,\text{s}$ ($20\,\text{Hz}$) corresponds to a rough estimate of the corner frequency for $M_L \approx 1$ events according to Michálek and Fischer [2013].

5.4.6 Undetected events

Referring to false negatives (FNs), i.e., undetected events, we recognized some common features. Looking at the false detections of each SLRNN realization we found that the FNs are usually the same. Typical examples of events undetected by the SLRNN network are shown in Figs. 5.13-5.16. Fig. 5.13 depicts undetected quite large events ($M_L = 2.3$ and 2.2) hidden in the coda of much stronger preceding event ($M_L = 3.8$). Even if seismograms of all the stations are available, only a very experienced interpreter would find these events and pick P- and S-wave onsets reliably. An example of an undetected very weak event ($M_L = -0.3$) on the KAC station is given in Fig. 5.14. The SNR on the KAC site is significantly lower than on other stations, so the P- and S-wave onsets are completely masked by noise. An example of an undetected event ($M_L = 0.2$) due to very small ground-motion velocity amplitudes on station POC, located at relatively large epicentral distance ($D = 13 \, \text{km}$), is demonstrated in Fig. 5.15. An example of detected and undetected weak events in the seismograms contaminated by strong disturbances at station KAC is shown in Fig. 5.16. As it results from Figs. 5.13-5.16, the event-detection failures can be reduced substantially by using station coincidence. This means the similarity of all the stations is seen even if the trace is very noisy on some stations. The detection should be based on the coincidence of more stations in a time window of appropriate length. Then the event-like disturbance on only one station should be eliminated.
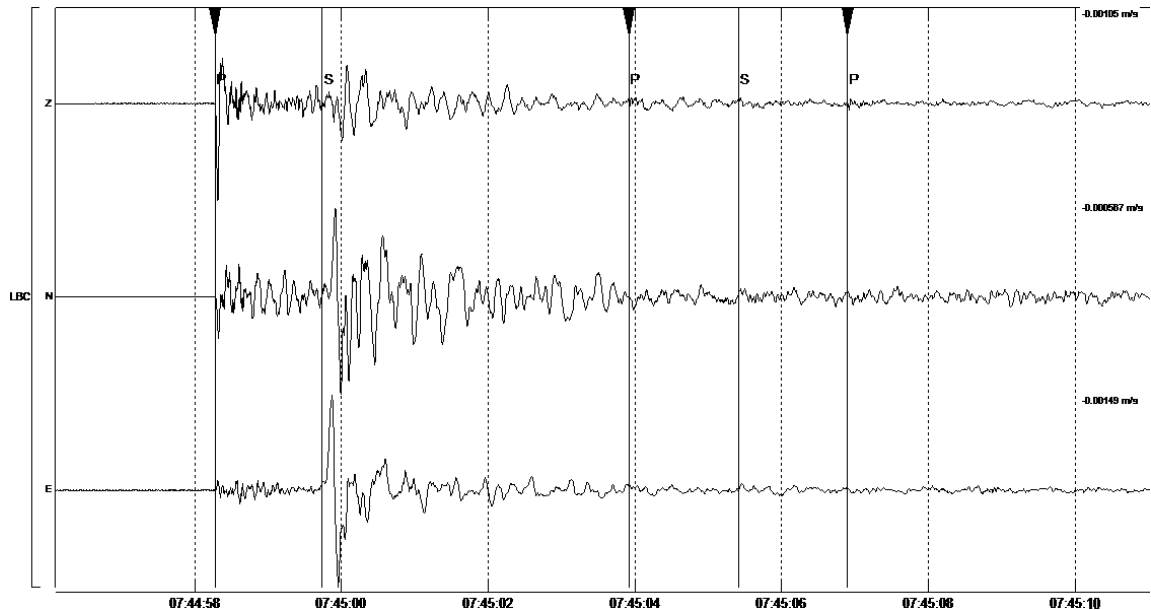
Figure 5.13: Example of undetected events with magnitudes $M_L = 2.3$ and $M_L = 2.2$ masked by a coda of the previous $M_L = 3.8$ earthquake (strongest event of the 2008 swarm, October 12, 07:44:56 UTC) on the LBC station. Even though the events are of relatively higher magnitudes, having the ground-motion-velocity amplitudes much higher than ambient noise, it is very difficult to recognize them in the coda. Vertical lines indicate the picks of the P- and S-wave onsets.
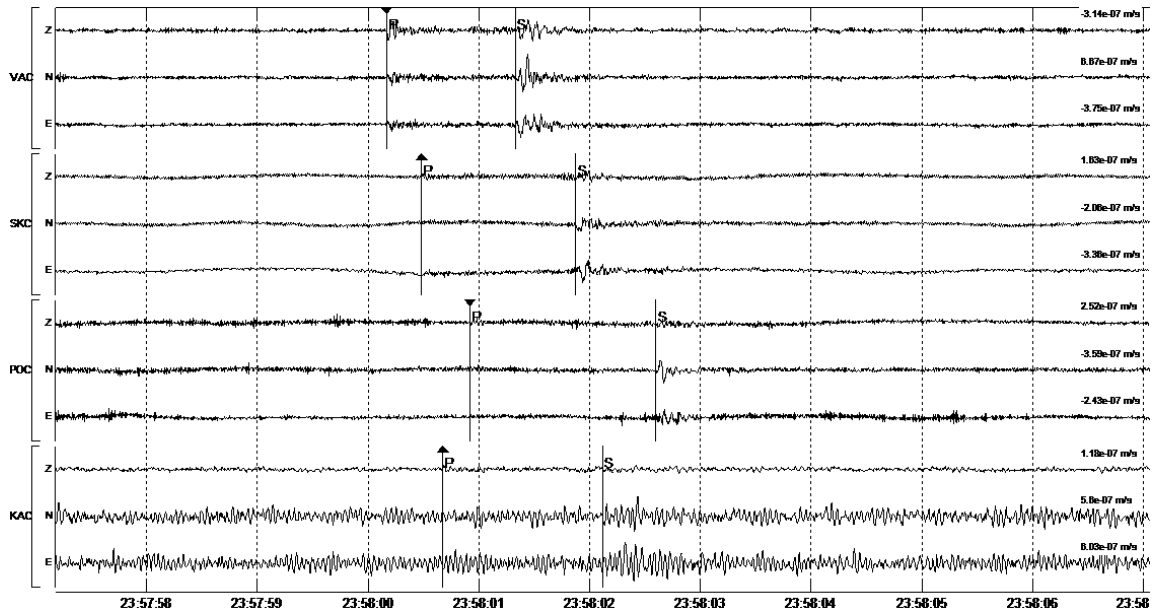
Figure 5.14: Example of a failed detection of $M_L = -0.3$ event on station KAC (bottom panel) and a successful detection of it on stations VAC, SKC and POC. Since the scale is the same for all traces it is evident that the waveform amplitudes on the KAC station are similar to those on other stations but noise on KAC is higher. Note a successful detection on stations SKC and POC (second and third panels from top), where the P waves of the event are practically invisible. Vertical lines indicate the picks of the P- and S-wave onsets, the arrows correspond to the P-onset polarity.
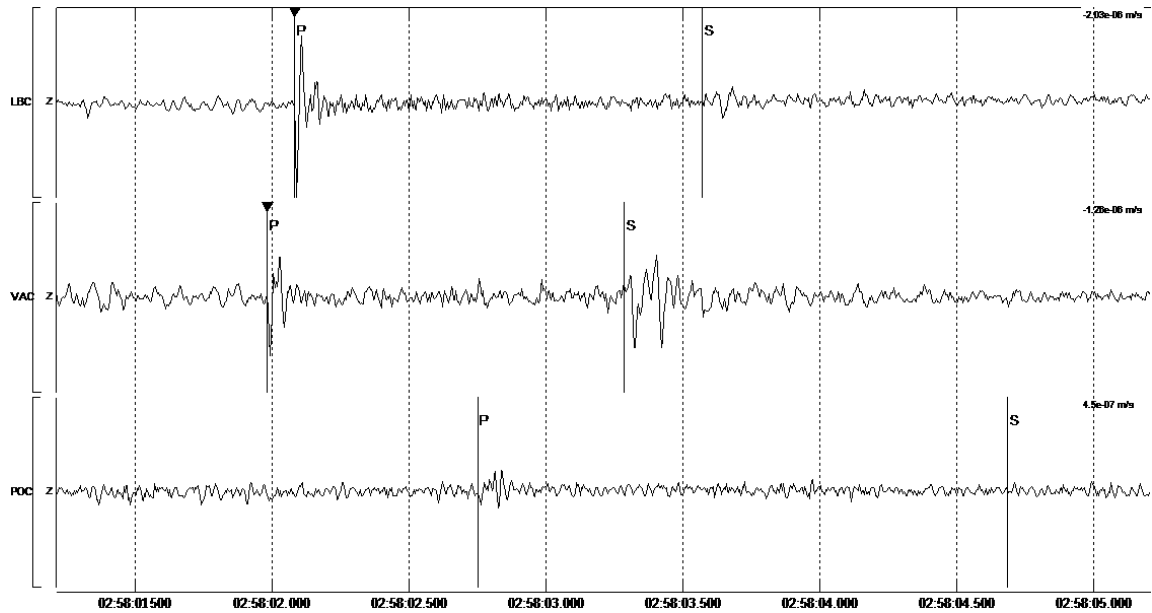
Figure 5.15: A failed detection of the $M_L = 0.2$ event on station POC ($D = 13\,\mathrm{km}$) due to a very weak P- and S-wave amplitudes. Two more stations, LBC ($D = 6\,\mathrm{km}$) and SKC ($D = 6\,\mathrm{km}$), with a successful detection of the event are added for comparison. Only vertical components are shown, all traces have the same scaling. It is obvious that the waveform amplitudes on POC are much weaker than at other stations, while the noise level is comparable. Weak amplitudes on POC are due two factors: the radiation pattern of the focus of the event and the larger epicentral distance.
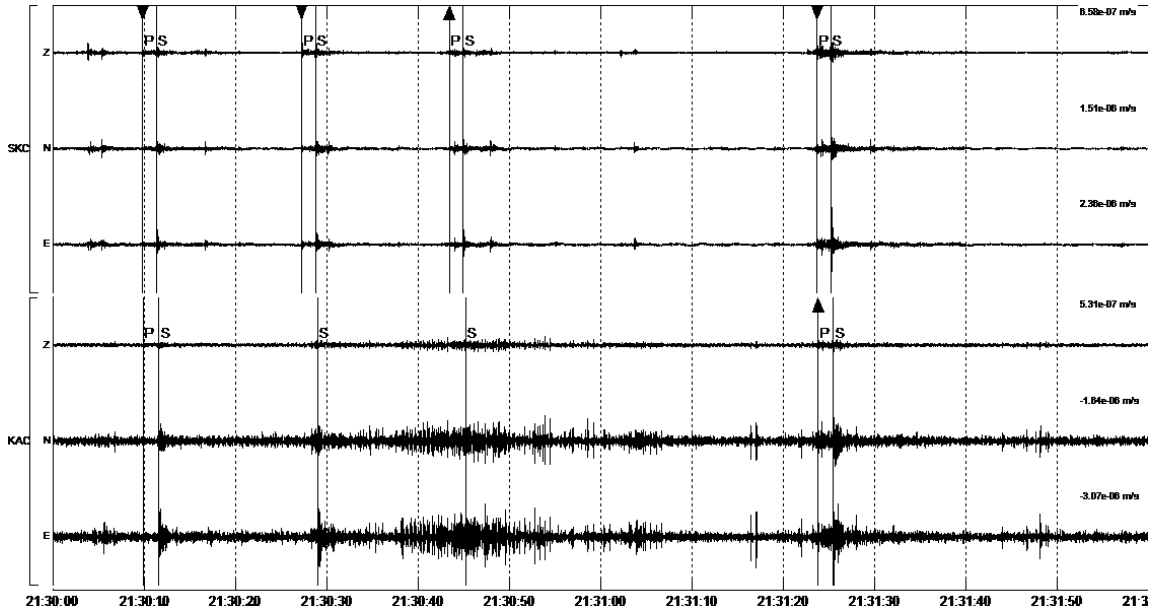
Figure 5.16: Example of detection performance in the disturbed seismogram at station KAC and in a seismogram with medium noise from station SKC. The seismograms include a sequence of four weak events (from left to right with magnitudes M_L of 0.3, 0.3, 0.3 and 0.6). All the events were detected on SKC while the detection of the third event on KAC failed due to strong disturbances. The scale is the same for all traces. Note that it is not possible to find the P waves of the second and third event in the POC seismogram, even if the processing would be performed by a skilled interpreter.

5.5   Multiple station detection

In order to reduce the number of false detections as well as the number of undetected events due to higher signal-to-noise ratio we search for detection on other stations in the network to confirm or discard the event detection. I designed a simple algorithm that rejects all detections which are not accompanied by enough detections on other stations of the seismic network. Fig. 5.17 depicts three component ground-velocity record of the KLV station of the REYKJANET network (for application of our trained SLRNN network to SW-Iceland events refer to Section 5.6.2) and corresponding SLRNN detection output. The detection is set whenever the detection output exceeds a certain threshold. The yellow stripes denote seismic events and one can see there are detections also in between the event stripes. The proposed algorithm first scans all detections (detection output above zero) on all stations of the seismic network and checks if there is a detection on a sufficient number of stations in the selected time window (we set it to 5 s with respect the size of the WEBNET and REYKJANET networks). In the next step we combine the detections together to make time intervals for events (see example in Fig. 5.18). As a result we define

time segments containing useful information. Thus, multiple overlapping events, especially during a swarm, lead to one time interval containing more events.

The number of stations, which are needed to declare an event, is closely related to the number of false detections. Additionally, too many stations required might cause loss of weaker events. Fig. 5.19 shows an example of a coincidence of four and six stations and their comparison with the events detections performed manually (by the experienced interpreter). If we compare the detection results of the four- and six-station coincidence with a precise manual ones, it can be seen that the six-station coincidence detects all the manually identified events correctly while four-station coincidence detects also false events or events which are not interpretable (three cyan stripes which do not coincide with the yellow ones). Moreover, four station coincidence detecting more events which merge into a wave train produce longer time window for detections of the events (broader stripes in Fig. 5.19). Two clearly separated event detections in six-station coincidence may merge into one longer event detection in case of four-station coincidence. For both networks—WEBNET and REYKJANET—the coincidence of six stations seems to be the best option (see Tables 5.1 and 5.2 in Section 5.6.1).
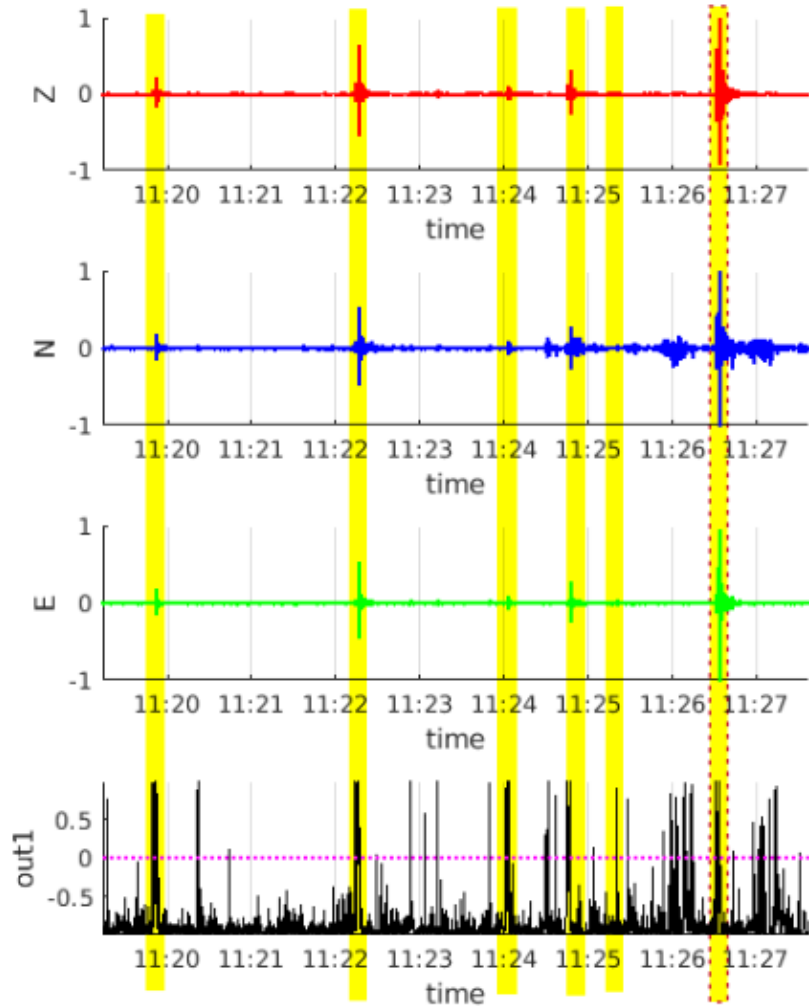
Figure 5.17: Example of the single-station detection. Seismogram from the REYK-JANET station KLV (2017 June 5, 11:20 to 11:27 UTC) filtered by BP of 1–40 Hz and detection output of the neural network (always in range between -1 and 1). From the top: vertical, north, east component of the ground-velocity record, detection output of our trained SLRNN neural network. Yellow stripes denote local seismic events from the Reykjanes Peninsula (after coincidence), the strongest event marked by red dashed line is an event included in catalog of the regional seismic network SIL ($M_L = 0.9$). The detection threshold (indicated by the purple dotted line) is exceeded even in between the events which could be due to both very weak events masked by noise and disturbances.
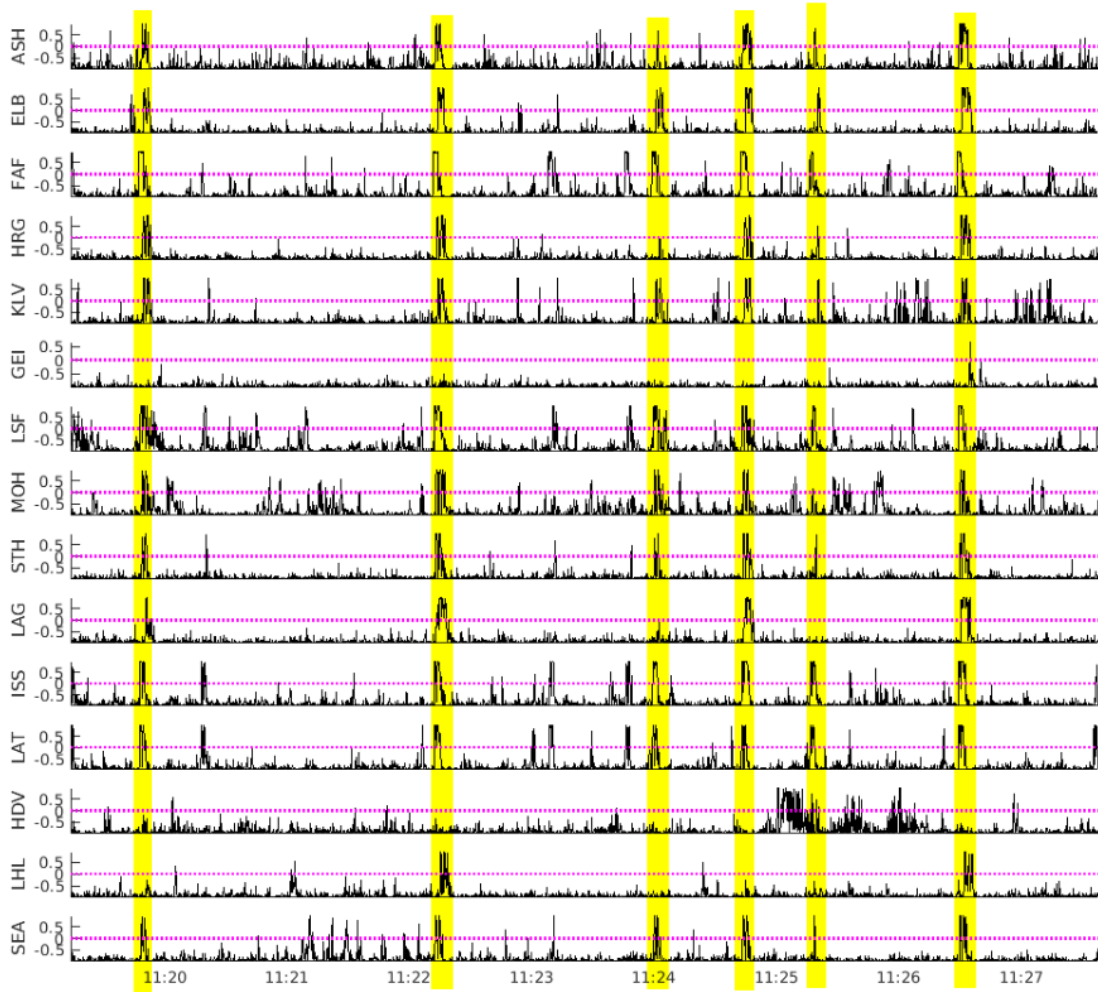
Figure 5.18: Example of the coincidence detection. Detection outputs of our SLRNN for all 15 stations of REYKJANET, detection on at least six stations required. The same time segment as in Fig. 5.17.
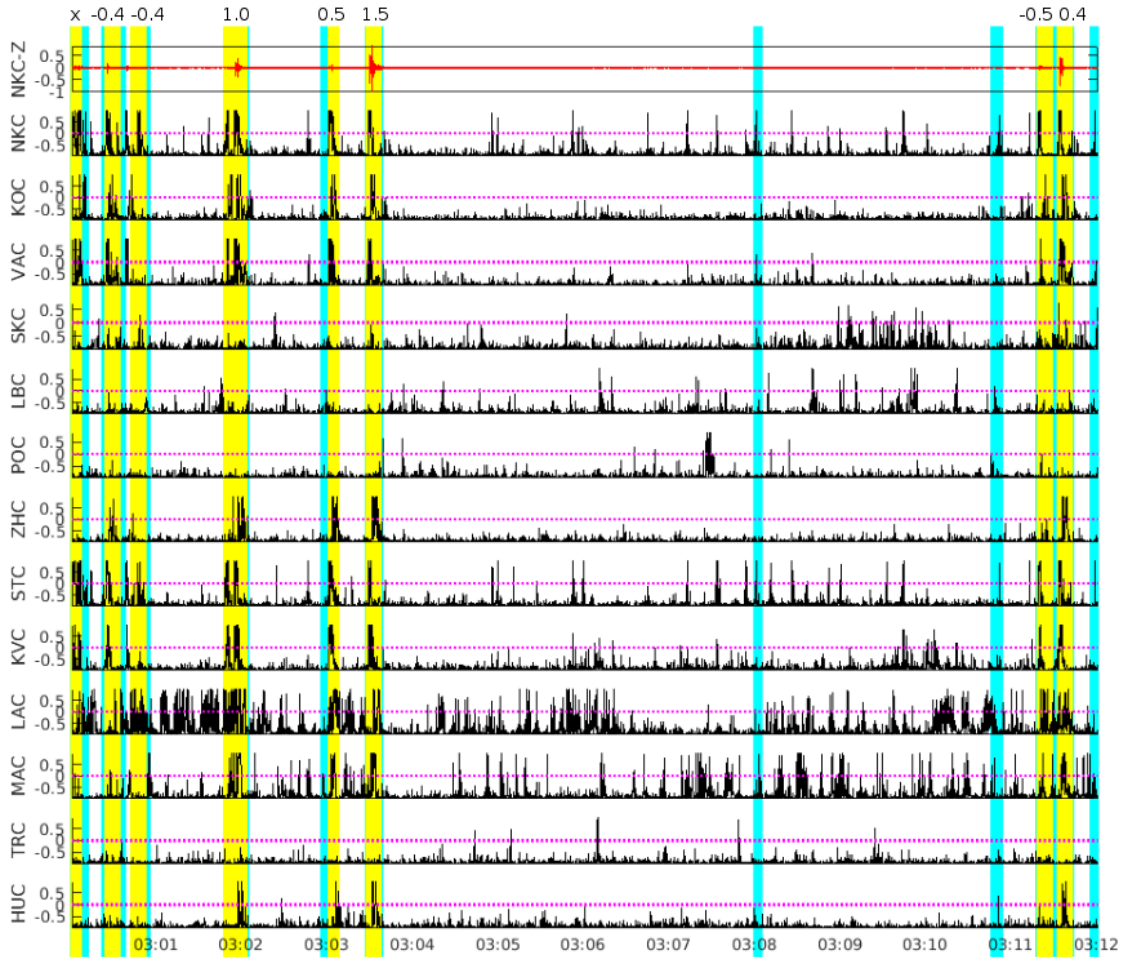
Figure 5.19: Example of the detection coincidence for four (cyan) and six (yellow) WEBNET stations. In case of concurrent event detection by four and six station coincidence the cyan stripes are overlaid by the yellow ones. Red trace above is the vertical component of seismogram from NKC station from 2018 August 24 3:00–3:12 UTC. All events in yellow were also detected manually, magnitudes M_L (from -0.5 to 1.5) are given above the yellow stripes. The first detected event in the seismogram is a multiple event consisting of several weak overlapping events, therefore the magnitude is not assigned (x sign is printed instead). Note the end of the record where two yellow events merge into one longer cyan event.

5.6 Application

5.6.1 WEBNET seismograms

The WEBNET data are first processed by the PePin software (Fischer [2003]) providing automatic locations in near-real time which are sufficient for preliminary interpretations. The events located by PePin are then re-interpreted by manual processing (adding or refining picks, location by NLLoc with more precise velocity model, and in case of more significant activities some more advanced analyses). In order to get good location residuals, the PePin software is set up to use only eight nearest stations around the Nový Kostel focal zone (the central part of the network) which contains more than 90 percent of the total seismic moment released in the whole seismoactive area since 1991 Jakoubková et al. [2018]). This unfortunately may result in omitting events outside the main focal zone. During November–December 2018 we compared in detail all event detections by the SLRNN (running in a pilot operation) with precise manual readings and with the PePin results. In this period the local seismicity was extremely low with maximum magnitude $M_{Lmax} = 1.3$. We took into account only events with magnitude above $M_L = -0.5$, which resulted in 183 events. The results of our analysis are summarized in Table 5.1 and 5.2 and displayed in Fig. 5.20. There are 106 events of $M_L > -0.5$ successfully detected by both SLRNN and PePin (red circles in Fig. 5.20), 73 events were successfully detected by the SLRNN only (they are missing in the PePin catalog, yellow circles in Fig. 5.20), and four events missing in the SLRNN list were successfully located by PePin (green circles in Fig. 5.20).

It is worth mentioning that significant part of the undetected events by the PePin algorithm are located outside the main focal zone of Nový Kostel. Tables 5.1 and 5.2 provide more detailed statistics including the comparison of the detection results of the SLRNN with coincidence of six and four stations. The six-station coincidence, which we found to be an optimum for the West Bohemia/Vogtland earthquake-swarm region, results in omitting four events which were located both manually and by PePin; all four undetected events have magnitude $M_{Lmax} \approx -0.5$. If we use four-station coincidence then all manually located events are successfully detected by the SLRNN but the number of event detections increase significantly. An example of one of the undetected events is given in Fig. 5.21. It is apparent that such small events may not be above noise level on sufficient number of stations.

5.6.2 REYKJANET seismograms

A potential ANN trained on the South-West Iceland data from REYKJANET poses quite a big problem because of the absence of complete catalogs/bulletins from the REYKJANET network which would be necessary to train the ANN. It is because of the REYKJANET recordings that have not been fully processed in detail like the WEBNET ones. To create relevant bulletins from the REYKJANET stations by manual processing of continuous recording would be extremely time-consuming, requiring an experienced specialist. Consequently, we mostly use the catalogs of a
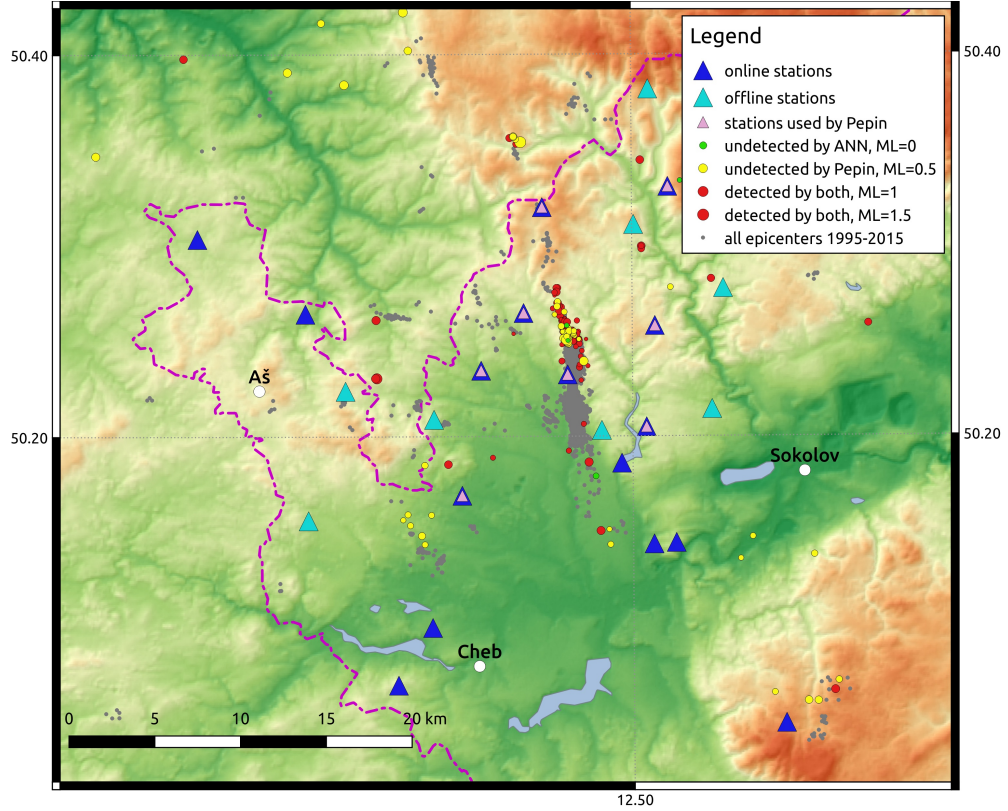
Figure 5.20: Detection results for local events during November and December 2018 in the map of West Bohemia/Vogtland. Blue triangles, on-line WEBNET stations; cyan triangles, off-line WEBNET stations; pink triangles, stations used for near-real time data processing by the PePin algorithm; grey dots, epicenters of events in time period 1995–2015; red circles, events located manually and by PePin and also detected by SLRNN; yellow circles, events located manually and detected by SLRNN (not located by PePin); green circles, events located manually and by PePin (not detected by SLRNN). Diameter of circles is scaled according to local magnitude.

Data set	Number of events
Manual events	317
SLRNN detections - 6 stations coincidence	392
SLRNN detections - 4 stations coincidence	840
PePin events	238

Table 5.1: Number of all events in the period November–December 2018 detected manually, by SLRNN and PePin algorithm. The manually detected events contain many very weak events ($M_L < -0.5$, compare with Table 5.2), majority of them is unsuitable for interpretation; similarly SLRNN detections contain very weak events or false detections. PePin events are declared after a successful location and thus they are assumed to be all real interpretable events.
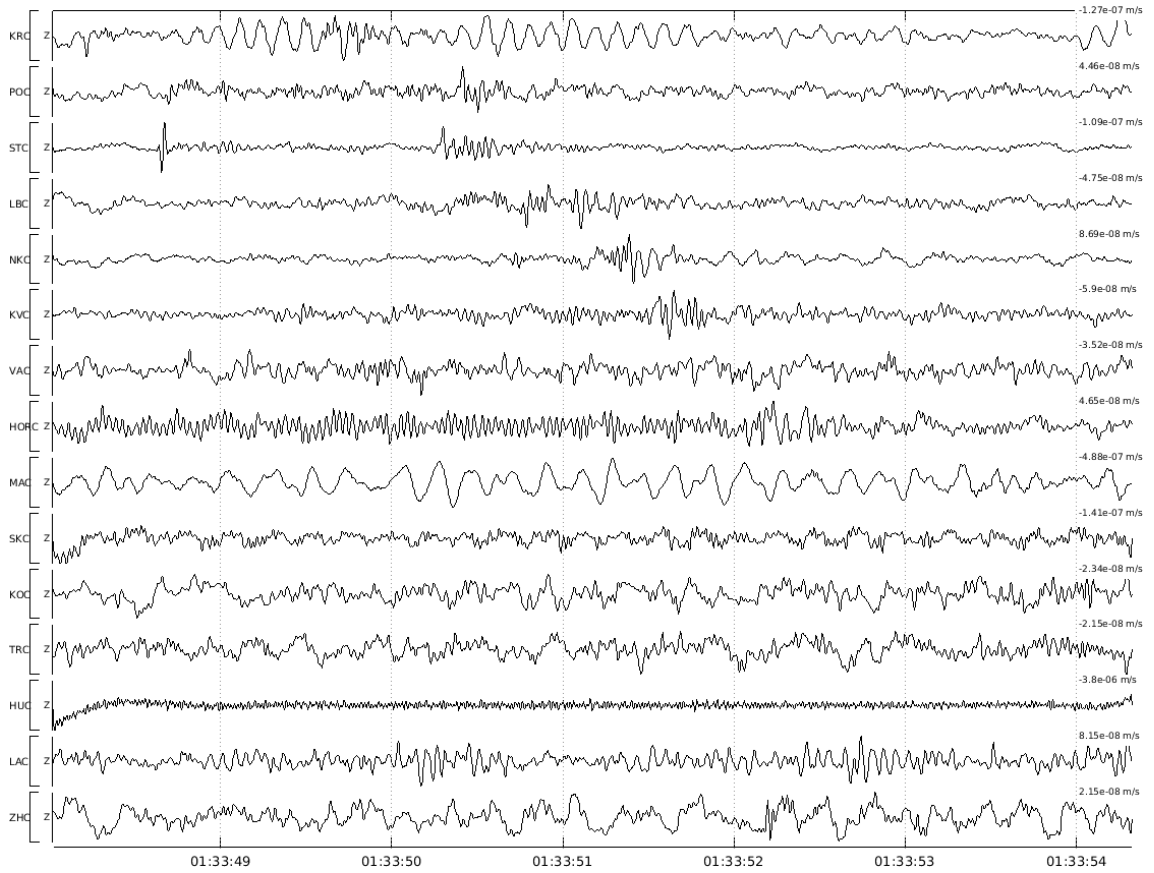
Figure 5.21: WEBNET seismograms of the local event (2008 November 14) unde-
tected by SLRNN with the six-station coincidence. Manually estimated magnitude
$M_L = -0.5$. Only vertical components of the ground-motion velocity (BP 1–40 Hz
applied) are displayed. Stations are sorted by epicentral distance (top trace corre-
sponds to the nearest station).

	Manual events	Subset in SLRNN-6	Subset in SLRNN-4	Subset in PePin
$M_L > -0.5$	183	179	183	110
$M_L > 0$	43	43	43	27

Table 5.2: Number of events compared to manual events for magnitude from $M_L > -0.5$ and $M_L > 0$, November–December 2018

50

	ANN	SIL	Antelope	PePin	Manual ($M_L > 0$)
(i) 30-31 Oct 2014	112	37	30	9	N/A
31 Mar 2015	216	30	37	29	N/A
28-30 Apr 2015	125	23	9	23	N/A
29-30 May 2015	937	167	34	25	N/A
(ii) 26 July 2017 11:00-12:00	124	56	N/A	N/A	281
(iii) 6-12 June 2017	184	34	N/A	N/A	64

Table 5.3: Number of events for all analyzed Reykjanes activities.

regional Icelandic network SIL provided by Icelandic Meteorological Office (IMO) for the REYKJANET-data analysis. But there are more detectable local events in the REYKJANET seismograms than those given in the SIL catalogs because REYK-JANET is an evidently denser network (15 stations) than a regional network SIL including seven stations in the area concerned (Fig. 5.22). Therefore, an application of the SLRNN network trained for the West Bohemia/Vogtland data (WEBNET) to data from South-West Iceland (REYKJANET) has been a challenging task. I used one of the best-performing SLRNNs as tested for WEBNET and applied it to the REYKJANET data. Since the deployment of the REYKJANET network in 2013, the seismicity on the Reykjanes Peninsula has typically been on a micro-earthquake level (magnitudes $M_L < 3$) except two earthquake swarms in October 2013 (which occurred on the tip of the peninsula out of the REYKJANET network immediately after putting the stations into operation) with $M_{Lmax} = 4.8$ and in July 2017 with $M_{Lmax} = 3.9$, and few weaker swarm-like episodes with magnitudes up to $M_{Lmax} = 3.5$. We analyzed in detail the detection results for

(i) four weak swarm-like activities from the period 2014–2015,

(ii) an intensive $M_{Lmax} = 3.9$ swarm of July 2017 and

(iii) scattered background seismicity on the Reykjanes Peninsula in June 2017

(for basic data and locations of the analyzed activities refer to Table 5.3 and Figs. 5.22 and 5.23).

The SIL catalog is the primary reference for evaluation of the SLRNN-detection results for both (i) and (ii). Besides, we used a catalog of the event detections produced by PePin algorithm (Section 5.1) and Antelope software package (by Boulder Real Time Technologies, Ltd.) that were applied to the REYKJANET data (i), and a detailed bulletin of the 2017 swarm containing manual onset picks from all the REYKJANET stations.

(i) First, we compared the total number of detected events by the SIL processing at IMO, PePin algorithm, Antelope software and SLRNN (also denoted as ANN) in the individual weak activities. The Antelope automatic location procedure uses weighted STA/LTA phase detections (mainly P-wave phases are correctly picked). The PePin algorithm uses polarization analysis for event detection. In the first step the S-wave arrivals (which are often clearly polarized) are identified then they are associated with matching P-wave arrivals in the given time window, finally the event is localized. However, in case of a false event location (e.g. due to the incorrect
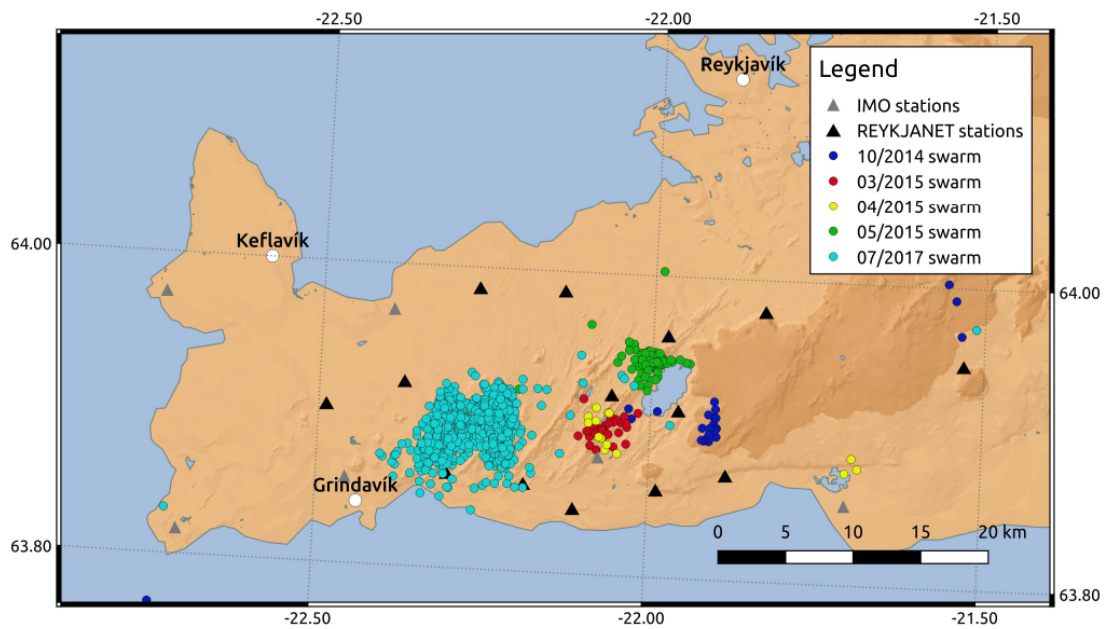
Figure 5.22: Distribution of analyzed seismic activities/events on the Reykjanes Peninsula. circles, epicenters of analyzed earthquake activities. Blue circles - 2014 October 30–31 ($M_{Lmax} = 2.8$), red circles - 2015 March 31 ($M_{Lmax} = 2.2$), yellow circles - 2015 April 28–30 ($M_{Lmax} = 1.6$), green circles - 2015 May 29–30 ($M_{Lmax} = 3.5$), cyan circles - 2017 July 26–28 ($M_{Lmax} = 3.9$). Black triangles denote REYKJANET stations, grey triangles mark IMO stations.
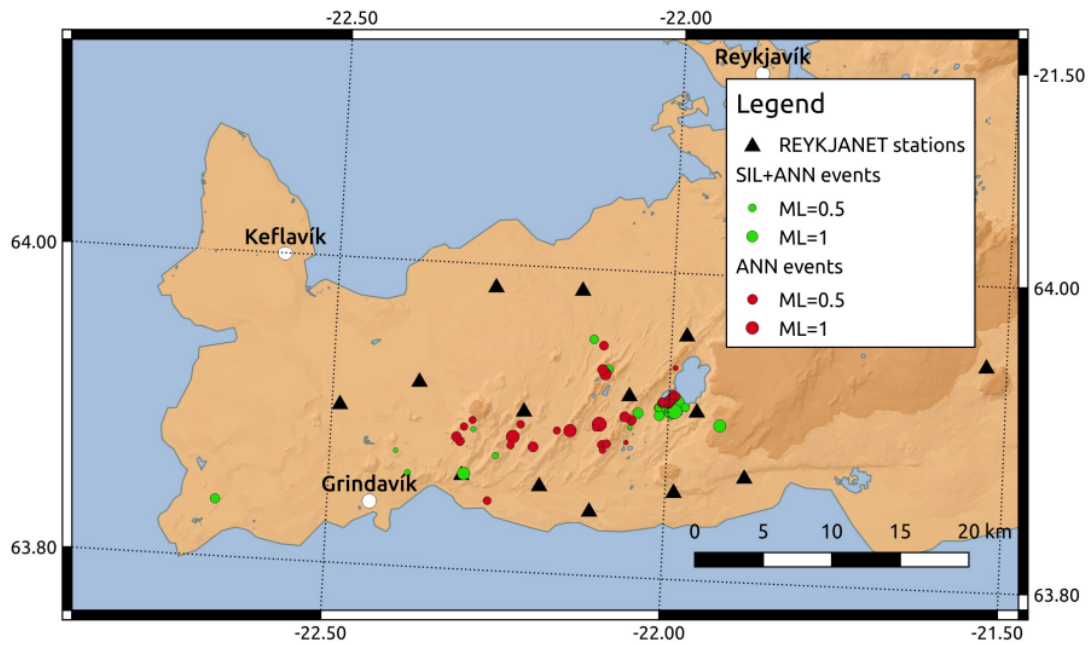
Figure 5.23: Examination of the SLRNN detections of background seismicity on the Reykjanes Peninsula in the period 2017 June 6–12. All 34 events listed in the SIL catalog (green circles) are successfully detected by the SLRNN. Another 37 events (red circles) detected by the SLRNN are located using manual picks of the P- and S-wave onsets. 112 more event detections indicated by the SLRNN are the events unfit for location due to lack of reliable P- and S-wave arrival times or false alarms in some cases.
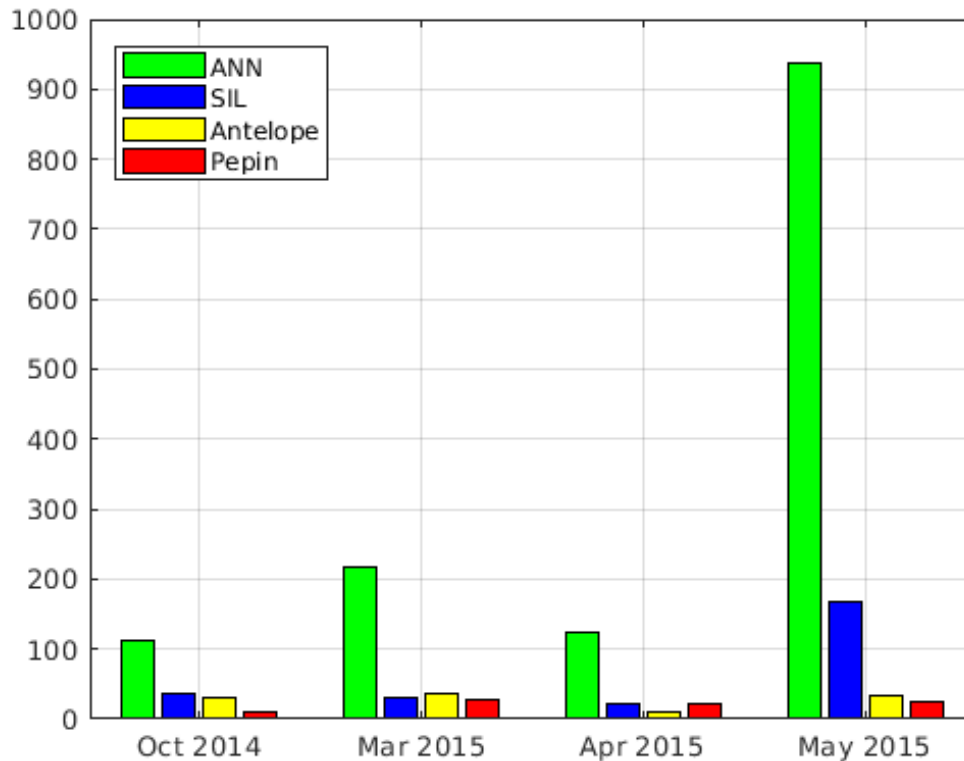
Figure 5.24: Number of detected events in analyzed micro-swarms on the Reykjanes Peninsula.

association of the P- and S-wave arrivals) the event is omitted in the uncatalogued (for more information about the PePin detector see Fischer [2003]). The comparison of the SIL, Antelope, PePin and ANN catalogs is depicted in Fig. 5.24.

It is apparent the number of events detected by SIL, PePin and Antelope is comparable for all the activities, while the number of detected events by the SLRNN is about five times higher. We manually checked one of the activities with a reasonable number of events—the mini-swarm of the 2015 March 31. In total, 30 events have been listed in the SIL catalog ($M_{Lmax} = 2.2$), 37 were located by Antelope and 28 by PePin. Inspecting the events manually, we found out none of the 'catalogs' (SIL, Antelope and PePin) to have been a complete subset of another one; each catalog contained some unique events which were missing in the other two catalogs (see Fig. 5.25). The SLRNN detector provided 217 events including all the detected events given in the SIL, PePin and Antelope catalogs. Fig. 5.25 represents the comparison of detected/undetected events from each catalog (SIL, PePin and Antelope) with those in the other two catalogs and with the SLRNN detections. By combining the SIL, PePin and Antelope catalogs we obtained 51 real events with minimum magnitudes $M_L \approx 0$. Our SLRNN detected all of them and in addition to that about three times more weak events. But many of the small detected events are unsuitable for

further processing because locating of such events would be unreliable due to unclear P- and S-wave onsets.

Nevertheless, Figure 5.28 demonstrates that even the small events are true local seismic events, even they are on most of the stations buried in the noise. We believe that further automatic processing leading to an event location would reject some of these event detections due to insufficient number of good quality phase readings; or some amplitude/power threshold may be used. Fig. 5.25 also point to the imperfect performance of the PePin algorithm because it missed two strongest and several other weaker events in the March 2015 activity (Fig. 5.25, top diagram in the figure). The PePin algorithm, which defines an event by associating the P- and S-wave phases, might have failed due to more complex waveforms resulting in the false association of the P- and S-wave phases (Section 5.1). Let me note that PePin has been tuned and routinely used for a near-real time processing of data from WEBNET.

(ii) A prominent earthquake swarm in July–August 2017 $M_{Lmax} = 3.9$ was fairly rapid. Most of the seismic moment released during 2 days from July 26 to 28 (Jakoubková et al. [2018]), more than 1500 $M_L > 0$ events have been listed in the SIL catalog for these days (Fig. 5.26). We concentrated on 1 hr of the swarm activity on July 26, from 11:00 to 12:00 UTC, that included the second strongest earthquake of the swarm ($M_L = 3.7$). This segment contains both calm and turbulent phase of the swarm (Fig. 5.26). We performed detailed manual processing of the continuous seismograms with the assistance of an experienced expert who found 441 events in total out of which 281 were reliably located with magnitude above $M_L > 0$. Then we compared the manually obtained events with detections provided by the SLRNN and with the list of events in SIL catalog. There were 56 events in SIL catalog and 124 event detections indicated by SLRNN (due to the turbulent nature of the swarm the detections often included more events). The results are shown in Figs 5.27 and 5.26. All of the manually picked events were correctly detected by the SLRNN and only one false SLRNN detection was found.

(iii) In order to prove the SLRNN ability to detect various local events on the whole Reykjanes Peninsula we selected a time segment containing scattered background non-swarm seismicity only (Fig. 5.23). We selected one week, 2017 June 6–12, where the seismic events included in the SIL catalog were scattered in the whole area covered by the REYKJANET network. The SLRNN detected 183 events, 34 events of which had been listed in the SIL catalog and no event present in SIL catalog was missed. By manual processing of the waveforms we were able to confirm reliably 37 new events which we located and for which we estimated M_L ranging from -0.5 to 1.3 (30 above $M_L = 0$). Remaining 112 events were mostly unfit for location due to insufficient number of clear P- and S-wave onset picks or they were real events hidden in ambient noise, and probably some of them were also false alarms.

5.6.3   Results and comments

The advantage of our neural network is the ability to recognize new types of local events (different shapes of waveforms due to different structure of a local upper crust) based on training examples (i.e., generalization capability) and very fast computa-
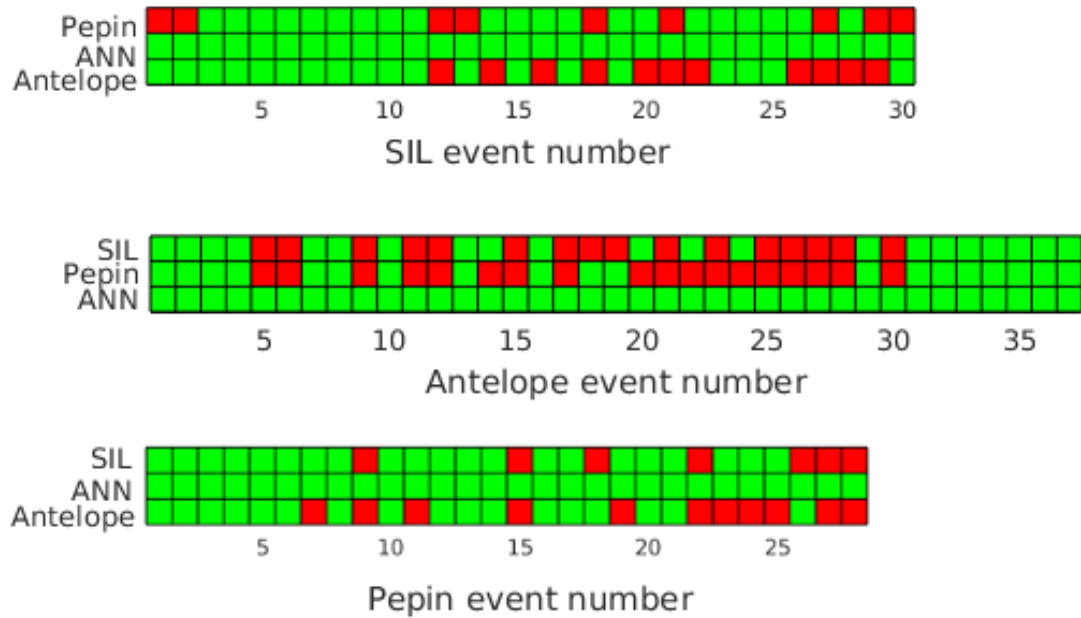
Figure 5.25: Detailed examination of the SLRNN detection results and the SIL, Antelope and PePin catalogs for mini-swarm of 2015 on the Reykjanes Peninsula. The diagrams represent the individual catalogs except SLRNN; from top to bottom: SIL, Antelope and PePin. Each column in the individual diagrams denotes a particular event in the respective catalog (thus the number of columns in each diagram equals to the number of events in the catalog). The events in the SIL and PePin diagrams are ordered according to magnitudes M_L given in the SIL and PePin catalogs from the strongest (on the left) to the weakest one (on the right); the events in the Antelope diagram are sorted according to the origin time. The rows in the diagrams denote events which are included (green cells)/missing (red cells) in the remaining three catalogs (indicated on the right). The SLRNN diagram is not presented because a total of 217 events are detected by our SLRNN including all the events given in the SIL, Antelope and PePin catalogs. Note that the each catalog (SIL, Antelope and PePin) contains some events detected only by ANN and missed in the other two catalogs
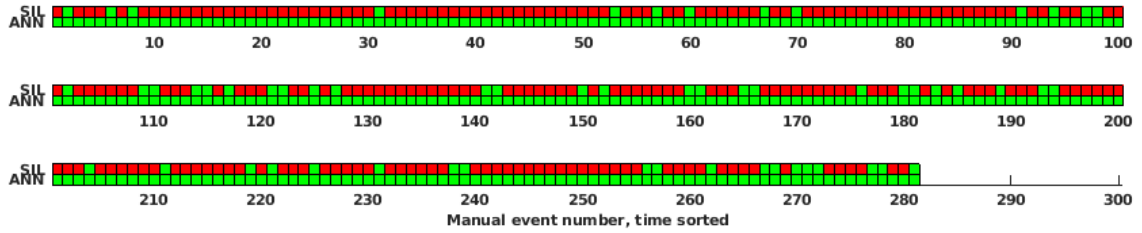
Figure 5.26: Comparison of the SLRNN detection results with the SIL and manual REYKJANET catalog for 1 hr period of a larger 2017 swarm on the Reykjanes Peninsula. High rate seismicity in the time window of 2017 July 26, 11:00 to 12:00 UTC, is examined. The diagram represents a comparison of the SLRNN results and SIL catalog with the REYKJANET catalog (281 $M_L > 0$ events) created manually by an experienced interpreter. For more information on the diagram structure refer to the caption of Fig. 5.25. The events are sorted according to the origin time.
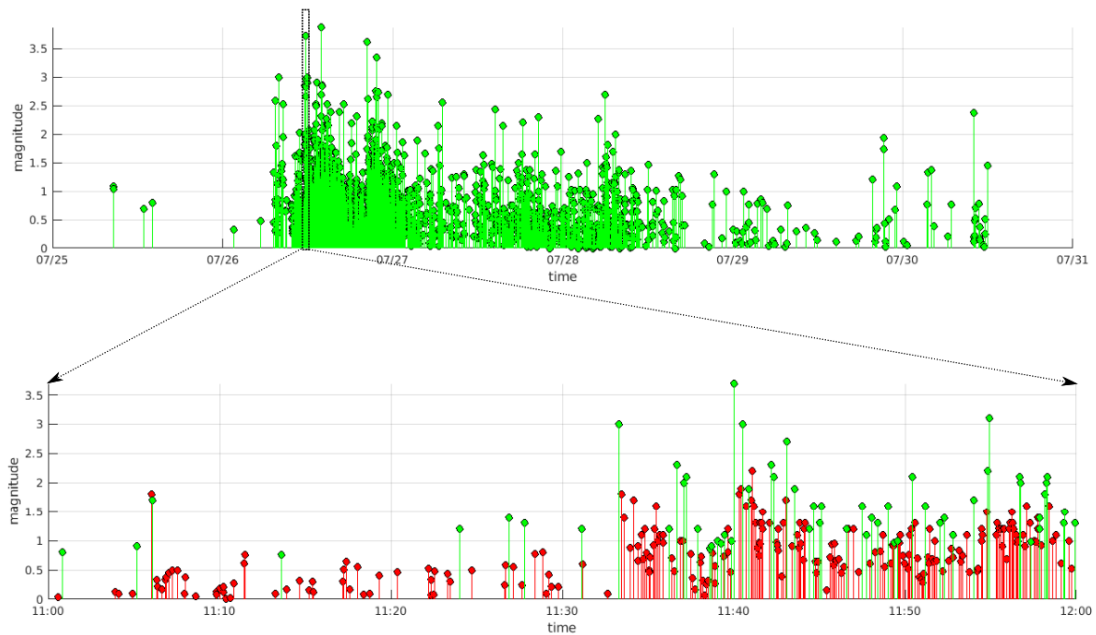
Figure 5.27: Magnitude-time distribution of the 2017 Reykjanes seismic swarm, only events with magnitude $M_L \geq 0$ are considered. Upper plot: the whole activity according to the SIL catalog; lower plot: 1 hr segment around the second strongest shock of $M_L = 3.7$ (2017 July 26, 11:00 to 12:00 UTC). Red points: events of the manually created REYKJANET catalog which were missing in the SIL catalog.
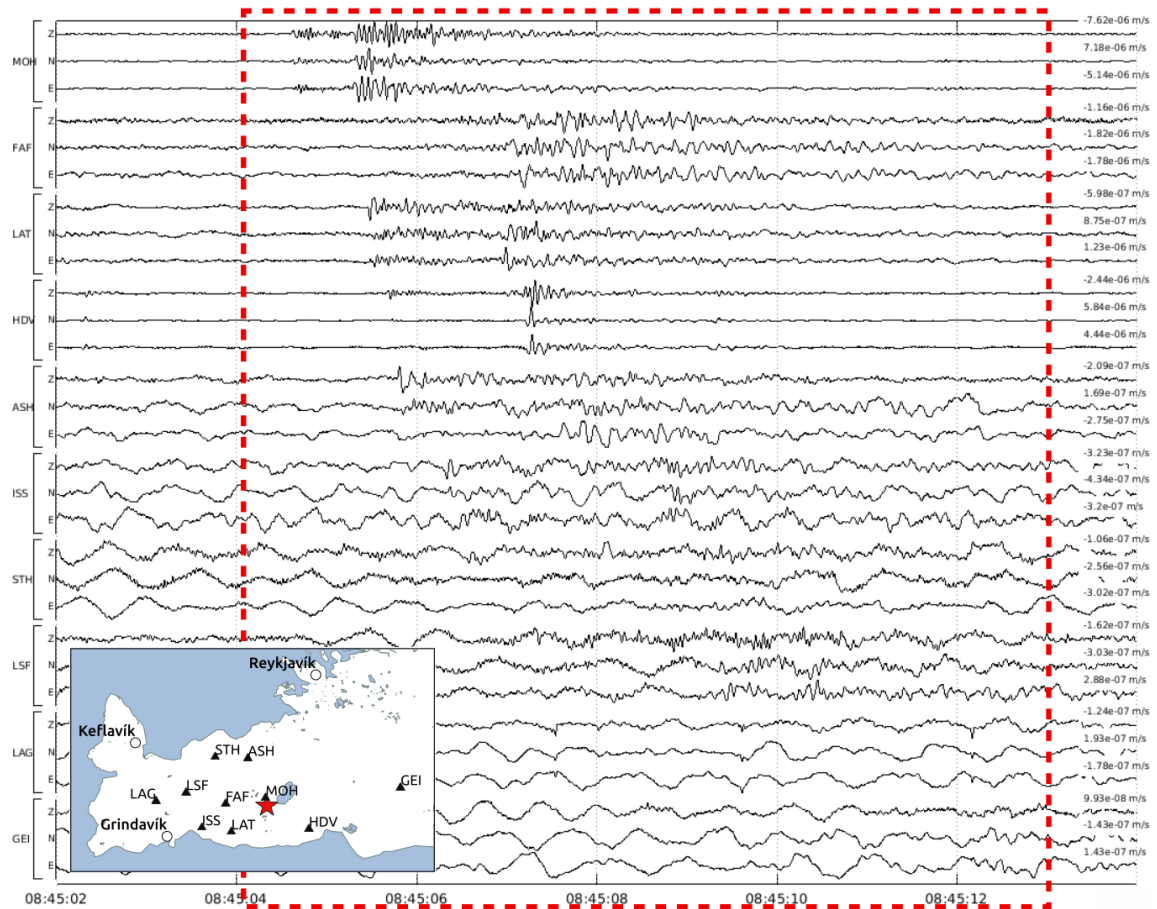
Figure 5.28: REYKJANET seismograms of one of the weakest events ($M_L = -0.6$, roughly estimated) of 2015 March 31 detected by the SLRNN with six-station coincidence. Seismograms for 10 stations are sorted by the epicentral distance and the map of stations with a rough epicentral location denoted by red asterisk is in lower-left corner. It is evident that the event is recognizable on the five nearest stations only, on the remaining stations its 'useful' signal is buried in noise. The event (its detection) is characterized by the maximum amplitude over all components of all stations in the whole detection time window (marked by dashed red line). Three component ground-motion velocity seismograms are filtered by BP of 1-40 Hz. The number above each trace gives the maximum amplitude of the ground-motion velocity in the displayed period.

tion of the trained network. The weaker point is the necessity to have very good manually prepared training data set. We showed that well-trained neural network can overcome this shortcoming and that a neural network trained on manually processed seismograms from WEBNET could be successfully applied to different local seismic network. Following the approach of the interpreters, more stations in the network must be considered. This is an algorithm we call coincidence and setting up the parameters for coincidence we can lower the detection threshold at the cost of potentially more false alarms; or lower the number of false alarms at the cost of omitting weaker events. The result of such a process is a list of time periods containing a useful signal, irrespective to the complexity of seismograms. This way all the multiple and overlapping events remain in consideration for further processing. The proposed neural network architecture (i.e., SLRNN with eight neurons) proved to be capable to detect local seismic events. Compared to automatic location algorithms based on searching for phase onsets the completeness achieved by detection is much higher. The reason is that the location algorithms must find sufficient number of correctly recognized onsets of seismic phases which is sometimes a challenging task even for trained experts. Additionally, the most effective detectors of S waves (as used among others in PePin) are based on polarization analysis, which tends to fail for weak events due to the high frequency content of the waveforms. If the number of phases found is not enough or they are incorrectly assigned, the event is usually irretrievably discarded. In case of event detection we only aim to recognize earthquake-like signals. This offers a considerable advantage for manual processing in terms there is no important event missing and the amount of data is substantially reduced. The data reduction is also improving efficiency of the automatic location algorithms.

A coincidence of six stations for both networks - WEBNET and REYKJANET - seems to be optimal. Such configuration ensures detection of all important events and low completeness magnitude still preserving the number of false detections reasonable even for manual processing (Table 5.4). For further processing of detected events we recommend to use some amplitude- or power-based criteria to sort the events. We used simply the largest amplitude in the event waveform which is obviously not an ideal criterion. On the other hand even such an easy operation gives some guidelines. A weak event can have large amplitudes (for example in case of disturbing signal on some stations), but the strong local event will never be of small amplitude. This way we can exclude unimportant or negligible events from further processing by setting a suitable amplitude threshold. Application to the REYKJANET data showed very good generalization ability of our trained neural network. Thanks to the generalization property of well-trained SLRNN we can use the same neural network for different region (Reykjanes Peninsula in SW Iceland), or in case of West Bohemia for detection of events from different epicentral zones outside the main focal zone. We expect our trained SLRNN to perform similarly when being applied to any seismic activity with the frequency content similar to that used for training. The only difference in sensitivity is given by the background noise level, so we can expect lower completeness magnitude for the WEBNET data showing generally higher signal-to-noise ratio compared to the REYKJANET data. On the other hand, the proposed

Data set	TP	FP	FN	TPR (recall)	PPV (precision)
REYKJANET (i): 2015 Mar 31, $M_L > 0$	51	165	0	1	0.236
REYKJANET (ii), $M_L > 0$	281	0	0	1	1
REYKJANET (iii), $M_L > 0$	184	120	0	1	0.605
WEBNET 6 sta, $M_L > -0.5$	179	213	4	0.978	0.457
WEBNET 4 sta, $M_L > -0.5$	183	657	0	1	0.206
WEBNET 6 sta, $M_L > 0$	43	349	0	1	0.11
WEBNET 4 sta, $M_L > 0$	43	797	0	1	0.051

Table 5.4: Precision and recall calculated for analyzed activities (only for those with manually processed events). The number of false positives (FP) is calculated with respect to a given magnitude threshold ($M_L > 0$ or $M_L > -0.5$) of reference manual events. For a lower magnitude threshold the number of FP decreases and the numbers of both TP and FN increase (compare line 4 and 6). REYKJANET (ii) activity is a piece of an intense swarm period, that is why there are no FPs and more detected events are often joined in one detection (as can be seen in Table 5.3). Denotation of data sets (i), (ii) and (iii) corresponds with that in Table 5.3. Abbreviation '6 sta' or '4 sta' denotes 6 or 4 station coincidence.

architecture could be possibly suitable for detection of regional or teleseismic events after new training and change of the input filter bank of the SLRNN.

The proposed SLRNN detector is nowadays routinely used for both networks WEBNET and REYKJANET. The WEBNET data are analyzed each day. After an event is found it is automatically imported to the database and a maximum amplitude of the waveform is saved. This amplitude helps to roughly estimate how strong the event is. During the manual processing the events with larger amplitude are analyzed first. Since the beginning of 2019 when the detector is used we have not observed a missed event of a significant magnitude.

In case of REYKJANET the detector has been used experimentally on portions of recordings containing some increased seismic activity (based on catalogs of IMO). In case of seismic swarms of Reykjanes Peninsula we observe a large number or events in short time period. This often results in multiple events in one detection period. Such a detection might not be easy for primary processing (picking of right P- and S-wave onsets of individual events), but the detection task is accomplished.

Chapter 6

Seismon_WB

Seismon_WB (Doubravová and Horálek [2013]) is a software which enables the interpreters to work with seismic data comfortably using graphical user interface (GUI). The experts in seismic-data processing and analyses do not need programming skills or heavy training to work with this user-friendly intuitive software. On the other hand anyone can develop new functions directly using MATLAB.

Seismon_WB is a modification of software Seismon created by Stefan Mertl in MATLAB (Mertl and Hausmann [2009]), in 2011 the original Seismon started to be rewritten in Python under a new name pSysmon (`http://www.mertl-research.at/projects/psysmon/`). The original program Seismon was designed as an universal tool for seismic experiments. For that purpose it consists of various tools and modules that can be adapted and developed by the users as it was provided under the GNU GPL license (the most widely used open source software license guarantee end users the freedom to run, study, share, and modify the software). The main advantage of that software is the close connection with the MySQL database. The database enables to store the results, network configuration, information about instruments used on particular stations at specific time and a list of available waveform files and the description of their contents. Well organized database is very important property of a software used for routine processing. Although Seismon offers various tools to comfortably access, list and view the database tables, these tables can be accessed separately and directly without Seismon quite comfortably by MySQL Workbench or phpMyAdmin or similar database manipulation tool. Unfortunately, Seismon did not meet all the requirements for routine processing of continual recordings from the WEBNET stations. It was therefore necessary to change many tools, often the whole behavior of the software and develop number of new modules to satisfy specific needs for the WEBNET data processing. This way I developed a new branch of Seismon differing significantly from the former one, which we started to call Seismon_WB (Seismon for the WeBnet data processing).

Seismon_WB was used experimentally from 2011 until it replaced an obsolete program Seisbase (Fischer and Hampl [1997], see Section 6.1) in 2013 and became the main processing tool for WEBNET data. Before introducing the Seismon_WB in daily routines for the WEBNET data we took care to ensure a compatibility with Seisbase and thus to preserve the consistency of the results over the years. The

behavior of Seismon_WB has been adapted to work similar to Seisbase in order to be comfortable for the interpreters used to the older program. Seisbase targeted to WEBNET data from the beginning was equipped with many useful functions that make the manual work easier and more effective. Unfortunately, Seisbase was unable to handle miniSEED file format, continuous records in general and it gradually became complicated to run this DOS-based software on new computers. I consulted the most common steps in routine work with the experienced interpreters and modified the program to be as helpful as possible for the users. That resulted in fairly comfortable software which on contrary lost some of its original universality. Seismon_WB has been used in continuous regime from September 2014.

The Fig. 6.1 shows the data flow around Seismon_WB. The program itself serves as an interface for the user that enables to access and process various data sets and to call external programs. The primary storage is MySQL database mainly accessed by Seismon_WB but it could be also fed by external programs. Most of the external programs used for data interpretation (location, moment tensor inversion etc.) are called by Seismon_WB and their results are saved to the database by Seismon_WB itself. The Archive DB block represents the export from Paradox database (formerly used by Seisbase) which can be converted to MySQL Seismon structure using specific Seismon_WB package of functions. This is one of the features that enabled the compatibility between Seismon_WB and Seisbase.
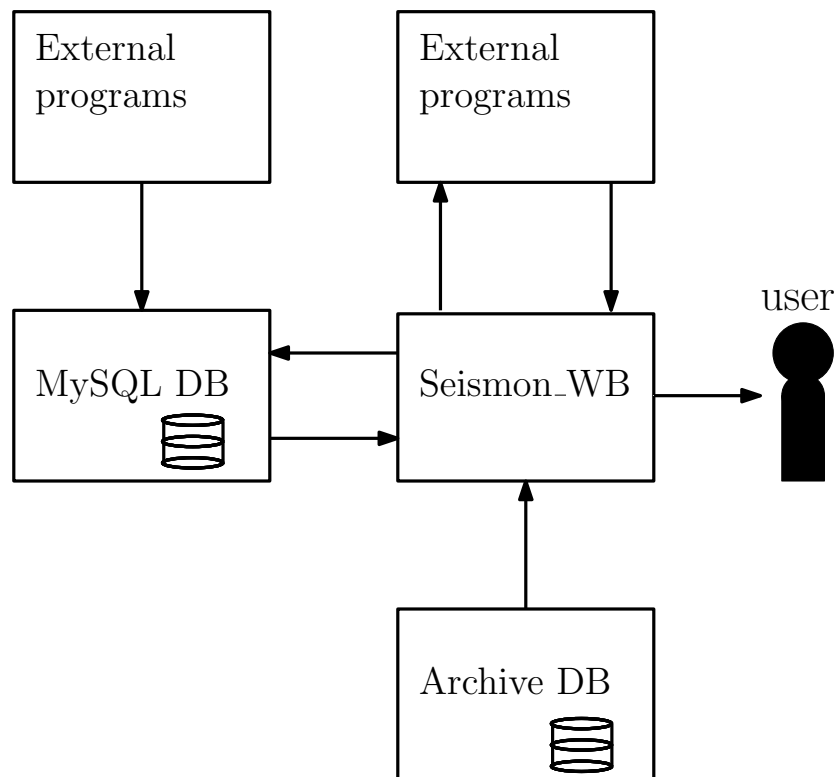
Figure 6.1: Seismon interaction scheme. The user interacts with Seismon_WB software to access the database and external programs. The archive data exported from Paradox database can be converted to MySQL database tables with Seismon_WB structure using specific packages of Seismon_WB itself.

6.1 Seisbase software and Paradox database

Seisbase program developed by T. Fischer and F. Hampl (Fischer and Hampl [1997]) during the 90's was written in Pascal and served to process triggered data from WEBNET network (in ESSTF, MARS-88 or GSE data format) until 2014. Seisbase enabled interactive work with seismograms and stored the results in Borland Paradox database. In consequence of the limitations originated in the computational power and memory capacity of personal computers that time the maximum length of seismic trace was 16 000 samples (i.e., 64 seconds of record with sampling frequency of 250 Hz). During the years it became more and more complicated to run this DOS-based software on new operating systems. The urgent need of the Seisbase replacement came with the necessity of continuous WEBNET recordings, processing of which was not possible with Seisbase. We needed to preserve all functions Seisbase offered and make all results created in Seisbase (e.g., the P- and S-phase onset picks, amplitude readings, event locations, etc.) accessible for future use in new software. The older database tables were imported into Seismon database (via Seismon_WB tool developed by J. Michálek) so the work on that data could consistently continue with the new Seismon_WB software.

6.2 MySQL Seismon database

For each Seismon project there is a separate set of database tables (this is the same for Seismon and Seismon_WB, there are some small differences in database table structures as Seismon_WB uses a few more columns). Some database tables serve as inputs for the Seismon_WB program because they store information of the seismic stations, their coordinates and instruments used, and available waveform files. Other database tables store outputs like information of event locations, magnitudes, phase picks or source parameters. Although one can export the database tables directly using some MySQL handling software, there are functions in Seismon_WB to export the information stored in the database in more suitable formats, e.g. the catalogs or bulletins that combine more database tables in one easily readable format.

6.3 External programs

External programs can interact with Seismon_WB directly or indirectly through the database. For example automatic everyday routines use database to store the results and make them accessible for the users of Seismon_WB. These are mainly (i) PePin automatic location, (ii) SLRNN event detection and (iii) import of new seismogram files.

The external programs used by Seismon_WB directly are usually those run by the Seismon_WB user upon request. That covers typically NLLoc (event location and magnitude computation Lomax et al. [2000, 2009]), AMT (amplitude-based moment tensor inversion Vavryčuk [2011]), TauP Toolkit (global travel time computation) or GoogleEarth (displaying Seismon_WB objects in satellite map).

6.4 Main program

To work with Seismon (either the original version or Seismon_WB) one needs to define at least one project which is a basic object of the program related to certain dataset, users and their specific settings. Each project is linked to its own set of database tables with information of the network configuration, location of waveform data files and various interpretation results. The projects can be made locally or on the server to be shared among users. That means that for the main routine processing of current seismic activity all the users share the same project saved on the server, but for some special studies anyone can define his own project (usually, but not necessarily, on local database). Each Seismon user has his own account linked to the database account. While working with the Seismon project, the settings remain saved for each user separately, so it enables to continue the interrupted work. In order to keep the size of database tables shorter we define separate project for each year of WEBNET and REYKJANET data.

Seismon is designed as a modular software in order to be highly flexible and effective. The task that needs to be performed is achieved by a sequence of modules, which are functional units performing particular operation (Fig. 6.2). An ordered set of modules is called a collection; typically each user defines few such collections for his/her own needs. For example the module *Select Seismon event* outputs a list of event IDs in the database matching selected criteria. That module followed by *Export bulletin* module form a collection that outputs a text file with catalog or bulletin of events. If the same module is followed by *View events in Google Earth* or *Display origins*, the collection serves to visualize the epicenters. The basic objects and philosophy of original Seismon were mostly preserved, although I developed many new modules (see Fig. 6.3) and modified the most of the existing ones.

Seismon is equipped with modules for viewing, modifying and exporting the database, working with events, data files and waveforms. Some modules are standalone, others need to be preceded or succeeded by another module, some modules are editable and by setting the parameters we define the input arguments of the module function (for example the criteria of above mentioned *Select Seismon event* like date, magnitude or depth of an event). The parameters are set by using a dialog windows.

The list of currently available modules sorted by the module categories is in Fig.6.3. The most of the modules must have been completely newly developed or substantially modified for Seismon_WB. Brief description of the modules is given in Appendix A.1. Special attention is paid to the *Trace display* module, which is the main module for interactive manual primary processing of the waveforms.

The main problems we needed to solve were among others overlapping signals or gaps in the continual seismogram files, missing channels, or different domains of the seismogram files (i.e., acceleration and velocity) which must be converted to the same domain for joint processing. To ease the routine interactive seismogram evaluation I added some automated or semi-automated functions together with keyboard shortcuts. For example, for each phase onset the amplitude reading is automatically found (it can be manually corrected although it is usually not necessary). P-wave ampli-
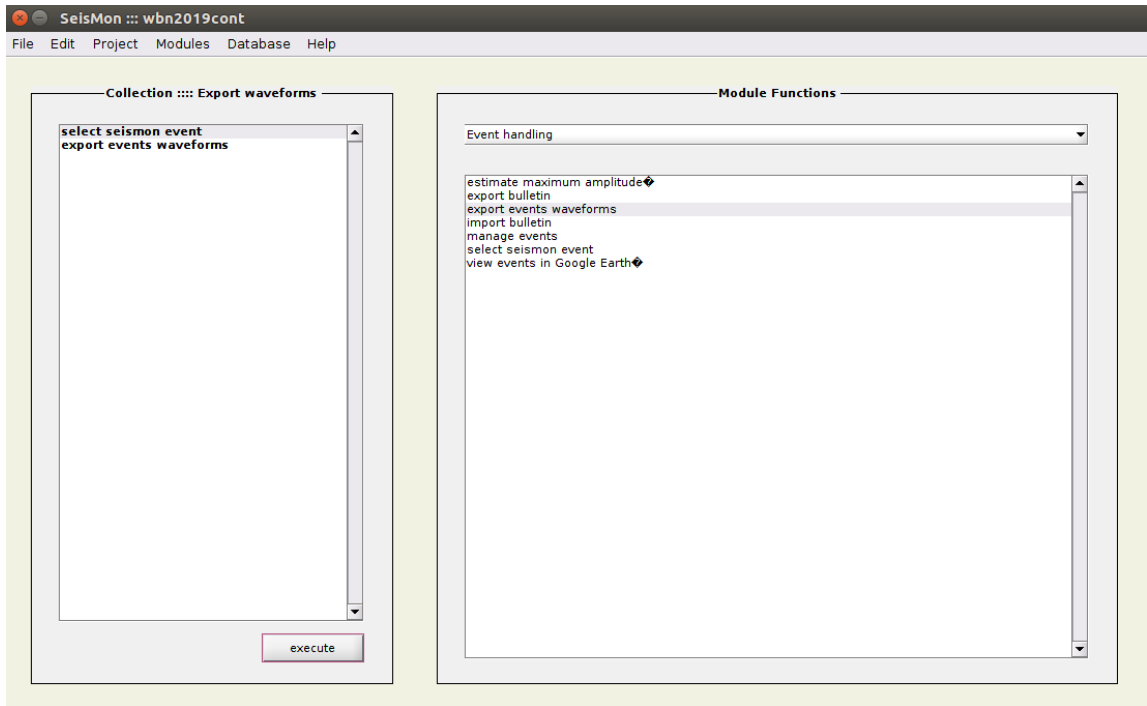
Figure 6.2: Main Seismon window. Panel on the left displays the active collection that exports parts of the seismograms as ASCII files of ground motion velocity. The subset of events to be exported is defined in dialog window of *Select Seismon event* module. The segments to be exported (which stations and channels, how long before/after P-wave onset or origin time to export) are set in *Export events waveforms* dialog window. Panel on the right side shows the list of available modules in a selected class of modules (in this case the *Event handling* functions).

DB Tools
- check the gaps *
- load from DB @
- load timespan from DB *
- show data coverage *

Display
- display origins *
- manage time segments *
- trace display @

Event handling
- estimate maximum amplitude *
- export bulletin *
- export events waveforms *
- manage events @
- select seismon events @
- view event in Google Earth @

File import
- ASCII import @
- Autodrm bulletin import @
- Convert ESSTF to GSE &
- GSE Import @
- GSE time shifts *
- Miniseed import @
- SAC import @
- Standard segy import @

Geometry
- Apply geometry @
- Edit Stations Database @
- Edit stations and Units Database *
- Edit Units Database @
- view geometry in Google Earth @

Moment tensor
- Moment tensor AMT *
- Import moment tensors *

NLLoc
- Create 1D model for NLLoc *
- Export NLLoc phase file @
- Localize events by NLLoc *
- Plot NLLoc Hypocenters *
- Run NLLoc *

Seisbase Tools
- Import station with coordinates to DB &
- Import sensor configuration to DB &
- Read Seisbase EXP tables &
- Insert Seisbase Evnets to DB &
- Scan for GSE files &

Autopick
- Automatic NLLoc picking *
- Automatic TauP picking *
- Automatic amplitude picking *

Figure 6.3: Seismon_WB modules. Modules denoted by asterisk (*) are newly developed by myself, modules with at symbol (@) are original Seismon modules (even though they have been substantially modified) and modules denoted by ampersand (&) have been developed by J. Michálek.
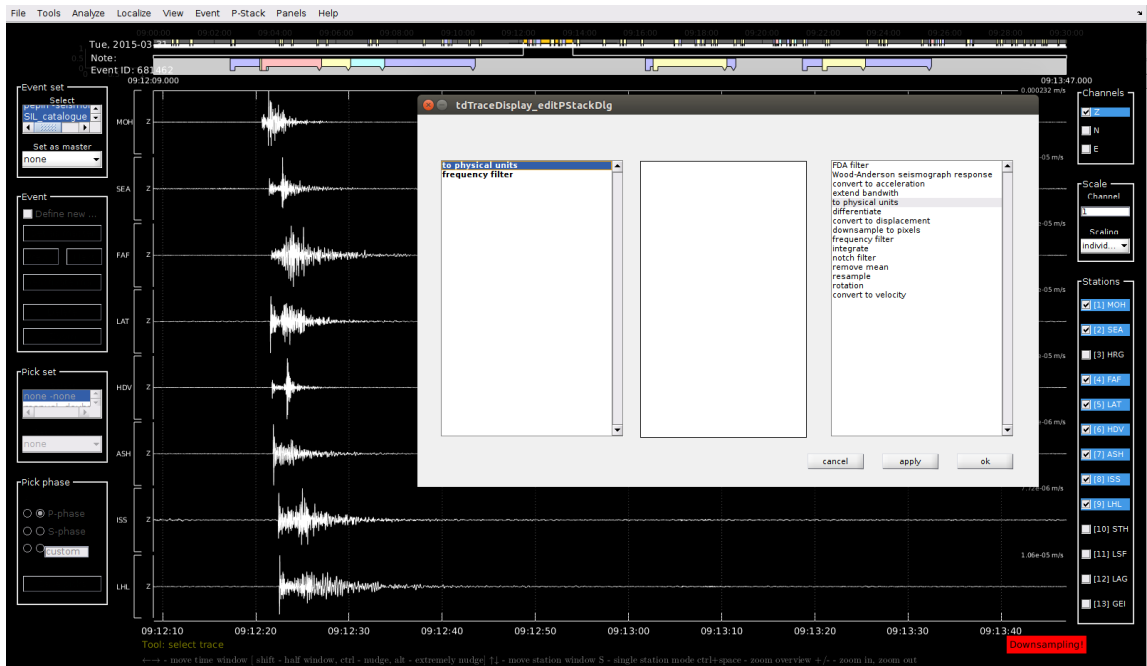
Figure 6.4: Screenshot of *Trace display* module. The *Trace display* module is the main tool for interactive manual processing of the waveforms. This example shows the use of Event sets for REYKJANET network on 31st March 2015. Each colorful patch at the top of the figure indicates a seismic event. Red color - PePin events, yellow - manual detections, light blue - SIL catalog and violet - events detected by SLRNN. The strongest event at the beginning is of local magnitude $M_L = 1.2$. The dialog window demonstrates the use of processing nodes. Right panel shows available processing nodes, left panel shows actual processing stack of processing nodes, in this case: first conversion from counts to meters per second, and second bandpass filter 1-40 Hz. Note that vertical channel of a few selected stations is displayed.

tude is found as the first local extreme after the onset in the ground-displacement waveforms, also the first motion direction is automatically assigned. The maximum S-wave amplitude, which is used for calculation of local magnitude M_L, is the global extreme of total vector of ground-velocity in a default 80 ms window after the onset, but the window length can be user-defined.

We also put strong emphasis on a precision of manual processing by adding a functionality of shifting picks, cursors or time window limits by one sample using keyboard, which is mainly useful when very precise P- and S-wave onset picks are needed (e.g., for the best possible location of a prominent event).

Seismon_WB enables to store and operate several "event sets" and "pick sets". Event set is a group of Seismon events - time defined segments of records. Each event is assigned to a class (typically local, regional or teleseismic event but also any type of recorded signal which is remarkable, e.g. records of quarry blasts). The same time segment of seismogram (usually a waveform) can be labeled as an event related to different event sets. Typically each method of event detection has its own event set. The pick set is a group of Seismon picks. The Seismon pick can be generally any time mark selected on the seismogram with assigned phase name and amplitude. Typically we use picks for P-wave onset, S-wave onset, P-wave amplitude and S-wave amplitude (each of the four types of pick is an object with name, time and amplitude but the amplitudes of onset picks are irrelevant and time of amplitude picks serve only to display which amplitude is considered). The picks of the same phase name for an event must be unique within a pick set. Similarly to event sets, different pick sets enable to distinguish the method which produced individual picks and therefore there can co-exist different picks for one event with the same phase name in different pick sets. That means the work can be done in several automatic and manual regimes simultaneously. For example, in practice the events generated automatically by the SLRNN algorithm are immediately copied to 'manual event set' designated for manual interpretation and also to 'automatic event set'. The automatic events in the 'manual event set' are then verified, corrected or approved by users while the same events in 'automatic event set' remain unchanged for potential later check of automatic detection results. This feature enables to check the automatic routines on the run and diagnose the cases when it fails.

In fact the automatic processing as a part of Seismon_WB itself or as an external program can be used at any stage of the processing and the visual inspection of automatic procedures can be comfortably supervised using Seismon_WB.

The program is written in MATLAB which offers advantages of well documented toolboxes and functions easy to use, on the other hand the commercial software limits the spreading of the code freely on any PC of user's choice. Therefore, I used Matlab Compiler toolbox and created standalone version of Seismon_WB, that can be run without MATLAB license, just using the MCR (Matlab Compiler Runtime) which is distributed freely. Additionally, the user of deployed application cannot change the code which prevents some unintended editing.

Seismon_WB can be generally used on Windows, Linux and MAC platforms, however only Windows and Linux versions have been tested. The main workaround in compatibility meant to implement platform related file paths and operating system

commands to run the external programs. The executable version of Seismon_WB must be compiled using the target platform (i.e., Window or Linux and 32-bit or 64-bit version).

The development of the Seismon_WB software is still continuing even though the evolution is much slower now. Besides adapting to new requirements of the users for new or improved functionality, the compatibility with up-to-date version of MATLAB is consistently maintained.

Chapter 7

Conclusion

Dense local seismic networks WEBNET and REYKJANET contribute to detailed studies of the seismic swarms dynamics, earthquake source and local structure of the Earth's crust. The detailed and systematic processing of large amount of data is an essential prerequisite for that. As the seismic stations advanced from triggered to continual recording, the manual processing became problematic because the qualified human work requirement increased dramatically. Without the automatic and semi-automatic processing of the seismic networks WEBNET and REYKJANET it would be impracticable to process the measured data in a full extent. My thesis consists of two parts: (i) Seismon_WB - a software for interactive data processing that enables also to control automatic and semi-automatic processing; and (ii) SLRNN detector of seismic events which is the fundamental step in automatic seismic data processing. The design, training, detailed testing and implementation of the SLRNN form a core part of this doctoral thesis and is described in detail in two attached papers.

(i) First, I needed to concern the comfortable way to manually process the seismic data. Especially the WEBNET data needed to be consistently processed following the works performed in Seisbase. I contributed extensively to a development of new software used by the WEBNET working group by modifying, extending and debugging an existing Seismon project. As a result Seismon_WB is an exclusive processing tool for all the routines applied to WEBNET (and REYKJANET) data since 2013. Not only classical manual processing is achieved by Seismon_WB but also an evaluation and check of automatic procedures applied. Nevertheless, the tuning and development of the software still continues. Although the software development is strictly practical result with very low direct scientific impact, it is an essential prerequisite for high quality processing of seismic data provided by the WEBNET group.

(ii) Next, the detection algorithm has been developed and tested. We designed a new artificial neural network concept and successfully applied it not only to WEBNET data used for training the neural network but also to data from REYKJANET network. The trained SLRNN is nowadays routinely used to detect events in recordings of local seismic networks WEBNET and REYKJANET.

The main results and lessons learned from the SLRNN may be summed up as follows:

- The SLRNN architecture is suitable for seismic event detection and eight neurons proved to be sufficient. The higher number of neurons does not improve the performance significantly as the training demands rise considerably. The detection performance is enhanced by coincidence in the network.

- The training data must be prepared with special care, missing P- and S-wave onset picks (especially if both are missing) complicate the proper training giving bad examples during the training. Even rough picks of noisy events helped the training significantly.

- The training using gradient-based methods requires many trials to repeat to find the optimum result. To evaluate the real detector performance, the sensitivity, specificity, precision and recall quantities must be used. To check the detection results properly a manual work is needed, because many of the SLRNN detections are low-magnitude events which are often missing in available catalogs.

- It is impossible to achieve good results with low completeness magnitude using one station detection. For fine result a coincidence in the network of seismic stations must be used. Six stations coincidence is a reasonable choice for both WEBNET and REYKJANET local seismic networks.

- Well-trained network can be successfully used for different region and a partly different waveforms. This is the generalization property of a neural network and the successful applicability of the detector trained on WEBNET data to REYKJANET data is an exemplary utilization of that.

In the near future there is a potential to use our neural network to pre-process data of the NEFOBS (Near Fault Observatory) deployed in the West Bohemia/Vogtland region consisting of four broad-band seismometers placed in shallow boreholes ($\approx$ 400 m deep) drilled within ICDP project *Drilling the Eger Rift* (more on `https://www.icdp-online.org/projects/world/europe/eger/` or Dahm et al. [2013]) supplemented with 3-D seismic arrays. The expected significantly larger amount of high-frequency micro-events (with local magnitudes as low as $M_L \approx -2$) might be successfully detected by our SLRNN.

The event detection is a starting point in the data processing chain for both automatic and manual processing. It's quality affects the whole processing results. I believe, I proved that the presented method provides high quality detections suitable for effective post-processing and thus high-quality investigation of the seismicity of the West Bohemia/Vogtland as well as South-West Iceland and potentially any other seismically active region.

Bibliography

T. Ahern, R. Casey, D. Barnes, Benson R., T. Knight, and C. Trabant. *SEED Reference Manual, version 2.4*. Incorporated Research Institutions for Seismology, 2009. URL `http://www.fdsn.org/seed_manual/SEEDManual_V2.4.pdf`.

H. Čermáková and J. Horálek. The 2011 West Bohemia (Central Europe) earthquake swarm compared with the previous swarms of 2000 and 2008. *Journal of Seismology*, pages 1–15, 2015. ISSN 1383-4649. doi: 10.1007/s10950-015-9502-3. URL `http://dx.doi.org/10.1007/s10950-015-9502-3`.

T. Dahm, P. Hrubcová, T. Fischer, J. Horálek, M. Korn, S. Buske, and D. Wagner. Eger rift ICDP: an observatory for study of non-volcanic, mid-crustal earthquake swarms and accompanying phenomena. *Scientific Drilling*, 16:93–99, 2013. doi: 10.5194/sd-16-93-2013. URL `https://www.sci-dril.net/16/93/2013/`.

H. Dai and C. MacBeth. The application of back-propagation neural network to automatic picking seismic arrivals from single-component recordings. *Journal of Geophysical Research: Solid Earth*, 102(B7):15105–15113, 1997. doi: 10.1029/97JB00625. URL `https://agupubs.onlinelibrary.wiley.com/doi/abs/10.1029/97JB00625`.

L. Dietz. Notes on configuring BINDER_EW: Earthworm's phase associator, 2002. URL `http://www.isti2.com/ew/ovr/binder{_}setup.html`.

J. Doubravová and J. Horálek. New interactive software for seismic data processing. In *Technical Computing Prague 2013 21st Annual Conference Proceedings*, 2013.

J. Doubravová, J. Wiszniowski, and J. Horálek. Single layer recurrent neural network for detection of swarm-like earthquakes in W-Bohemia/Vogtland - the method. *Computers & Geosciences*, 93:138 – 149, 2016. ISSN 0098-3004. doi: https://doi.org/10.1016/j.cageo.2016.05.011. URL `http://www.sciencedirect.com/science/article/pii/S0098300416301327`.

J. Doubravová and J. Horálek. Single Layer Recurrent Neural Network for detection of local swarm-like earthquakes—the application. *Geophysical Journal International*, 219(1):672–689, 07 2019. ISSN 0956-540X. doi: 10.1093/gji/ggz321. URL `https://doi.org/10.1093/gji/ggz321`.

F. U. Dowla, S. R. Taylor, and R. W. Anderson. Seismic discrimination with artificial neural networks: preliminary results with regional spectral data. *Bulletin of the Seismological Society of America*, 80(5):1346–1373, 1990.

P. Einarsson. *Encyclopedia of Earthquake Engineering*, chapter Plate boundaries, rifts and transforms in Iceland. Springer-Verlag Berlin Heidelberg 2021, 2008. doi: 10.1007-978-3-642-36197-5{_}298-1.

P. Einarsson. *Encyclopedia of Earthquake Engineering*, chapter Mechanisms of Earthquakes in Iceland. Springer-Verlag Berlin Heidelberg 2021, 2014. doi: 10.1007-978-3-642-36197-5{_}298-1.

J. L. Elman. Finding structure in time. *Cognitive Science*, 14(2):179–211, 1990. ISSN 1551-6709. doi: 10.1207/s15516709cog1402{_}1. URL `http://dx.doi.org/10.1207/s15516709cog1402{_}1`.

A. M. Esposito, F. Giudicepietro, S. Scarpetta, L. D'Auria, M. Marinaro, and M. Martini. Automatic discrimination among landslide, explosion-quake, and microtremor seismic signals at Stromboli volcano using neural networks. *Bulletin of the Seismological Society of America*, 96(4A):1230–1240, 2006.

T. Fischer. Automatic location of swarm earthquakes from local network data. *Studia Geophysica et Geodaetica*, 47(1):83–98, 2003. ISSN 0039-3169. doi: 10.1023/A: 1022251605990. URL `http://dx.doi.org/10.1023/A%3A1022251605990`.

T. Fischer and F. Hampl. SEISBASE - Principles of a Program and Database for Routine Analysis of Data from Local Seismic Networks, Version 4.7. *Acta Montana*, Ser. A(11):15–34, 1997.

T. Fischer, J. Horálek, J. Michálek, and A. Boušková. The 2008 West Bohemia earthquake swarm in the light of the WEBNET network. *Journal of Seismology*, 14(4):665–682, 2010a. ISSN 1383-4649. doi: 10.1007/s10950-010-9189-4. URL `http://dx.doi.org/10.1007/s10950-010-9189-4`.

T. Fischer, J. Horálek, J. Michálek, and A. Boušková. The 2008 West Bohemia earthquake swarm in the light of the WEBNET network. *Journal of Seismology*, 14(4):665–682, Oct 2010b. ISSN 1573-157X. doi: 10.1007/s10950-010-9189-4. URL `https://doi.org/10.1007/s10950-010-9189-4`.

T. Fischer, J. Horálek, P. Hrubcová, V. Vavryčuk, K. Bräuer, and H. Kämpf. Intra-continental earthquake swarms in West-Bohemia and Vogtland: A review. *Tectonophysics*, 611:1 – 27, 2014. ISSN 0040-1951. doi: https://doi.org/10.1016/j.tecto.2013.11.001. URL `http://www.sciencedirect.com/science/article/pii/S0040195113006458`.

T. Fischer, C. Matyska, and J. Heinicke. Earthquake-enhanced permeability - evidence from carbon dioxide release following the M_L 3.5 earthquake in West Bohemia. *Earth and Planetary Science Letters*, 460:60–67, 2017.

H. Geirsson, T. Árnadóttir, S. Hreinsdóttir, J. Decriem, P.C. LaFemina, S. Jónsson, R.A. Bennett, S. Metzger, A. Holland, E. Sturkell, T. Villemin, C. Völksen, F. Sigmundsson, P. Einarsson, M.J. Roberts, and H. Sveinbjörnsson. Overview of results from continuous GPS observations in Iceland from 1995 to 2010. *Jökul*, 60: 3–22, 2010.

S. Gentili and A. Michelini. Automatic picking of P and S phases using a neural tree. *Journal of Seismology*, 10(1):39–63, 2006. ISSN 1383-4649. doi: 10.1007/ s10950-006-2296-6. URL http://dx.doi.org/10.1007/s10950-006-2296-6.

V. Gravirov, K. Kislov, and T. Ovchinnikova. Neural network method for identification of earthquake phases in increased noise level conditions. In *EGU General Assembly Conference Abstracts*, volume 12, page 2434, 2010.

G. E. Hinton. Connectionist learning procedures. *Artificial Intelligence*, 40:185 – 234, 1989. doi: http://dx.doi.org/10.1016/0004-3702(89)90049-0. URL http: //www.sciencedirect.com/science/article/pii/0004370289900490.

J. Horálek. Reykjanet, 2013. URL http://www.fdsn.org/networks/detail/7E_ 2013/.

J. Horálek and T. Fischer. Role of crustal fluids in triggering the West Bohemia/Vogtland earthquake swarms: Just what we know (a review). *Studia Geophysica et Geodaetica*, 52(4):455, Feb 2008. ISSN 1573-1626. doi: 10.1007/ s11200-008-0032-0. URL https://doi.org/10.1007/s11200-008-0032-0.

J. Horálek and T. Fischer. Intraplate earthquake swarms in West Bohemia/Vogtland (Central Europe). *Jokull*, 60:67–88, 2010.

J. Horálek and J. Šílený. Source mechanisms of the 2000 earthquake swarm in the West Bohemia/Vogtland region (Central Europe). *Geophysical Journal International*, 194(2):979–999, 05 2013. ISSN 0956-540X. doi: 10.1093/gji/ggt138. URL https://doi.org/10.1093/gji/ggt138.

J. Horálek, T. Fischer, A. Boušková, and P. Jedlička. The Western Bohemia/Vogtland region in the light of the WEBNET network. *Studia Geophysica Et Geodaetica*, 44(2):107–125, 2000a.

J. Horálek, J. Šílený, T. Fischer, A. Slancová, and A. Boušková. Scenario of the January 1997 West Bohemia earthquake swarm. *Studia Geophysica et Geodaetica*, 44(4):491–521, Oct 2000b. ISSN 1573-1626. doi: 10.1023/A:1021811600752. URL https://doi.org/10.1023/A:1021811600752.

A S C R Institute of Geophysics. West Bohemia local seismic network, 1991. URL http://www.fdsn.org/networks/detail/WB/.

S. Jakobsdóttir. Seismicity in Iceland: 1994-2007. *Jökull*, 58:75–100, 2008.

S. Jakobsdóttir, G. B. Guðmundsson, and R. Stefánsson. Seismicity in Iceland 1991-2000 monitored by the SIL seismic system. *Jökull*, 51:87–94, 2002.

H. Jakoubková. *Earthquake swarms in diverse tectonic environments.* PhD thesis, Charles University in Prague, 2018.

H. Jakoubková, J. Horálek, and T. Fischer. 2014 mainshock-aftershock activity versus earthquake swarms in West Bohemia, Czech Republic. *Pure and Applied Geophysics*, 175(1):109–131, Jan 2018. ISSN 1420-9136. doi: 10.1007/s00024-017-1679-7. URL https://doi.org/10.1007/s00024-017-1679-7.

M. I. Jordan. Attractor dynamics and parallelism in a connectionist sequential machine. *In: Proceedings of the Eighth Annual Conference of the Cognitive Science Society*, (Elbraum, Hillsdale, NJ):531–546, 1986.

H. Kao and S. Shan. The source-scanning algorithm: mapping the distribution of seismic sources in time and space. *Geophysical Journal International*, 157 (2):589–594, 2004. doi: 10.1111/j.1365-246X.2004.02276.x. URL http://gji.oxfordjournals.org/content/157/2/589.abstract.

H. S. Kuyuk, E. Yildirim, E. Dogan, and G. Horasan. An unsupervised learning algorithm: application to the discrimination of seismic events and quarry blasts in the vicinity of Istanbul. *Natural Hazards and Earth System Sciences*, 11(1): 93–100, 2011.

R. Le Bras, H. Swanger, T. Sereno, G. Beall, and R. Jenkins. Global association. design document and user's manual. Technical report, DTIC Document, 1994.

A. Lomax, J. Virieux, P. Volant, and C. Berge-Thierry. *Probabilistic Earthquake Location in 3D and Layered Models*, pages 101–134. Springer Netherlands, Dordrecht, 2000. ISBN 978-94-015-9536-0. doi: 10.1007/978-94-015-9536-0_5. URL https://doi.org/10.1007/978-94-015-9536-0_5.

A. Lomax, A. Michelini, and A. Curtis. *Earthquake Location, Direct, Global-Search Methods*, pages 2449–2473. Springer New York, New York, NY, 2009. ISBN 978-0-387-30440-3. doi: 10.1007/978-0-387-30440-3_150. URL https://doi.org/10.1007/978-0-387-30440-3_150.

G. Madureira and A. E. Ruano. A neural network seismic detector. *Acta Technica Jaurinensis*, 2(2):159–170, 2009.

S. Mertl and H. Hausmann. Seismon-a flexible seismic processing software. In *EGU General Assembly Conference Abstracts*, volume 11, page 4266, 2009.

J. Michálek and T. Fischer. Source parameters of the swarm earthquakes in West Bohemia/Vogtland. *Geophysical Journal International*, 195(2):1196–1210, 2013. doi: 10.1093/gji/ggt286. URL http://gji.oxfordjournals.org/content/195/2/1196.abstract.

A. Morales-Esteban, F. Martínez-Álvarez, and J. Reyes. Earthquake prediction in seismogenic areas of the Iberian peninsula based on computational intelligence. *Tectonophysics*, 593:121 – 134, 2013. ISSN 0040-1951. doi: https://doi.org/10.1016/j.tecto.2013.02.036. URL http://www.sciencedirect.com/science/article/pii/S0040195113001467.

S. M. Mousavi, S. P. Horton, C. A. Langston, and B. Samei. Seismic features and automatic discrimination of deep and shallow induced-microearthquakes using neural network and logistic regression. *Geophysical Journal International*, 207 (1):29–46, 07 2016. ISSN 0956-540X. doi: 10.1093/gji/ggw258. URL https://doi.org/10.1093/gji/ggw258.

S. M. Mousavi, W. Zhu, Y. Sheng, and G. C. Beroza. CRED: A deep residual network of convolutional and recurrent units for earthquake signal detection, 2018.

K.S. Narendra and K. Parthasarathy. Gradient methods for the optimization of dynamical systems containing neural networks. *Neural Networks, IEEE Transactions on*, 2(2):252–262, Mar 1991. ISSN 1045-9227. doi: 10.1109/72.80336.

A. Panskkat and H. Adeli. Neural network models for earthquake magnitude prediction using multiple seismicity indicators. *International Journal of Neural Systems*, 17(01):13–33, 2007. doi: 10.1142/S0129065707000890. URL https://doi.org/10.1142/S0129065707000890. PMID: 17393560.

J. Reyes, A. Morales-Esteban, and F. Martínez-Álvarez. Neural networks to predict earthquakes in Chile. *Applied Soft Computing*, 13(2):1314 – 1328, 2013. ISSN 1568-4946. doi: https://doi.org/10.1016/j.asoc.2012.10.014. URL http://www.sciencedirect.com/science/article/pii/S1568494612004656.

A. T. Ringler and J. R. Evans. A Quick SEED Tutorial. *Seismological Research Letters*, 86(6):1717–1725, 09 2015. ISSN 0895-0695. doi: 10.1785/0220150043. URL https://doi.org/10.1785/0220150043.

G. Romeo. Seismic signals detection and classification using artiricial neural networks. *Annals of Geophysics*, 37(3), 1994.

Z. E. Ross, M. Meier, E. Hauksson, and T. H. Heaton. Generalized seismic phase detection with deep learning. *Bulletin of the Seismological Society of America*, 108 (5A):2894–2901, 2018.

K. Sæmundsson and P. Einarsson. Notes on the tectonics of Reykjanes. report no. ísor-2013/003, 2014.

R. Sleeman and T. van Eck. Robust automatic P-phase picking: an on-line implementation in the analysis of broadband seismogram recordings. *Physics of the Earth and Planetary Interiors*, 113(1–4):265–275, 1999. ISSN 0031-9201. doi: http://dx.doi.org/10.1016/S0031-9201(99)00007-2. URL http://www.sciencedirect.com/science/article/pii/S0031920199000072.

J. A. Swets. *Signal detection theory and ROC analysis in psychology and diagnostics: collected papers.* Scientific psychology series. Lawrence Erlbaum Associates, 1996. ISBN 9780805818345. URL `https://books.google.cz/books?id=1vkMAQAAMAAJ`.

T. Tiira. Discrimination of nuclear explosions and earthquakes from teleseismic distances with a local network of short period seismic stations using artificial neural networks. *Physics of the earth and planetary interiors*, 97(1-4):247–268, 1996.

T. Tiira. Detecting teleseismic events using artificial neural networks. *Computers I& Geosciences*, 25(8):929 – 938, 1999. ISSN 0098-3004. doi: http://dx.doi.org/10.1016/S0098-3004(99)00056-4. URL `http://www.sciencedirect.com/science/article/pii/S0098300499000564`.

V. Vavryčuk. Principal earthquakes: Theory and observations from the 2008 West Bohemia swarm. *Earth and Planetary Science Letters*, 305(3):290 – 296, 2011. ISSN 0012-821X. doi: https://doi.org/10.1016/j.epsl.2011.03.002. URL `http://www.sciencedirect.com/science/article/pii/S0012821X11001373`.

J. Wang and T. Teng. Artificial neural network-based seismic detector. *Bulletin of the Seismological Society of America*, 85(1):308–319, 1995. URL `http://www.bssaonline.org/content/85/1/308.abstract`.

J. Wang and T. Teng. Identification and picking of S phase using an artificial neural network. *Bulletin of the Seismological Society of America*, 87(5):1140–1149, 1997. URL `http://www.bssaonline.org/content/87/5/1140.abstract`.

P. J. Werbos. Backpropagation through time: what it does and how to do it. *Proceedings of the IEEE*, 78(10):1550–1560, Oct 1990. ISSN 0018-9219. doi: 10.1109/5.58337.

R. J. Williams and D. Zipser. A learning algorithm for continually running fully recurrent neural networks. *Neural Comput.*, 1(2):270–280, June 1989. ISSN 0899-7667. doi: 10.1162/neco.1989.1.2.270. URL `http://dx.doi.org/10.1162/neco.1989.1.2.270`.

J. Wiszniowski, B.M. Plesiewicz, and J. Trojanowski. Application of Real Time Recurrent Neural Network for Detection of Small Natural Earthquakes in Poland. *Acta Geophys.*, 62(3):469–485, 2014.

M. Withers, R. Aster, C. Young, J. Beiriger, M. Harris, S. Moore, and J. Trujillo. A comparison of select trigger algorithms for automated global seismic phase and event detection. *Bulletin of the Seismological Society of America*, 88(1):95–106, 1998. URL `http://www.bssaonline.org/content/88/1/95.abstract`.

M. Withers, R. Aster, and C. Young. An automated local and regional seismic event detection and location system using waveform correlation. *Bulletin of the Seismological Society of America*, 89(3):657–669, 1999. URL `http://www.bssaonline.org/content/89/3/657.abstract`.

M. H. Zweig and G. Campbell. Receiver-operating characteristic (ROC) plots: a fundamental evaluation tool in clinical medicine. *Clinical chemistry*, 39(4):561–577, 1993.

List of Figures

84

List of Tables

List of Abbreviations

ANN Artificial Neural Networks

BP Band Pass

BPTT Back Propagation Through Time

CAS Czech Academy of Sciences

CF Compact Flash

FFT Fast Fourier Transform

FN False Negative

FP False Positive

GPL General Public License

GPS Global Positioning System

GUI Graphical User Interface

ID IDentificator, here: a unique number in the database

IG Institute of Geophysics

IMO Icelandic Meteorological Office

IRIS Incorporated Research Institutions for Seismology

IRSM Institute of Rock Structure and Mechanics

LIWE Learning Importance Weight of Events

LTA Long Time Average

MCR Matlab Compiler Runtime

MLP Multi-Layer-Perceptron

MRTG Multi Router Traffic Grapher

NARX Nonlinear Autoregressive Neural Network

PCA Principal Component Analysis

ROC Receiver Operating Characteristic

RTRN Real Time Recurrent Network

SD Secure Digital

SEED Standard for Exchange of Earthquake Data

SLRNN Single Layer Recurrent Neural Network

SNR Signal-to-Noise Ratio

SOH State of Health

SSH Secure SHell

STA Short Time Average

TCP/IP Transmission Control Protocol/Internet Protocol

TN True Negative

TNR True Negative Rate

TP True Positive

TPR True Positive Rate

UHF Ultra High Frequency

List of publications

Doubravová et al., 2016: J. Doubravová, J. Wiszniowski, and J. Horálek. Single layer recurrent neural network for detection of swarm-like earthquakes in W-Bohemia/Vogtland - the method. *Computers & Geosciences*, 93:138 – 149, 2016. ISSN 0098-3004. doi: https://doi.org/10.1016/j.cageo.2016.05.011. URL `https://www.sciencedirect.com/science/article/pii/S0098300416301327`

Doubravová and Horálek, 2019: J. Doubravová and J. Horálek. Single Layer Recurrent Neural Network for detection of local swarm-like earthquakes—the application. *Geophysical Journal International*, 219(1):672–689, 07 2019. ISSN 0956-540X. doi: 10.1093/gji/ggz321. URL `https://doi.org/10.1093/gji/ggz321`

Appendix A

Attachments

A.1 Seismon_WB modules

A.1.1 DB Tools

Set of functions to import or interpret database tables related to record files. These modules serve for data selection or data consistency check.

Load from DB A module that selects list of appropriate files from the database for selected timespan, stations and channels. The available and selected data are visualized (Fig.A.1). The module's output serves as an input for other modules like *Trace display.*

Load timespan from DB Similar to *Load from DB* module, but only time beginning and time end is defined. The module then loads the list of all the available waveforms. It is faster than *Load from DB* module because no visual interpretation of available data is present.

Check the gaps This module is standalone without inputs from previous modules and outputs to succeeding modules. Editable parameters are start and end time of the analyzed data. The module then scans the database table of seismogram files and comparing the beginning and end times of records for individual stations lists the gaps larger than a specified value into a text file.

Show data coverage Similar to *Check the gaps* but the module represents the available data in a graphical form (Fig.A.2). It serves to overview longer data segment and does not consider all channels, only vertical ones are used. First, it was designed to check all channels of the stations, but for a quicker result it was simplified to check the presence of the vertical component only.
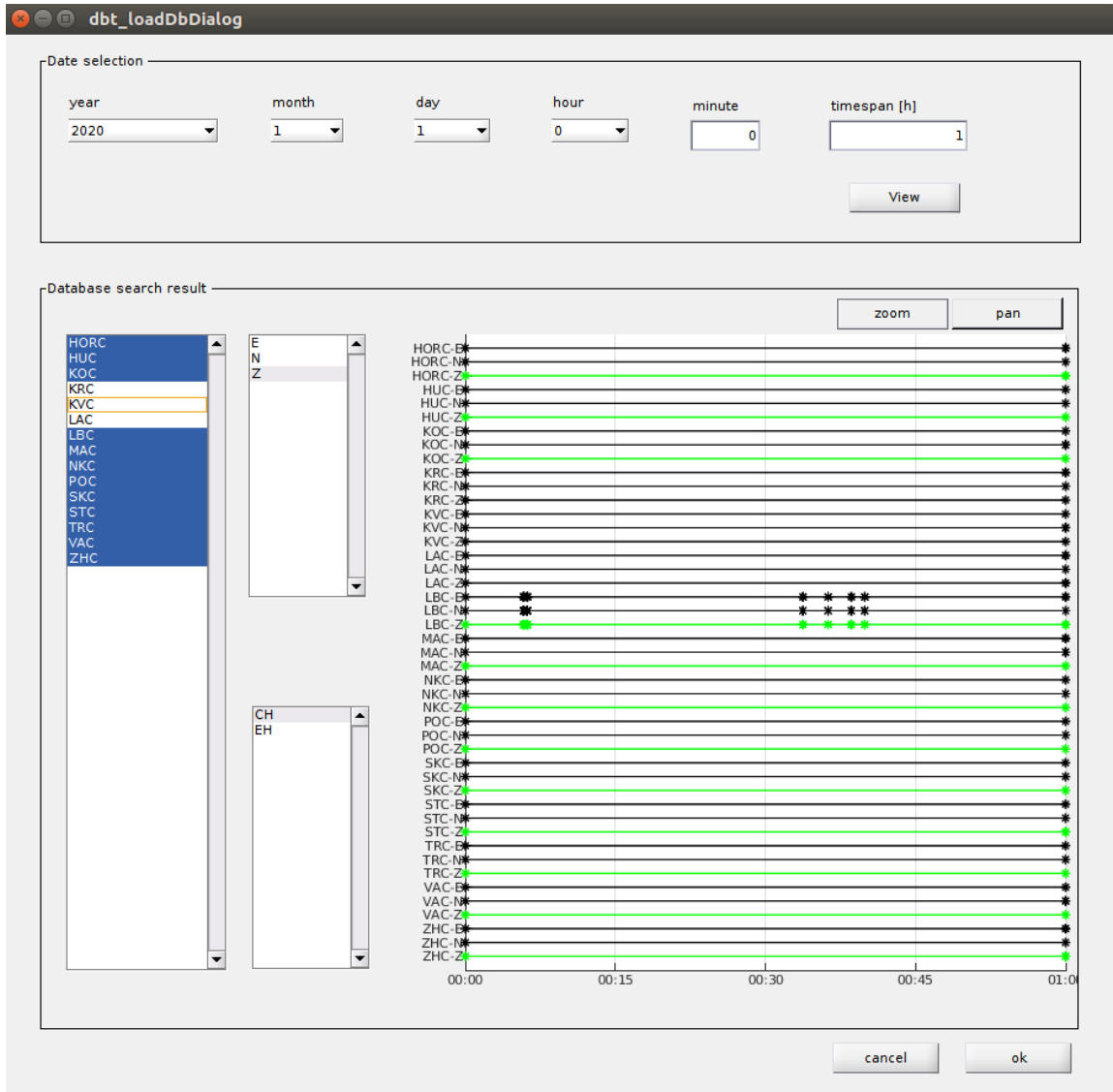
Figure A.1: Load from DB dialog window for setting the selection. The available recordings are depicted by black vertical lines, currently selected data are represented by green color.
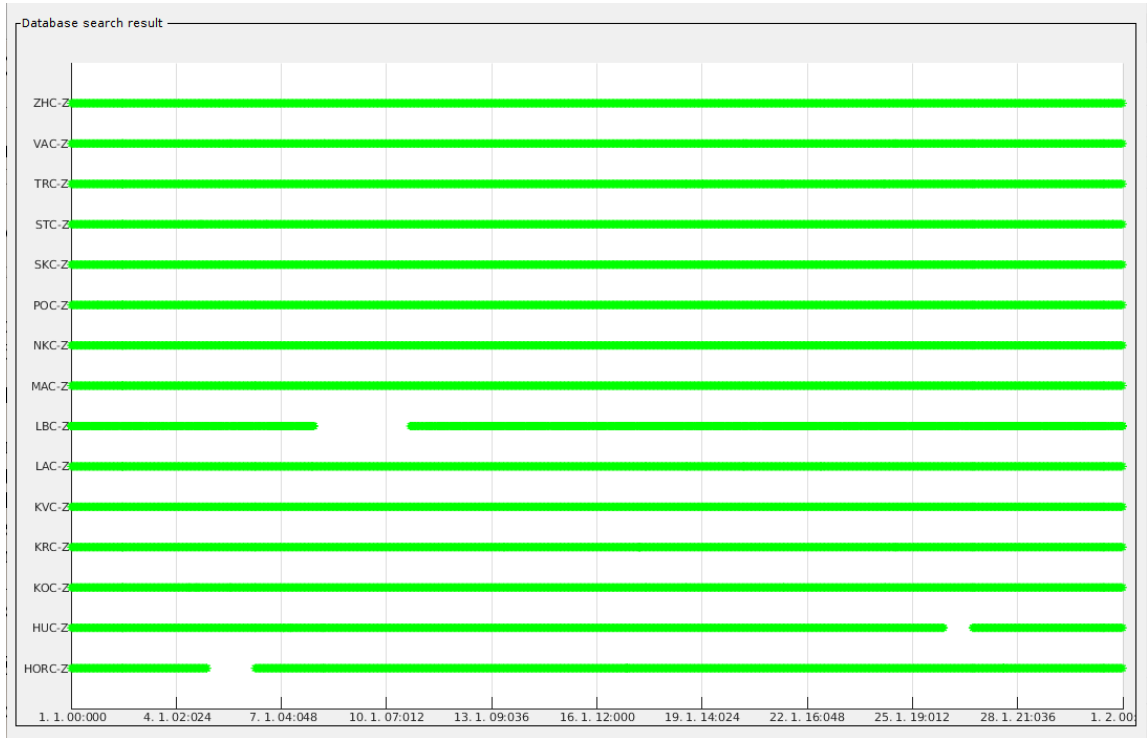
Figure A.2: Show data coverage example

A.1.2 Display

Functions used for visualizing the recorded data and epicenters. The most important is *Trace display* module which is the main tool for manual inspection of seismic records.

Display origins This module displays the map view of epicenters. It must be preceded by event selection and the type of location must be specified, because each event can have more locations by different methods. When the map is displayed the user can select a group of events by click-and-drag and the selection or inverse selection is then saved to a text file. The text file with the list of event IDs can be then used as an input to *Select Seismon event* module.

Manage time segments Module preceded by selection of waveforms (like *Load from DB*) that prepares shorter segments of equal length with defined overlap to go quickly through continuous data (usually when there is no event detection or catalog available). Each segment then defines inputs for *Trace display*, that is then called by context menu.

Trace display The main module for interactive manual work is called *Trace display*. This module enables to visualize waveforms and under a control of an interpreter to define events, pick phase arrivals, locate and estimate source parameters. For this purpose is *Trace display* equipped with tools and processing nodes. Tools
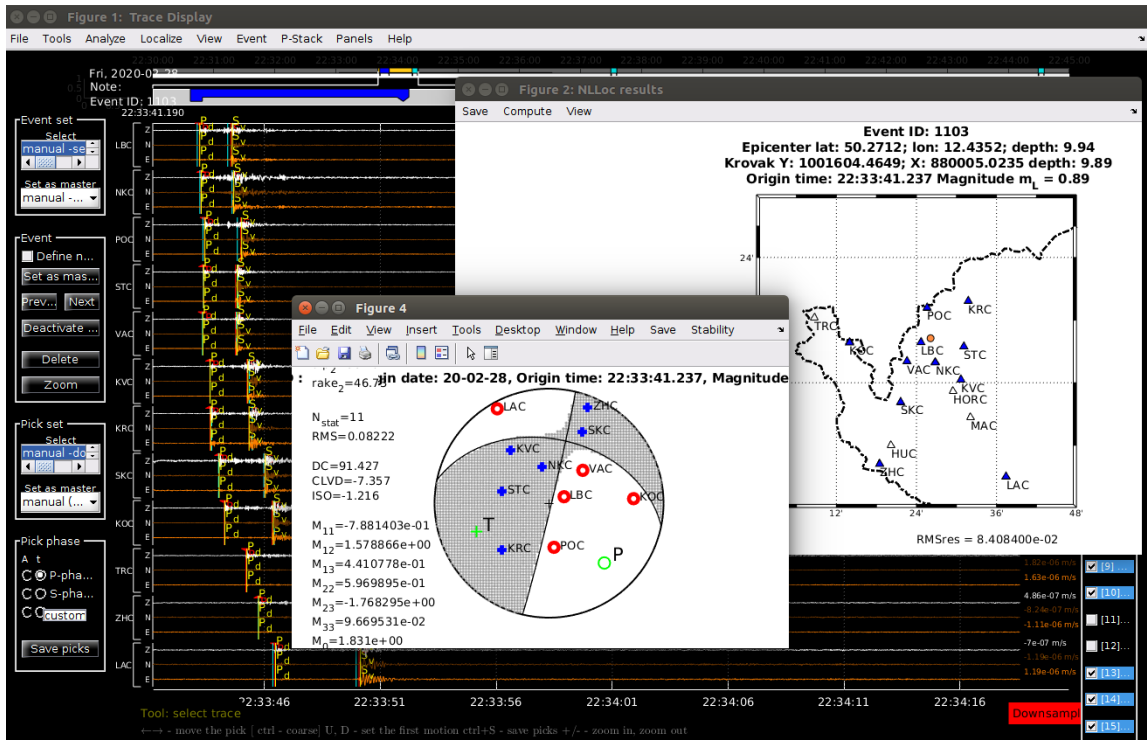
Figure A.3: *Trace display* main window with an event display together with its location and focal mechanism

are determined to analyze the signal (frequency spectrum, spectrogram, polarization analysis, particle motion plot, envelope, location, moment tensor inversion, etc.) while processing nodes modify the signal waveforms (filtration, domain conversion, rotation, etc.). The processing stack enables to control the settings and the order of the processing nodes applied. The module must be preceded by some data selection module. The *Trace display* module can be also called indirectly by other modules (like *Manage events* or *Manage time segments*), when the module is not in the collection but it can be called in interactive way - for example if the user displays a list of events and their characteristics and wants to inspect the waveforms, the *Trace display* module is called upon request.

A.1.3 Event handling

Set of functions designed for work with seismic events. Modules for event handling are very often used because event is a basic object used in Seismon.

Select Seismon event   This module enables to select events from the database in a user friendly way. The events can be filtered by event set, event class, time, location, magnitude or ID. The resulting table can be then sorted and a subset of rows can be selected. The module's output serves as an input for many other modules working with events.
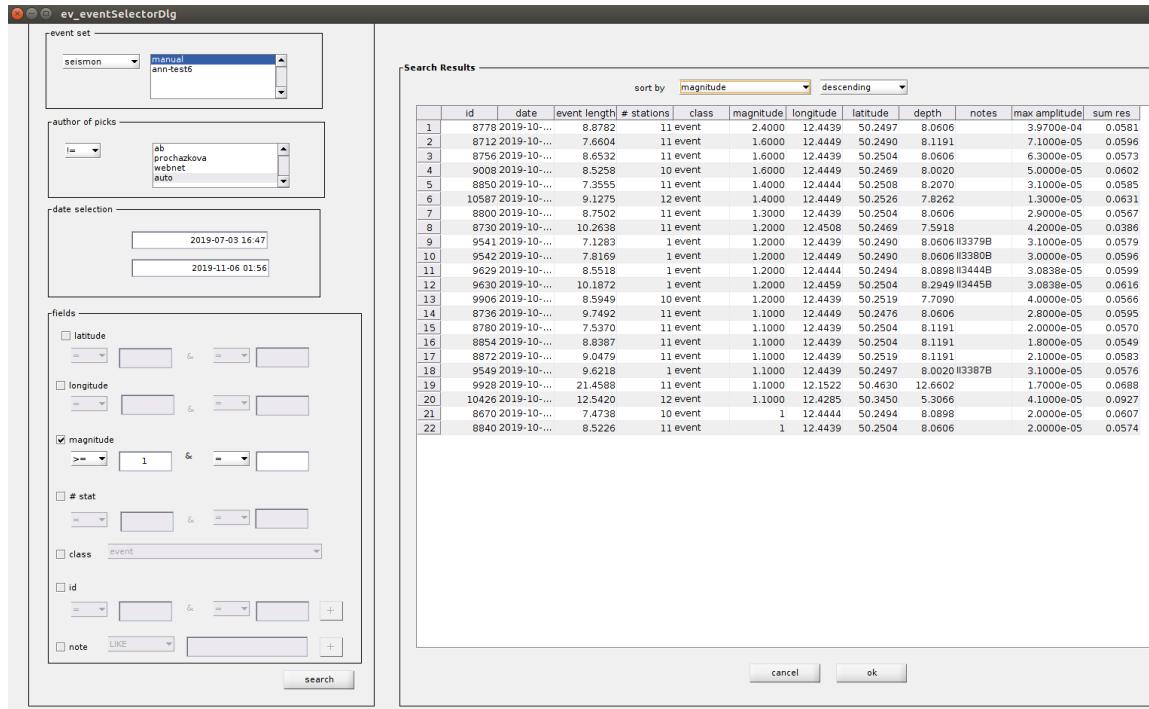
Figure A.4: *Select Seismon event* dialog window

Estimate maximum amplitude   This module preceded by event selection assigns the maximum amplitude of ground motion of the waveforms within the event duration and inserts such information to the database record of the event. This helps to sort the events prior to location and magnitude is computed.

Export bulletin   This module needs an event selection input from previous module. The editable parameters regard to the output format of the bulletin. The various text formats help the subsequent users to easily use the bulletin or catalog.

Export event waveforms   The module exports waveforms of individual events to separate ASCII or GSE2.0 files. The time limits of the waveforms can be defined either relatively to the P-wave onset or to the origin time of the event. This module needs an event selection input from previous module or from external file.

Import bulletin   This module is standalone one. It is designed to read the text file of a bulletin and import it to the project's database tables. The editable parameters define the input format of the bulletin and to which set to assign the obtained information (i.e., what kind of events, picks and locations is present).

Manage events   The module enables to inspect the events. The selected events (provided by preceding module) are listed in an interactive window. The user can view and edit the parameters of the events, sort or delete the events, inspect in detail the locations assigned to the events and also run the *Trace display* for selected event
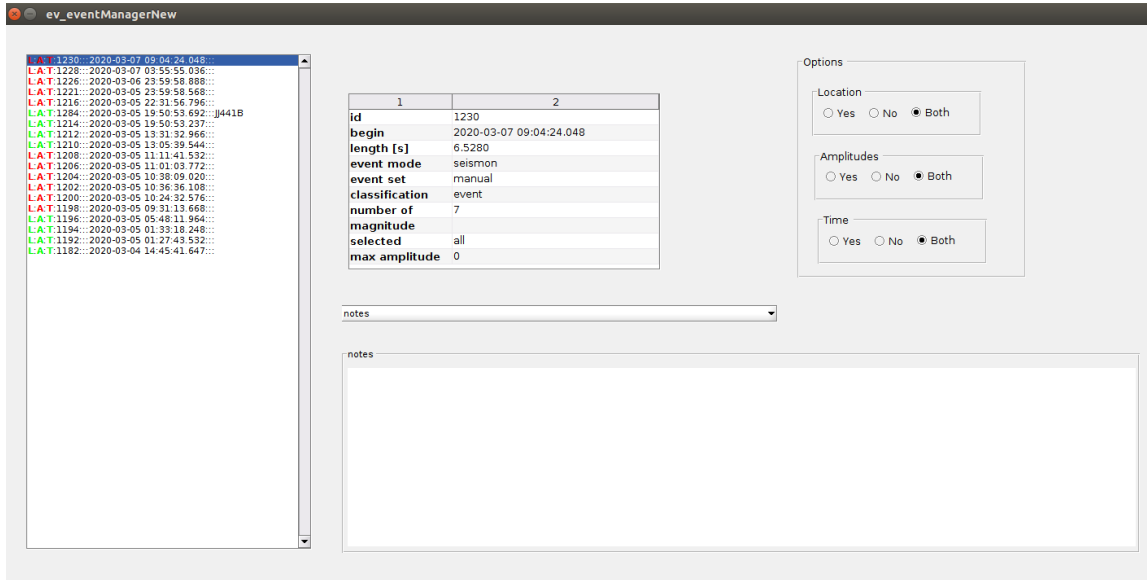
Figure A.5: Event manager window

(Fig.A.5). In an everyday manual routine, the events are interpreted in this way - sorted by preliminary magnitude, maximum amplitude or time they are one by one viewed and edited in *Trace display* called from event manager.

View events in GoogleEarth   Preceded by *Select Seismon event* this module prepares a .kml file (a file format used to display geographic data in an Earth browser such as Google Earth) and runs external program Google Earth with the .kml file as an input argument. The epicenters are then plotted on the Google Earth map.

A.1.4   File import

Set of modules to import new recordings to the database for different file-types and other supporting functions for file handling. After a file import, *Apply Geometry* module must be called to connect the data-files with instruments.

ASCII/GSE/Miniseed/SAC/Segy import   Standalone modules to import waveform files to Seismon. All these file types are accepted by Seismon and these modules add the records about the files to the database table. During that process the header information (station, channel, time) is written to the database.

Convert ESSTF to GSE   This module converts the ESSTF files to GSE2.0. The ESSTF format is original Lennartz acquisition system data format.

GSE time shifts   This module shifts the time in GSE files. This was needed for some older data converted to GSE without taking into account the differences
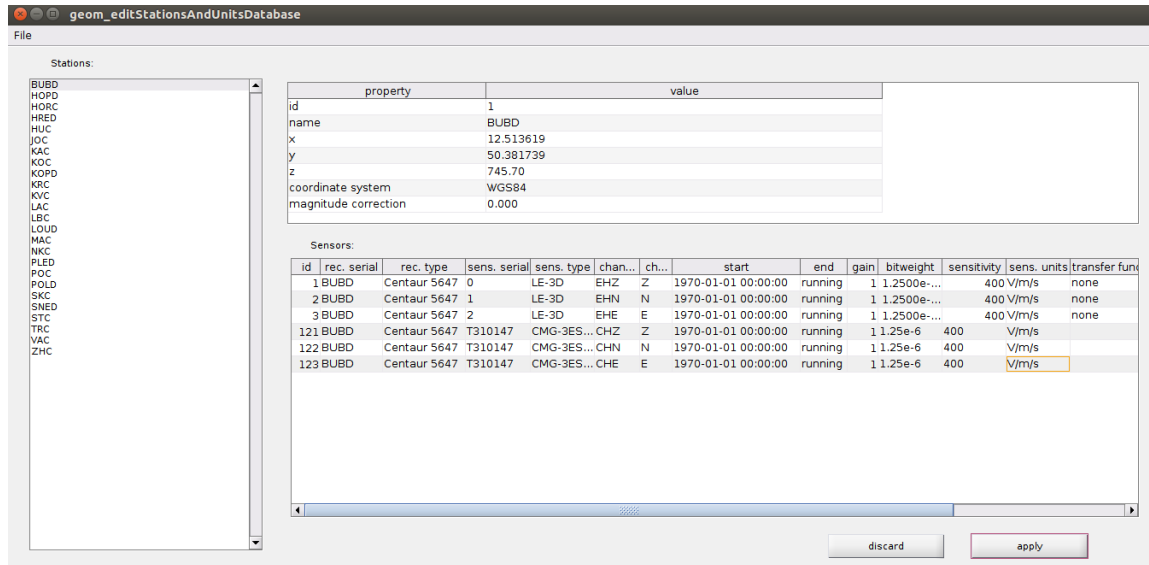
Figure A.6: *Edit stations and units database* module dialog window

between waveform data transmission delay and the DCF77 timestamps.

A.1.5 Geometry

The term Geometry in Seismon means the location and instrumentation information of the seismic stations. These modules enable to view, edit or create geometry entries.

Edit stations database A standalone module for editing, exporting and importing station database table. Station is defined by the station code and geographical coordinates. The instrumentation in Seismon is held by units and sensors objects. This module enables to define or edit stations by filling the fields in a form and import/export the stations in Seismon text format SSF. If a new Seismon project is defined with the same instrumentation, the export and import of SSF files becomes very helpful.

Edit units database A standalone module for editing, exporting and importing database tables of units and sensors. Units and sensors are linked to the station and represent the instrumentation. This module enables to define or edit units and sensors by filling the fields in a form and import/export the sensors and units in Seismon text format SUF. If a new Seismon project is defined with the same instrumentation, the export and import of SUF files becomes very helpful.

Edit stations and units database A module that enables to edit stations, units and sensors at once. It prevents inconsistency errors that may occur editing stations and units separately (Fig. A.6).

View geometry in Google Earth   This module prepares a .kml file and runs external program Google Earth with the .kml file as an input argument. The stations are then plotted on the Google Earth map.

Apply Geometry   This standalone module connects instrumentation and waveform file tables. It is called after a waveform files import (i.e., *ASCII/GSE/Miniseed/SAC/Segy import* module). During the waveform files import the traceheader database table is filled with file names, paths, station name, channel name and time period. Calling the module *Apply geometry* will fill traceheader table with valid station ID, unit ID and sensor ID. Loading waveform files by Seismon is then controlled by the IDs of stations/units/sensors.

A.1.6   Moment tensor

Functions for moment tensor computation or import the results. Routinely the moment tensors are computed in interactive regime right after a location in *Trace Display module.*

Moment tensor AMT   This module preceded by *Select Seismon event* uses P-wave amplitude picks to compute amplitude moment tensors with an external program AMT by Václav Vavryčuk (method described in Vavryčuk [2011]).

Import moment tensors   Import of computed moment tensors in a text format provided by Václav Vavryčuk's programs.

A.1.7   NLLoc

Set of functions based on NLLoc (Lomax et al. [2000, 2009]). For a routine location in interactive mode the NLLoc can be run also from the *Trace Display module.*

Create 1D model for NLLoc   Interactive standalone module for running NLLoc Grid2Time and Time2Grid programs to prepare new travel time grids for a new 1-D layered model (used rarely).

Export NLLoc phase file   Exports an .obs phase file that can be used with NLLoc (not usually used while the NLLoc is routinely used after picking in *Trace display* module). As an input *Select Seismon event* is required. The editable parameter is the pickset (type of wave-onset readings, e.g. automatic vs. manual) which should be used.

Localize events by NLLoc   This module preceded by *Select Seismon event* module runs a batch NLLoc location for those events. The results can be saved in a text file or in the Seismon database. The editable module parameters are local

paths to NLLoc, location model, pickset, stations used for location, stations used for magnitude and phases used (only P and/or S can be selected).

Plot NLLoc hypocenters A standalone module that plots the hypocenters provided by NLLoc. An editable parameter is the .hyp file path.

Run NLLoc The module preceded by *Export NLLoc phase file* module or a standalone one with defined path to .obs file is nowadays used seldom. It calls NLLoc on a remote server and outputs the .hyp file (the output file with location provided by NLLoc). It was designed for Windows users before the successful compilation of NLLoc under Windows was achieved. The module uses WinSCP program to upload/download the input/output files for NLLoc. The editable parameters are the local and remote paths and the connection details. The remote location can be used also when NLLoc is called from the *Trace display* module.

A.1.8   Seisbase Tools

A set of tools for importing Seisbase results to Seismon database implemented by J. Michálek.

Import station with coordinated to DB This module reads the station configuration exported from Seisbase and creates database records to Seismon database table.

Import Sensor configuration to DB This module reads the sensor configuration exported from Seisbase and creates database records to Seismon database tables.

Read Seisbase EXP tables This module reads the events, picks and locations exported from Seisbase tables. This module must be succeeded by *Insert Seisbase events to DB*.

Insert Seisbase events to DB This module uses output of *Read Seisbase EXP tables* and creates database records to Seismon database tables.

Scan for GSE files Scans the directory structure used by Seisbase to make a list of all GSE files. The module should be succeeded by *Import GSE files*.

A.1.9   Autopick

Simple automatic picking routines. It serves to forward computation of arrival times based on known origin time of the events or adding amplitude picks to existing time picks.

Automatic NLLoc picking   The module preceded by *Select Seismon event* runs a batch of NLLoc locations, then save the result to the database or to the output text file.

Automatic TauP picking   For selected events the automatic time picks will be computed using TauP and saved to the database.

Automatic amplitude picking   For selected events the automatic amplitude picks according to the WEBNET interpretation routines will be assigned (i.e., first local extreme after P-wave onset in displacement and maximum in a $80\,\mathrm{ms}$ long time window after S-wave onset in velocity, both with $1\,\mathrm{Hz}$ high-pass filter applied). The event selection module must be preceding.
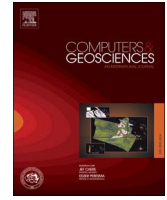
Research paper

Single Layer Recurrent Neural Network for detection of swarm-like earthquakes in W-Bohemia/Vogtland—the method

CrossMark

Jana Doubravová [a,b,*], Jan Wiszniowski [c], Josef Horálek [a]

[a] Institute of Geophysics, Czech Academy of Sciences, v. v. i., Boční II 1401, 14131 Prague, Czech Republic
[b] Charles University in Prague, Faculty of Mathematics and Physics Ke Karlovu 3, 121 16 Prague, Czech Republic
[c] Institute of Geophysics, Polish Academy of Sciences, Księcia Janusza 64, 01–452 Warsaw, Poland

ABSTRACT

In this paper, we present a new method of local event detection of swarm-like earthquakes based on neural networks. The proposed algorithm uses unique neural network architecture. It combines features used in other neural network concepts such as the Real Time Recurrent Network and Nonlinear Autoregressive Neural Network to achieve good performance of detection. We use the recurrence combined with various delays applied to recurrent inputs so the network remembers history of many samples. This method has been tested on data from a local seismic network in West Bohemia with promising results. We found that phases not picked in training data diminish the detection capability of the neural network and proper preparation of training data is therefore fundamental. To train the network we define a parameter called the learning importance weight of events and show that it affects the number of acceptable solutions achieved by many trials of the Back Propagation Through Time algorithm. We also compare the individual training of stations with training all of them simultaneously, and we conclude that results of joint training are better for some stations than training only one station.

© 2016 Elsevier Ltd. All rights reserved.

1. Introduction

Automatic seismic event detection is crucial in seismic data processing. Generally, seismic stations record huge volumes of continuous data which can be evaluated either automatically, or manually, or both. Effective manual processing inevitably requires excellent automatic event detection. We apply the method presented here to the earthquake swarm region in West Bohemia. During the swarms we have to process a large number of events which occur during short periods of time (i.e., hundreds of events per day). It is excessively time consuming to process events manually, and yet swarms are still processed this way. In past years short term averaging/long term averaging (STA/LTA) triggered recordings with coincidence on stations through the network were used. The number of the triggers was much higher than the number of local events (it also contained regional or teleseismic events and quarry blasts, storms or coincidental disturbances). On the other hand, during the swarms some weaker events were missing. That necessitated the use of a reliable automatic detector of local seismic events. In this paper we present

the use of the Artificial Neural Network (ANN) to distinguish between disturbances (any signal except for local events) and local events.

After good detection the event could be then processed further manually or automatically. Firstly, the P-and S-phases are picked, the event is localized and the focal mechanism is computed. But with very weak events this task might even be impossible. Then detecting the event can indicate useful local seismic events which may be beneficial to complete the event statistics, i.e., lower the magnitude of completeness in a range which is unrealizable manually.

2. Brief overview of the detection approaches

Automatic processing of seismic events could be performed in different ways. The first approach accords with the steps of manual processing. Initially, an event must be detected, then the P- and S-phases are picked and the location of the event is computed using those picks (as in Sleeman and van Eck, 1999). In the second approach, a search is made for all possible phases to combine them to satisfy the events, which are subsequently located (Le Bras et al., 1994; Dietz, 2002; Fischer, 2003). During the third approach a search is made through all possible hypocenters ensure concurrence with real data, and an event is declared without picking

(Withers et al., 1999; Kao and Shan, 2004). We apply the first processing scheme which begins with detecting an event.

There are several methods of detection, which can be sorted into the time domain methods, the frequency domain methods, particle motion processing, and pattern matching (Withers et al., 1998). All groups of detection can be achieved through the Artificial Neural Networks. The advantage of ANN detection methods is the ease of adjusting parameters of detection by training in the ANN. Consequently, a detailed description of what are common features for events, or on the other hand, what are the most significant differences between events and disturbances, are not required. Therefore, ANNs were widely used for seismic event detection or phase picking. ANNs were applied to detection in the time domain (Wang and Teng, 1995, 1997; Gentili and Michelini, 2006), the frequency domain (Wang and Teng, 1995; Tiira, 1999), as well as pattern matching (Madureira and Ruano, 2009; Tiira, 1999). Mostly all of these methods are based on feed-forward multi-layer-perceptron (MLP) networks with one hidden layer, where the ANN is fed by moving window vectors. Wang and Teng (1995) compared the detection performance of two ANN detectors with MLP architecture. The first was fed by consecutive samples of STA/LTA of the whole full frequency band signal, while the input of the second one was samples of moving window spectra. The authors concluded that a spectral content must be considered for successful detection. The work of Tiira (1999) uses MLP fed by STA/LTA of different lengths in seven frequency bands to detect teleseismic events. He also experimented with recurrent networks having one state neuron—Elman (1990) and Jordan (1986) networks but both performed worse than MLP. Madureira and Ruano (2009) designed an MLP network whose inputs are frequency samples in consecutive time windows. Another solution to incorporate the history of the signal is to use a network with recurrent neurons (Tiira, 1999; Wiszniowski et al., 2014). Detection of small local events by a Real Time Recurrent Network (Williams and Zipser, 1989) was undertaken by Wiszniowski et al. (2014). The network with 17 inputs of STA/LTA in narrow frequency bands and 12 recurrent neurons with one step delay compared to STA/LTA with filtration and proved to be better especially when signal to noise ratio was small. Nevertheless, the result shows the rapid forgetfulness of a recurrent network with single delay units, which limits discrimination in the time domain.

The method introduced is applied to data from the West Bohemia earthquake-swarm region, which is now automatically processed by two algorithms. The first (Fischer, 2003) is based on looking for all possible phases first, searching for such groups of picks that will comprise a local event. All events with small number of picks or with large residual of locations are then removed. The other method uses automatic locations from Antelope software. Antelope locations are usually more scattered and many smaller events are omitted.

3. Data

A local seismic network WEBNET (operated by the Institute of Geophysics, 1991 and Institute of Rock Structure and Mechanics of the Czech Academy of Sciences (CAS)) has been monitoring the seismicity in the West Bohemia earthquake-swarm region since the 1980s. At present there are a total of 22 seismic stations. They operate in two different data-transfer regimes. The first one is an on-line data transmission mode used at 13 stations, and the second one is an off-line data collection mode used on the 9 remaining stations. Available immediately are data from on-line stations (Fig. 1), while off-line stations data are collected while visiting the sites. Until upgraded in 2015, the stations were equipped with short period seismometers, mostly SM3, LE-3D and one broadband CMG-40 T seismometer. Since we want to apply our method to a quick estimation of current activity, we use on-line stations only.

All data used are continuous three component ground-velocity records sampled at 250 Hz. Until 2013 some of the stations were operated in triggered mode only and we do not use them (KOC, LAC, TRC, NKC). During more than 30 years of observation several earthquake swarms were recorded well (Horálek et al., 2000; Čermáková and Horálek, 2015). The most recent installed station (in 2006) is ZHC (see Fig. 1), therefore we focus on activity since 2006. We chose the swarms in 2008 and 2010 without swarm-like seismicity as training data and the swarm of 2011 to test the results.

In addition, we use manual P- and S-wave picks that serve to
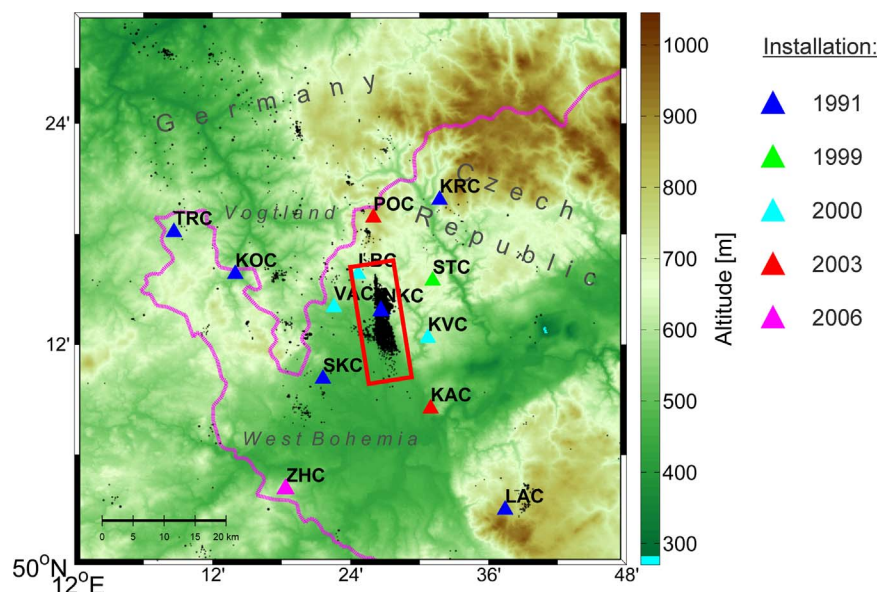
Fig. 1. On-line stations of WEBNET (triangles) and epicenters (black dots) of the swarm-like events in West Bohemia and adjacent territory of Germany. The red rectangle marks the main epicentral area where more than 90 percent of events have occurred in the last 30 years. The years of getting the individual stations into operation are indicated by colors. (For interpretation of the references to color in this figure caption, the reader is referred to the web version of this paper.)

define an event during the training process. A number of events have not been picked manually in the 2008-swarm recordings. The implication is that during the training process all unpicked events are treated as disturbances and during the evaluation of results are wrongly considered as false detections.

4. Method

4.1. Single Layer Recurrent Neural Network and its configuration for the WEBNET detector

The Single Layer Recurrent Neural Network (SLRNN) consists of a set of m artificial neurons. The i-th artificial neuron (Fig. 2) at moment t has an output value

$$V_i = g\left(\sum_{j=1}^{n} w_{ij} v_j\right) \tag{1}$$

where w_{ij} are weight coefficients of the neuron inputs, $v_j(t)$ are input values, $V_i(t)$ is an output value, and $g(.)$ an activation function. The activation function defines a neuron activation behavior depending on the neuron's weighted input. In our case a widely used hyperbolic tangent is used (the neuron outputs are limited from -1 to 1). The SLRNN was based on the Real Time Recurrent Network (RTRN, Williams and Zipser, 1989) and the Nonlinear Autoregressive Neural Network (NARX, Narendra and Parthasarathy, 1991). The structure of the SLRNN is shown in Fig. 3.

It is a Single Layer Recurrent Artificial Neural Network similar to the RTRN. Each SLRNN neuron has the following inputs:

$$v_j(t) = \begin{cases} V_K(t - D_c) & j = 1, \dots, n_r; K = 1, \dots, m; c = 1, \dots, d & \text{recurrent inputs} \\ x_i(t) & j = n_r, \dots, n-1; i = 1, \dots, p & \text{inputs of the SLRNN} \\ 1 & j = n & \text{constant value 1, bias} \end{cases} \tag{2}$$

where m is the number of neurons, n is the number of inputs of the neurons $(n = p + n_r + 1)$, p is the number of inputs of the SLRNN, $n_r = m \cdot d$ is the number of recurrent inputs, and d is the number of delay units. As opposed to the RTRN, which has one step delay between output and input, the delay in the SLRNN is variable similar to the NARX. One output of neuron can be connected to many inputs of neurons with different delays. Consequently, there can be more recurrent inputs than neurons. An output of K-th neuron is delayed by D_1 to D_d steps and fed back as a part of the first n_r inputs of the neurons. The use of delays of more time steps allows remembering time relations longer compared to the RTRN (Wiszniowski et al., 2014). Thus, the inputs from 1 to n_r are the recurrent ones, the inputs from $n_r + 1$ to $n - 1$ are those of the whole network, and the n-th input (also called bias) is connected to a constant value of 1. As opposed to the NARX, only a part of neural outputs (k) are outputs of the SLRNN. Other hidden neurons allow building self-adapted time relations not controlled by expected outputs.

Our SLRNN, designed for detection of small natural earthquakes in WEBNET, consists of 8 neurons and 18 inputs. The feedback connections of the output of each neuron are delayed by 1, 2, 4, and 8 time steps. Thus the neurons have 32 feedback inputs, 18
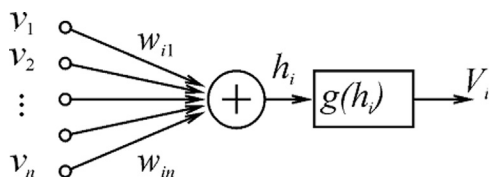
Fig. 2. Single i-th neuron with n inputs (from v_1 to v_n), weight coefficients (from w_{i1} to w_{in}), adder with output $h_i = \sum w_{ij} v_j$, activation function $g(.)$ with output $V_i = g(h_i)$.
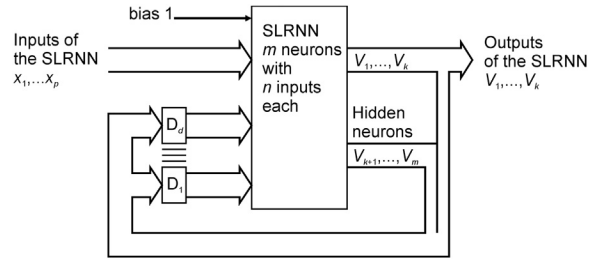
Fig. 3. Schema of SLRNN: p inputs of the network $x_1, \dots, x_p$; k outputs, which are output of neurons $V_1, \dots, V_k$; and $m - k$ hidden neurons $V_{k+1}, \dots, V_m$. Output of each neuron is connected to d inputs delayed by the corresponding (D_c) number of cycles, $c = 1, \dots, d$. $D_1, \dots, D_d$ are delay units.

inputs of the network, and 1 bias input. The 18 inputs come from a filter bank of STA/LTA ratios. The filter bank is an array of narrow band-pass filters that separate the input signal into multiple components, each one carrying an isolated frequency band of the original signal (Fig. 4).

The outputs of the first three neurons, which are also outputs of the SLRNN, correspond to: V_1—detection of event, V_2—detection of P wave onset (P onset hereafter), and V_3—detection of S wave onset (S onset hereafter). This is achieved by adjusting the weights w_{ij} during the training process (in our case for $32 + 18 + 1 = 51$ inputs and 8 neurons it is 408 weights). After successful training, the V_1 output is used for event detection, while the rest of the outputs (outputs of the hidden neurons and phase detections) are used only as feedback. The detection outputs V_2 and V_3 cannot be used as pickers because of a long time step of the SLRNN (0.2 s).

4.2. Input data

Here we describe processing the data before it is used as SLRNN inputs (Fig. 5). Original data is three component seismic records (N, north-south; E, east-west; Z, vertical). First, we filter the signals by a filter bank. It consists of nine half-octave IIR filters which filter out the narrow frequency bands (0.6–1 Hz, 1–1.6 Hz, 1.6–2.5 Hz, 2.5–4 Hz, 4–6.3 Hz, 6.3–10 Hz, 10–16 Hz, 16–25 Hz, 25–40 Hz) see Fig. 4. After filtration we compute a total horizontal component $\sqrt{N^2 + E^2}$. Then, we calculate the STA/LTA ratios. The length of the short term average (STA) window is two times longer than the shortest period (defined by the higher corner frequency of each filter) and the long term average (LTA) window is ten times longer than the longest period (defined by the lower corner frequency of each filter). The original sample rate is then decimated to 5 Hz, because the SLRNN works in 0.2 s time steps. The time step of the neural network is a compromise between the acceptable
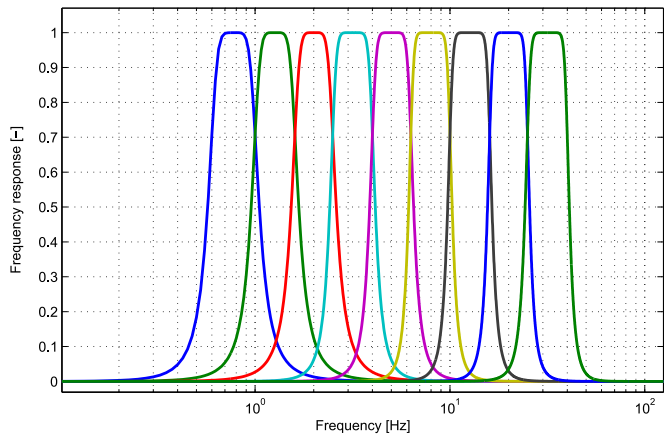
Fig. 4. Filter bank frequency response. Each half-octave filter filters out a narrow frequency band from the input signal.
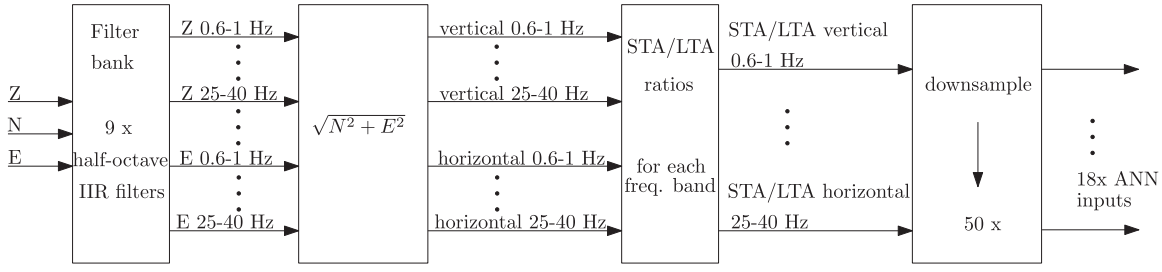
Fig. 5. Processing scheme of the SLRNN input data. Three-component raw seismograms are processed into 18 SLRNN inputs.

computational load and a good separation of individual waves.

4.3. Training algorithm

We applied a supervised learning algorithm, which implies that neuron weights w_{ij} are changed in order to get the best possible fit of the real and required outputs of the SLRNN. It is achieved by minimizing the cost function of real and required outputs. Consequently, the required outputs of the network and the cost function E must be defined. The output of a well-trained network ought to fall below a certain threshold during the occurrences of seismic noise and disturbance, whereas it must significantly exceed the threshold during the seismic local event. In our case, the threshold was zero. However, the detection is not required to exceed the threshold at the beginning of the event. It can occur any time during the event. It is not even recommended to exceed the threshold at the beginning until, for example, secondary waves come. Otherwise, some disturbances similar in shape to the P waves might generate detection. Therefore, the required output is negative at the beginning of an event, whereas after the S onset the positive output is strongly enforced. The error between required and real output is weighted in order to ignore or emphasize the error. The cost function E for one waveform in the training set is defined as a sum of output errors in the form:

$$E = \sum_t \sum_{i=1}^{3} \eta_i(t) \big[\zeta_i(t) - o_i(t) \big]^2,$$
(3)

where ζ_i is the expected output of i-th neuron, η_i is the learning-error weighting coefficient (learning coefficient hereafter) and o_i is the real output of the SLRNN ($i = 1, 2, 3$, corresponding to outputs V_1, V_2 and V_3). Both ζ and η depend on the P and S phases of the seismic event. The learning coefficient defines how sensitive is the learning process of SLRNN to certain periods of the event waveform (Figs. 6 and 7).

To improve generalization of the detection, we implemented the weight decay regularization method (Hinton, 1989) into SLRNN learning. Hinton showed that it is possible to improve generalization by adding a term that amounts to the sum of squares of the network weights to the cost function. Then the cost function is

$$E = \gamma \sum_t \sum_{i=1}^{3} \eta_i(t) \big[\zeta_i(t) - o_i(t) \big]^2 + (1 - \gamma) \sum_{i=1}^{m} \sum_{j=1}^{n} w_{ij}^2.$$
(4)

where the regularization parameter γ controls the extent to which the second penalty term influences the cost function. The minimization is based on a gradient of (4) according to the formula

$$\frac{\partial E}{\partial w_{pq}} = 2\gamma \sum_t \sum_{i=1}^{3} \eta_i(t)[\zeta_i(t) - o_i(t)]\frac{\partial o_i(t)}{\partial w_{pq}} + 2(1 - \gamma)w_{pq}.$$
(5)

Two methods most often used to compute the gradient of cost function of recurrent neural networks are the Real Time Learning algorithm (Williams and Zipser, 1989) used by Wiszniowski et al. (2014) and Back Propagation Through Time (BPTT) algorithm (Werbos, 1990). Regarding the SLRNN, we chose BPTT because it is faster and it is implemented in Matlab Neural Network Toolbox
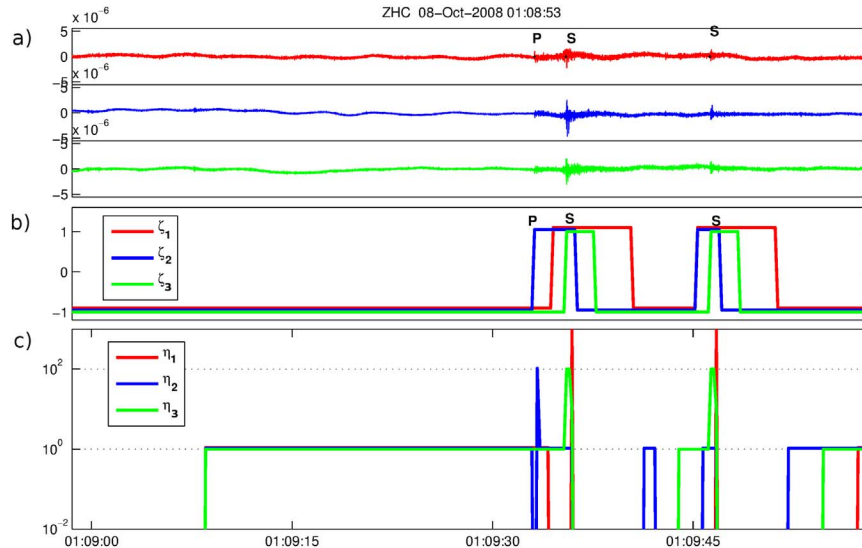
Fig. 6. Example of SLRNN learning on the ZHC station from the 8 Oct 2008 event with P- and S-wave onset picks, and a later event with S pick only. (a) The seismic signal with marked phases, red—Z component, blue—N component, green—E component, (b) expected outputs of the SLRNN, red—event detection, blue—P wave detection, green—S wave detection, (c) learning coefficient, red—event detection, blue—P wave detection, green—S wave detection. (For interpretation of the references to color in this figure caption, the reader is referred to the web version of this paper.)
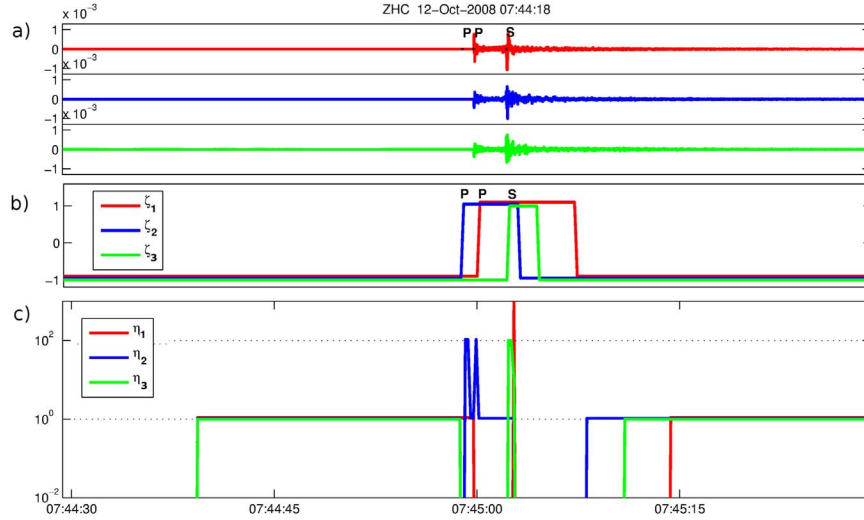
Fig. 7. Example of SLRNN learning on the ZHC station from 8 Oct 2008 event with P- and S-wave onset picks, preceded by small event with P pick only. (For further details legend see Fig. 6). (For interpretation of the references to color in this figure caption, the reader is referred to the web version of this paper.)

that we use.

We define the values of the expected outputs (Figs. 6 and 7b) as:

$$\zeta_1(t) = 1: t \in \langle T_P + 1.4 \text{ s}, T_S + 5 \text{ s}\rangle, \tag{6a}$$

$$\zeta_1(t) = -1: \text{otherwise}, \tag{6b}$$

$$\zeta_2(t) = 1: t \in \langle T_P, T_S + 1 \text{ s}\rangle, \tag{6c}$$

$$\zeta_2(t) = -1: \text{otherwise}, \tag{6d}$$

$$\zeta_3(t) = 1: t \in \langle T_S, T_S + 2 \text{ s}\rangle, \tag{6e}$$

$$\zeta_3(t) = -1: \text{otherwise}, \tag{6f}$$

where ζ_1 is the expected output corresponding to event detection, ζ_2 is the expected output corresponding to P wave, ζ_3 is the expected output corresponding to S wave, and T_P and T_S are picked onset times of the P and S phases. Since many disturbances may have similar shape to P phase, we want the decision of detection to be made later, not based on P-phase onset shape. Therefore we define an expected event detection signal to be high later after P onset (6a). The values of learning coefficients (Figs. 6 and 7c) vary according to formulas:

$$\eta_1(t) = 0: t \in \langle T_0, T_0 + 10 \text{ s}\rangle \tag{7a}$$

$$\eta_1(t) = 1: t \in \langle T_0 + 10 \text{ s}, T_P + 1 \text{ s}\rangle \tag{7b}$$

$$\eta_1(t) = 0: t \in \langle T_P + 1 \text{ s}, T_S + 0.6 \text{ s}\rangle \tag{7c}$$

$$\eta_1(t) = LIWE: t \in \langle T_S + 0.6 \text{ s}, T_S + 0.8 \text{ s}\rangle \tag{7d}$$

$$\eta_1(t) = 0: t \in \langle T_S + 0.8 \text{ s}, T_S + 12 \text{ s}\rangle \tag{7e}$$

$$\eta_2(t) = 0: t \in \langle T_0, T_0 + 10 \text{ s}\rangle \tag{7f}$$

$$\eta_2(t) = 1: t \in \langle T_0 + 10 \text{ s}, T_P\rangle \tag{7g}$$

$$\eta_2(t) = 0: t \in \langle T_P, T_P + 0.2 \text{ s}\rangle \tag{7h}$$

$$\eta_2(t) = LIWE_{10}: t \in \langle T_P + 0.2 \text{ s}, T_P + 0.6 \text{ s}\rangle \tag{7i}$$

$$\eta_2(t) = 1: t \in \langle T_P + 0.6 \text{ s}, T_S + 0.8 \text{ s}\rangle \tag{7j}$$

$$\eta_2(t) = 0: t \in \langle T_S + 0.8 \text{ s}, T_S + 5.6 \text{ s}\rangle \tag{7k}$$

$$\eta_3(t) = 0: t \in \langle T_0, T_0 + 10 \text{ s}\rangle \tag{7l}$$

$$\eta_3(t) = 1: t \in \langle T_0 + 10 \text{ s}, T_S + 0.2 \text{ s}\rangle \tag{7m}$$

$$\eta_3(t) = LIWE_{10}: t \in \langle T_S + 0.2 \text{ s}, T_S + 0.4 \text{ s}\rangle \tag{7n}$$

$$\eta_3(t) = 0.1 \cdot LIWE_{10}: t \in \langle T_S + 0.4 \text{ s}, T_S + 0.6 \text{ s}\rangle \tag{7o}$$

$$\eta_3(t) = 0: t \in \langle T_S + 0.6 \text{ s}, T_S + 8.2 \text{ s}\rangle \tag{7p}$$

where T_0 is the beginning of each record in the training set. The values of learning coefficients are set to zero at the beginning of the record (7a), (7f), (7l). It is a technical requirement. The output values of neurons are initially set to zero and neurons need a few time steps to reach their typical operating values. In our case it is
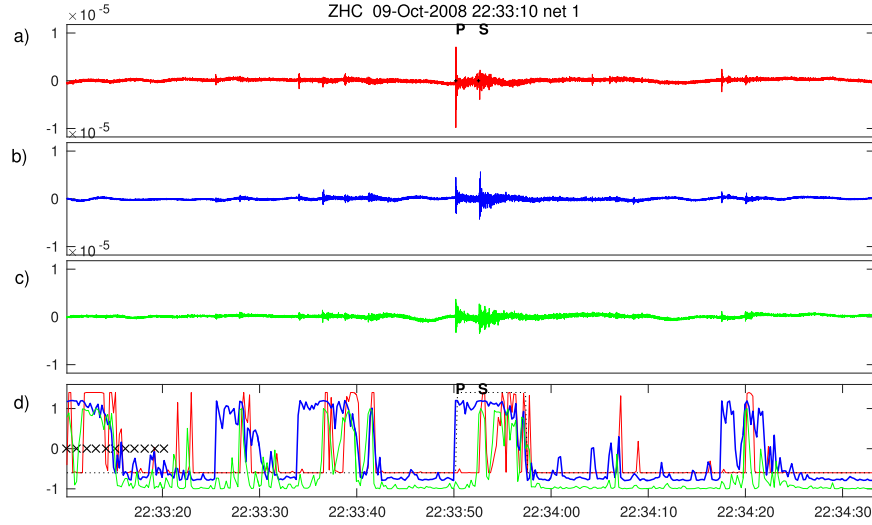
Fig. 8. An example of one properly picked event and events not picked (before and after). Seismogram (the ground velocity in m/s) from station ZHC: (a) Z component with marked phases, (b) N component, (c) E component, (d) detection signals: red—event detection, blue—P wave detection, green—S wave detection. (For interpretation of the references to color in this figure caption, the reader is referred to the web version of this paper.)

50 time steps corresponding to 10 s; as seen in Fig. 8d (area marked by signs x), this period is sufficient. Low values of learning coefficients block the training process until neurons reach their usual values. The first 10 s are not used for training the SLRNN.

At the beginning of event recording the detection output V_1 is forced at a low level in order to use more information for earthquake identification than the P-wave onset. Therefore, the expected output is then low (6a) and learning coefficient $\eta_1 = 1$ by one second (7b). This is sufficient time to diminish the P-wave and is the minimum delay between P and S waves in WEBNET. Then the output V_1 could have any value ($\eta_1 = 0$) (7c). Finally, after onset of S wave the signal must be detected and the value of η_1 is very high (7d).

With respect to noise and disturbances, it is clear what shape of the output signal of detection is required; it should be -1 all the time. In case of events we cannot determine the shape and additionally it is not important. There is just one requirement, that signal has to exceed the threshold of detection. We decided, that the high detection signal was required during the training only in one point, but with a large weight. Therefore, just after the S-wave onset the value of η_1 is very high (7d). Earlier and later, the output detection V_1 can take on any value, both high and low, but none of the values are forced during training the SLRNN (7c) and (7e). Output is ignored especially at the tail of waveforms (7e). The learning coefficient must be greater in this point than in points of noises to have equivalent values of E for noises and events. It takes the value of the Learning Importance Weight of Events (LIWE), which was defined in this paper. A few values of LIWE in the range of (10,1000) were tested.

In the case of seismic waves P and S the η values are high one step after the onset, but not as high as with detection. The value $LIWE_{10} = LIWE/10$ (7i), (7n). The output of P is important until onset of the S wave (7j), because the information about the appearance of a P-wave in the past is helpful for S wave identification. The S output is important until detection (7o). Then outputs are irrelevant (7k) and (7n).

Many seismograms of small events do not have visible P or S waves. In these cases, expected outputs and learning coefficients are calculated in a different way.

When only the P wave is picked, the output ζ_1 is $+1$ for a seismic signal from 1.2 s after the onset of the P phase to eight seconds after the P wave otherwise it is -1. The expected detection signal is not high just after the P onset because the decision of

detection should be produced later. The ζ_2 output is $+1$ from the beginning of the phase P to the three seconds after that, -1 otherwise (Fig. 7b). The output ζ_3 is irrelevant, so the expected value is taken as -1 and $\eta_3 = 0$ (9n). Forcing the detection is delayed 2.8 s to the expected time of S wave (9c, (9d), (Fig. 7c).

$$\zeta_1(t) = 1: t \in \langle T_P + 1.4 \text{ s}, T_P + 8 \text{ s}\rangle \tag{8a}$$

$$\zeta_1(t) = -1: \text{otherwise} \tag{8b}$$

$$\zeta_2(t) = 1: t \in \langle T_P, T_P + 3.4 \text{ s}\rangle \tag{8c}$$

$$\zeta_2(t) = -1: \text{otherwise} \tag{8d}$$

$$\zeta_3(t) = -1 \tag{8e}$$

The values of the learning error weighting coefficient vary when the S wave is missing according to formulas:

$$\eta_1(t) = 0 : t \in \langle T_0, T_0 + 10 \text{ s}\rangle \tag{9a}$$

$$\eta_1(t) = 1 : t \in \langle T_0 + 10 \text{ s}, T_P + 1 \text{ s}\rangle \tag{9b}$$

$$\eta_1(t) = 0 : t \in \langle T_P + 1 \text{ s}, T_P + 2.8 \text{ s}\rangle \tag{9c}$$

$$\eta_1(t) = LIWE : t \in \langle T_P + 2.8 \text{ s}, T_P + 3.4 \text{ s}\rangle \tag{9d}$$

$$\eta_1(t) = 0 : t \in \langle T_P + 3.4 \text{ s}, T_P + 12 \text{ s}\rangle \tag{9e}$$

$$\eta_2(t) = 0 : t \in \langle T_0, T_0 + 10 \text{ s}\rangle \tag{9f}$$

$$\eta_2(t) = 1 : t \in \langle T_0 + 10 \text{ s}, T_P\rangle \tag{9g}$$

$$\eta_2(t) = 0 : t \in \langle T_P, T_P + 0.2 \text{ s}\rangle \tag{9h}$$

$$\eta_2(t) = LIWE_{10} : t \in \langle T_P + 0.2 \text{ s}, T_P + 0.6 \text{ s}\rangle \tag{9i}$$

$$\eta_2(t) = 1 : t \in \langle T_P + 0.6 \text{ s}, T_P + 2.4 \text{ s}\rangle \tag{9j}$$

$$\eta_2(t) = 0 : t \in \langle T_P + 2.4 \text{ s}, T_P + 8.4 \text{ s}\rangle \tag{9k}$$

$$\eta_3(t) = 0 : t \in \langle T_0, T_0 + 10 \text{ s}\rangle \tag{9l}$$

$$\eta_3(t) = 1 : t \in \langle T_0 + 10 \text{ s}, T_P\rangle \tag{9m}$$

$$\eta_3(t) = 0 : t \in \langle T_P, T_P + 12 \text{ s}\rangle \tag{9n}$$

When only the S wave is picked, the ζ_2 is irrelevant (11h). Detection output ζ_1 is high from a second before the S onset to a few seconds after that (Fig. 6b).

$$\zeta_1(t) = 1: t \in \langle T_S - 1 \text{ s}, T_S + 5 \text{ s}\rangle \tag{10a}$$

$$\zeta_1(t) = -1: \text{otherwise} \tag{10b}$$

The values of the learning error weighting coefficient vary in consonance with formulas (Fig. 6c):

$$\eta_1(t) = 0 : t \in \langle T_0, T_0 + 10 \text{ s}\rangle \tag{11a}$$

$$\eta_1(t) = 1 : t \in \langle T_0 + 10 \text{ s}, T_S - 2 \text{ s}\rangle \tag{11b}$$

$$\eta_1(t) = 0 : t \in \langle T_S - 2 \text{ s}, T_S + 0.6 \text{ s}\rangle \tag{11c}$$

$$\eta_1(t) = LIWE : t \in \langle T_S + 0.6 \text{ s}, T_S + 0.8 \text{ s}\rangle \tag{11d}$$

$$\eta_1(t) = 0 : t \in \langle T_S + 0.8 \text{ s}, T_S + 11 \text{ s}\rangle \tag{11e}$$

$$\eta_2(t) = 0 : t \in \langle T_0, T_0 + 10 \text{ s}\rangle \tag{11f}$$

$$\eta_2(t) = 1 : t \in \langle T_0 + 10 \text{ s}, T_S - 4 \text{ s}\rangle \tag{11g}$$

$$\eta_2(t) = 0 : t \in \langle T_S - 4 \text{ s}, T_S - 0.4 \text{ s}\rangle \tag{11h}$$

$$\eta_2(t) = 1: t \in \langle T_S - 0.4 \text{ s}, T_S + 0.8 \text{ s}\rangle \tag{11i}$$

$$\eta_2(t) = 0: t \in \langle T_S + 0.8 \text{ s}, T_S + 6 \text{ s}\rangle \tag{11j}$$

$$\eta_3(t) = 0 : t \in \langle T_0, T_0 + 10 \text{ s}\rangle \tag{11k}$$

$$\eta_3(t) = 1 : t \in \langle T_0 + 10 \text{ s}, T_S\rangle \tag{11l}$$

$$\eta_3(t) = 0 : t \in \langle T_S, T_S + 0.2 \text{ s}\rangle \tag{11m}$$

$$\eta_3(t) = LIWE_{10} : t \in \langle T_S + 0.2 \text{ s}, T_S + 0.6 \text{ s}\rangle \tag{11n}$$

$$\eta_3(t) = 0.1 \cdot LIWE_{10}: t \in \langle T_S + 0.6 \text{ s}, T_S + 0.8 \text{ s}\rangle \tag{11o}$$

$$\eta_3(t) = 0 : t \in \langle T_S + 0.8 \text{ s}, T_S + 8, 6 \text{ s}\rangle \tag{11p}$$

It should be noted that the cost function is not described well in the absence of the phases. However, these cases concern the weakest events, detection of which is the hardest. It is impossible to remove them from training since the larger events are usually accompanied by nearby small events.

4.4. Training data

The SLRNN network was trained by using the Levenberg–Marquardt BPTT algorithm. The training data was divided randomly into an actual training set (80% of data) and the validation set (20% of data). Each step of the training procedure reduces the cost function of the training set and in addition computes the cost function of the validation set, which is not used for training. As long as the cost function of the training set and cost function of the validation set decrease, training continues. If the cost function of the validation set starts to increase, the training stops. This prevents overtraining the network when it would perfectly detect the training events but would not recognize other events well. Because of the strong nonlinearity of the cost function, the training was performed numerous times with different random initial neuron weights w_{ij}. The regularization parameter γ is set to 0.6. For training the SLRNN we used data from the earthquake swarms of 2008 and 2010. The 2008 data include thousands of local swarm events with manually picked P- and S-wave onsets which are consistent throughout the whole period. We chose randomly about one hundred events for each station with different magnitudes, locations or focal mechanisms. Additionally, a similar number of examples of disturbances and non-local events were needed. For this purpose we chose the 2010 data because it exhibited low local seismicity without earthquake swarms in 2010, so finding a variety of well recognized disturbances was easy. We used manually classified quarry blasts, regional or teleseismic events, disturbances by wind or storms and other unspecified disturbances.

Major problems in our training process are lacking picks which may be due to higher noise masking onsets or to unclear P onsets on stations placed near nodal planes of a particular event, rarely due to a failure during the manual processing. When the P and S picks are missing, the SLRNN network is forced to learn that the signal is a disturbance, causing the training to act in just the opposite way. Additionally, during the evaluation of network performance on the test set many right detections not verified by manual picks are wrongly treated as false detections. To eliminate
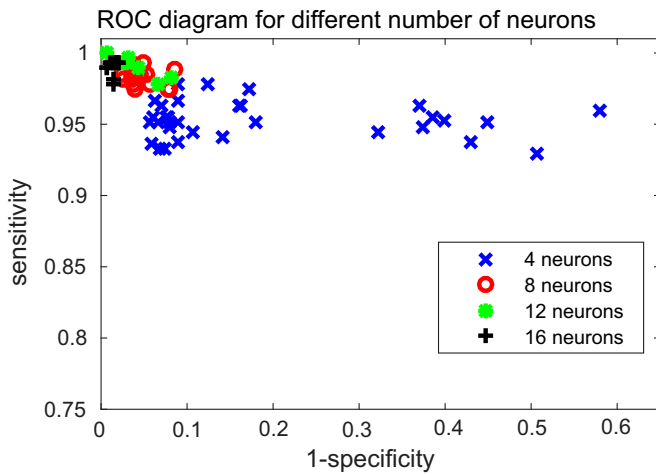
ROC diagram for different number of neurons

Fig. 9. ROC diagram for different number of neurons—results of a few trails of training when all stations were trained together.

this problem it was necessary to complete the P and S picks even if their right position was not clear (considering that the step of our SLRNN is 50 samples, i.e., 0.2 s). Accordingly, we must have picked both the training and test sets several times. An example of an unpicked event is shown Fig. 8. At least three events were unpicked. They were detected by the SLRNN, which shows that the network can work trained by partly wrong data.

5. Tests

5.1. Sensitivity, specificity and receiver operating characteristic

Although training the SLRNN minimizes the cost function *E*, the quality of detection depends on number of events detected and number of false detections, which are not wholly related to *E*. To assess the SLRNN performance we evaluate three characteristics—specificity, sensitivity and receiver operating characteristic (Zweig and Campbell (1993)). All of them are obtained based on the values of:

- true positive (TP)—number of correctly detected events,
- false negative (FN)—number of undetected events,
- true negative (TN)—number of correct rejections,
- false positive (FP)—number of false detections.

The training set consists of recordings with local seismic events and recordings with any other signal regarded as a disturbance. In the case of the picked seismic events the number of true positives is incremented if the detection output is above zero ($V_1 > 0$) a few seconds after the P onset (Fig. 8), but if $V_1 < 0$ the number of false negatives is incremented. The event detections outside picked events are ignored because there may be some unpicked events (mostly very weak ones as in Fig. 8) which are detected by the SLRNN. Regarding non-local earthquakes or disturbances the number of false positives is incremented if there is at least one point where detection output was above zero. Otherwise, the number of true negative is incremented.

The sensitivity, also designated as the true positive rate (TPR), is calculated according to the formula

$$\text{TPR} = \frac{TP}{TP + FN},$$

$$(12)$$

where (TP + FN) is the sum of all detected and undetected events. The specificity (also designated as the true negative rate (TNR)) is

calculated according to the formula

$$\text{TNR} = \frac{TN}{TN + FP}.$$

$$(13)$$

It is the ratio of true negatives to the total number of all disturbances (TN + FP). The sensitivity, which is required to be 1, i.e., all local earthquakes are detected. Low TNR means that algorithm tends to produce an excess of false detections. Increasing the number of detections for small events is always associated with expanding the number of false detections. Therefore, slightly lower sensitivity could be acceptable together with a high specificity value. The relation of the sensitivity and specificity is described by the receiver operating characteristic (ROC) that is usually depicted by the ROC diagram (Swets, 1996). When the sensitivity and specificity depends on the parameters of the detection algorithm or on the parameters of training the neural network, the ROC-curves represent a relation between the sensitivity and the specificity for various values of parameters.

5.2. Number of neurons

Estimating the number of neurons is always a difficult task. Generally, it is a parameter empirically set by the designer. On the one hand, it must be the lowest possible to have reasonable time for training and good generalization, but on the other hand, it must be high enough to satisfy the complexity of the problem. We tested 4,8,12,16 neurons which is in our case 140, 408, 804 and 1328 weights. A lesser number of recurrent neurons simplify the ANN to ANN detectors in the frequency domain (Wang and Teng, 1995). The ROC characteristic in Fig. 9 shows that the detection is significantly inferior to four neurons. Increasing the number of neurons to 12 or 16 improved the detection only slightly while the training got significantly more time-consuming.

5.3. Comparison of training results for different training parameters and stations

Firstly we evaluated the impact of the *LIWE* value (7d), (7i), (11n) on the learning process. We tested the training of the SLRNN with *LIWE* values of 1000, 500, 200, 100, 50, 20, and 10. The same set of the *LIWE* values are also used in additional tests. The sensitivity of the SLRNN trained with *LIWE* = 1000 was high, but there were too many false detections and the specificity was low. Therefore smaller values of *LIWE* were tested, i.e., 500, 200, 100, 50, 20, and 10.

The cost function is strongly nonlinear, having a number of local minima which results in some of them stopping the SLRNN learning, a tendency increases with the value of *LIWE*. Fig. 10 shows the sum of cost function values over the training set for 2000 trials of the training detection for station POC for the set of *LIWE* values. The POC station was chosen because it was one of stations showing the best detection results.

Fig. 11 shows similar results for 500 trials for each *LIWE* value on all the WEBNET stations; the number of trials was reduced due to demands on training time. When *LIWE* was small (10–100), only 30–40% of training periods failed completely. In the case of big *LIWE* (1000) more than 60–70% of periods of training failed. Figs. 10 and 11 show there is not the same best value of *E* among the training trials. That suggests there is not one best solution, so the former training might still not be the optimal solution. The *LIWE* value significantly affects the nonlinearity of training. The BPTT algorithm must be iterated more times or nonlinear optimization methods should be applied instead.

To assess detector performance we examined the sensitivities and specificities. For *LIWE* values we computed the sensitivities and specificities for 10 training results with the smallest cost
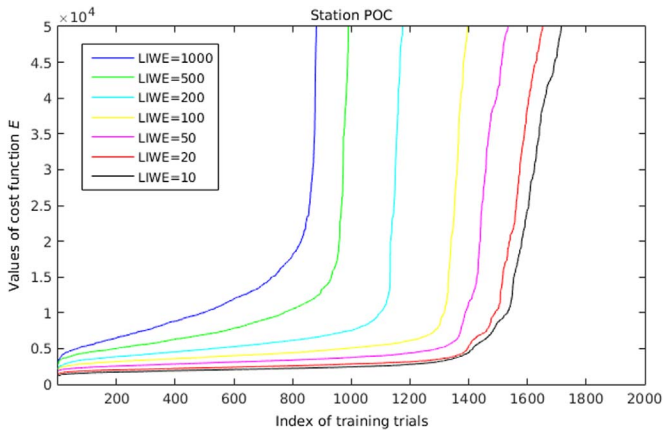
Fig. 10. Sum of E-values over the training set for 2000 trials of training detection for one station POC for the individual $LIWE$ values. Each of 2000 training periods for each $LIWE$ finished at some of the local minimum of the cost function. For each trial the value of the cost function has been computed and results for each $LIWE$ were sorted from best to worst (from lowest E to highest E). The curves show how many trials failed. The number of successful training periods is higher for lower $LIWEs$.
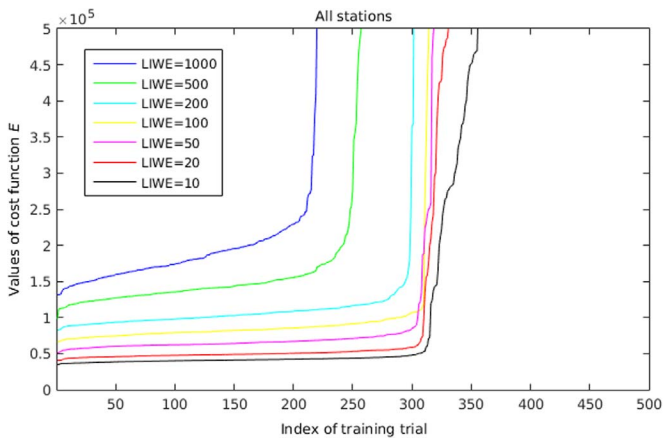
Fig. 11. Sum of E-values over the training set for 500 trials of the training detection for all the stations for various $LIWEs$, from best to worst.

function.

The influence of the $LIWE$ value on sensitivity and specificity is presented in Fig. 12a and b. For greater $LIWEs$ the specificity decreases, which means that the number of wrong detections is growing. On the other hand, for smaller $LIWEs$ the sensitivity

decreases, so more events are not detected. This implies that the best $LIWE$ value is between of 50 and 200.

The detection ability of our SLRNN was tested in two ways. First, the network was trained and used individually for each station. The results for all the WEBNET stations, which were trained individually with $LIWE=100$ are shown in the ROC diagram (Fig. 13a).

Second, the network was trained for all stations together. The result is shown in Fig. 13, where sensitivity is computed individually for each station. There are large differences between stations. The ROCs show that some stations like POC and LBC have 100% sensitivity and high specificity >90%, whereas some other stations like KAC, ZHC, NKCN have 99.5% sensitivity and smaller specificity. Results of training all stations together are similar; stations POC, LBC, and NKCN are the best, whereas stations KAC, and ZHC are significantly worse. The difference between joint and individual training at NKCN is probably caused by the lack of many picks at this station. The reason is that the former station NKC which was located at the same site as NKCN (parallel operation) was routinely used for event location until recently. That is why a number of smaller events have not been picked on NKCN, but NKC was operated in the triggered mode, so the data from this station is not used for training the SLRNN.

5.4. Comparison with signal-to-noise ratio on the stations

Testing revealed the obvious: some stations always detect events as being worse than the others, so we compared it to signal-to-noise ratios (SNR) on individual WEBNET stations. We processed five local events with local magnitude of $M_L \approx 1$ so as to have reasonable signal power and spectral content. Events with lower magnitudes may be contaminated by noise, while events with higher magnitudes have lower frequencies. We computed fast Fourier transform (FFT) spectra of noise just before the event and the spectra of the event. The signal and noise spectra of five events were averaged and the resulting SNRs were smoothened by moving average (window length 5 Hz). To eliminate the signal decay due to different hypocentral distances, the SNR for the individual stations is corrected by factor R corresponding to the hypocentral distance in km.

$$SNR = 20 \cdot \log\left(\frac{S(f)}{N(f)} \cdot R \right).$$

$$(14)$$

The resultant SNRs are depicted in Fig. 14. It is obvious from this fact that the SNR pattern of the three components is consistent which implies that the SNR is consistent on all channels. We thus
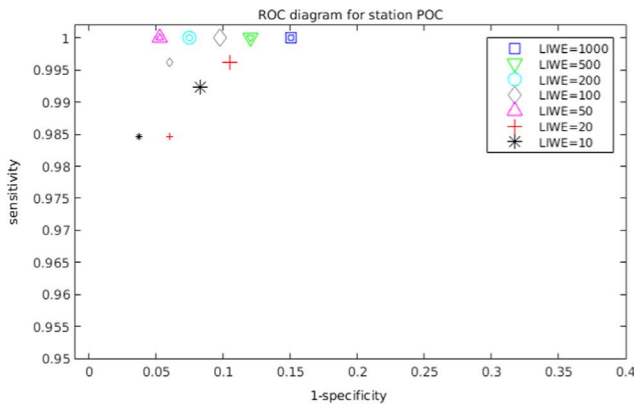
(a) ROC for the POC station
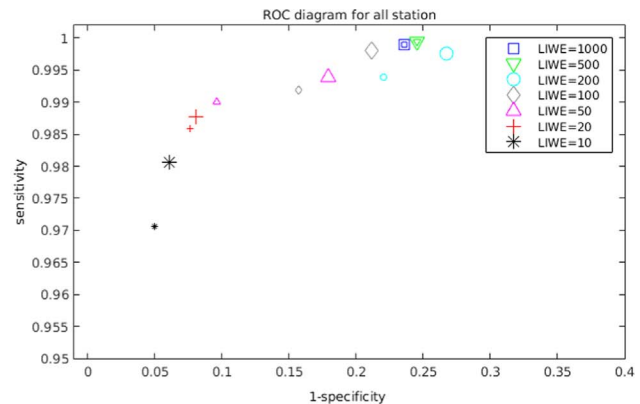
(b) ROC for all the stations

Fig. 12. The ROC diagram for the set of $LIWEs$ for station POC and all stations together. To reduce number of points in the ROC diagrams, only two of the 10 sensitivities (TPRs) and specificities (TNRs) are presented. Both TPR and TNR are required to be the highest possible (equal to 1), thus our figures show the result with maxima of TPR·TNR (smaller symbols), and maxima of TNR for the best TPR (bigger symbols). (a) ROC for the POC station. (b) ROC for all the stations.

(a) Each station trained individually.

(b) All stations trained together

Fig. 13. ROC diagrams for individual and joint training—maxima of TPR·TNR (bigger symbols), and maxima of TNR for the best TPR (smaller symbols). Individual training stations KAC and ZHC reveal the worst results. The joint training improved results in some cases, e.g., NKCN and ZHC.

(a) E component

(b) N component

(c) Z component
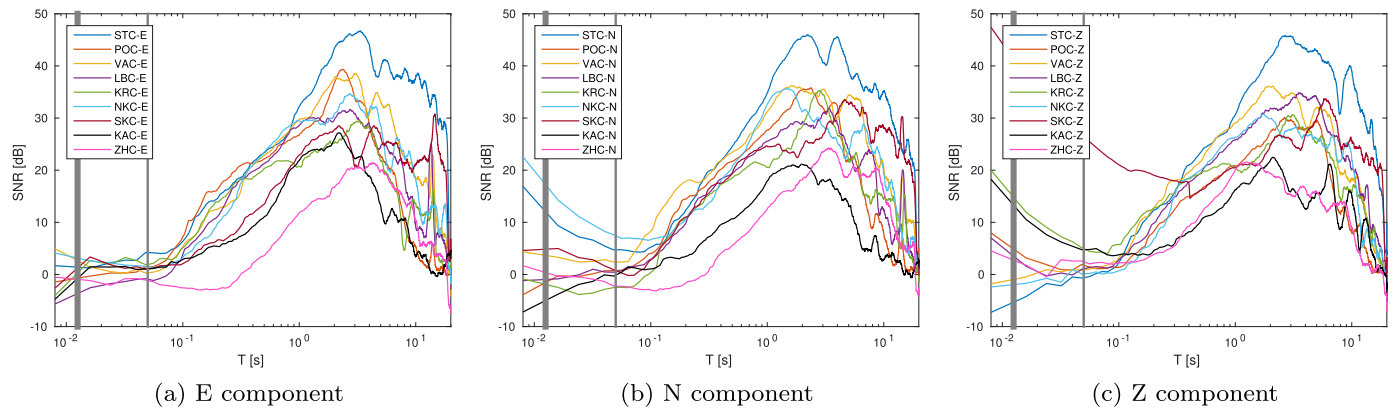
Fig. 14. SNR for all stations used for events with local magnitude $M_L \approx 1$ corrected by the distance factor R. The thicker vertical line at 0.0125 s (80 Hz) corresponds to the corner frequency of the anti-aliasing filter in recording units, and the thinner one at 0.05 s (20 Hz) corresponds to a rough estimate of the corner frequency for $M_L \approx 1$ events according to Michálek and Fischer (2013).

assume it is mostly a question of the site effects. Stations ZHC and KAC having the lowest SNR between 1.0 and 80 Hz also indicate the worst ROC. A lower SNR on these stations may be due to a shallower installation of sensors when contrasted with other stations; additionally, the ZHC station is situated close to a TV tower and also a larger town, so the higher noise cannot be avoided. Two gray lines are plotted there We wish to emphasize that the signal-to-noise ratio at frequencies between 5 and 40 Hz are of crucial importance for a detection performance of our SLRNN, particularly for detection of weak local events.

6. Preliminary results

6.1. False detections

We tested the performance of our trained SLRNN using data from earthquake swarm 2011 for the POC station. We chose station POC since it was used to test *LIWE* values during the training process. The results showed a large number of false detections (a few hundred depending on the SLRNN training result). After an experienced interpreter inspected the 2011 waveforms and catalogues, we found that there were a number of unpicked smaller events. So we checked carefully only 5 h of the swarm-activity recording. In this way six previously picked events with magnitudes between $M_L = 0.6$ and $M_L = 0.9$ were supplemented with 154 new events having magnitudes $M_L = -0.3$ to $M_L = 0.6$. The next test at the same time period showed a huge improvement; many

false detections switched to true ones but still some remained (from tens to a hundred). The networks with the lowest number of false detections generally do not detect some of the events. After the interpreter's inspection we found that some of the events are visible in the seismogram but definitely impossible to be picked. Besides, many other of detected events might be buried under noise. We wish to note that neural networks with very low false positives often have a tendency to increase the false negative.

6.2. Undetected events

Referring to false negatives (FNs), i.e., undetected events we recognized some common features. Looking at the false detections of each SLRNN realization we found that the FNs are usually the same. Typical examples of events undetected by the SLRNN network are shown in Figs. 15–18. Fig. 15 depicts undetected events hidden in the coda of the preceding event. Even if all the stations are available, only a very experienced interpreter would find those events and pick P and S onsets reliably. An example of an undetected event on the KAC station is given in Fig. 16. The SNR on the KAC site is significantly lower than on other stations. An example of an undetected event due to very small ground-motion-velocity amplitudes on station POC, located at the largest epicentral distance (DI=13 km), is demonstrated in Fig. 17. An example of detected and undetected weak events in the seismograms contaminated by strong disturbances at station KAC is shown in Fig. 18.

As evident in Figs. 16–18, the event-detection failures,
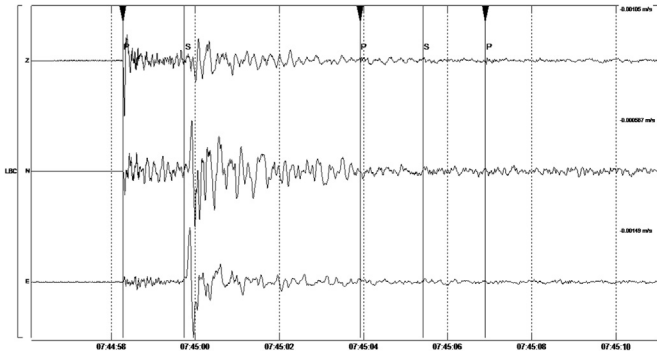
Fig. 15. Undetected events with magnitudes $M_L = 2.3$ and $M_L = 2.2$ masked by a coda of the previous $M_L = 3.8$ earthquake on the LBC station. Even though the events are of relatively higher magnitudes, having the ground-motion-velocity amplitudes much higher than ambient noise, it is very difficult to recognize them in the coda. Vertical lines indicate the picks of the P- and S-wave onsets.

Fig. 16. Example of a failed detection of $M_L = -0.3$ event on station KAC (bottom panel) and a successful detection of it on stations VAC, SKC and POC. Since the scale is the same for all traces it is evident that the waveform amplitudes on the KAC station are similar to those on other stations but noise on KAC is higher, so the P- and S-wave onsets are completely masked by noise. Note a successful detection on stations SKC and POC (second and third panels from top), where the P waves of the event is practically invisible. Vertical lines indicate the picks of the P- and S-wave onsets, the arrows correspond to the P-onset polarity.
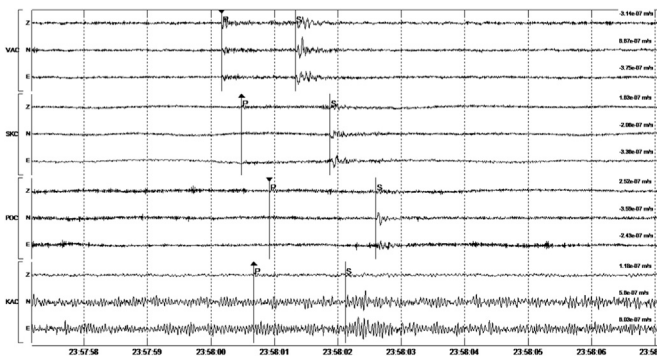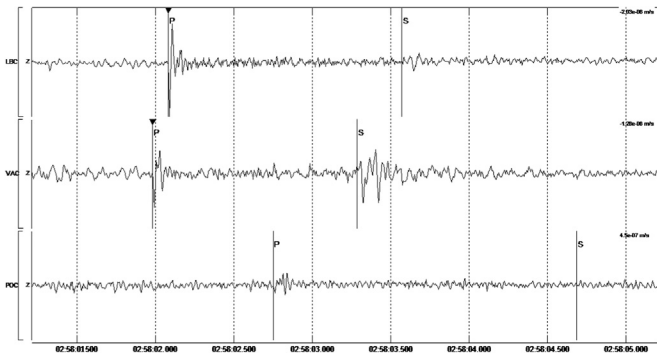

Fig. 17. A failed detection of the $M_L = 0.2$ event on station POC due to a very weak P- and S-wave amplitudes. Two more stations, LBC and SKC, with a successful detection of the event are added for comparison. Only vertical components are shown, all traces have the same scaling. It is obvious that the waveform amplitudes on POC are much weaker than at other stations, while the noise level is comparable. Weak amplitudes on POC are due two factors: the radiation pattern of the focus of the event and the larger epicentral distance of about 14 km.

demonstrated in these figures can be reduced substantially by using station coincidence. This means the similarity of all the stations is seen even if the trace is very noisy on some stations. The detection should be based on the coincidence of more stations in a time window of appropriate length. Then the event-like disturbance on only one station should be eliminated.
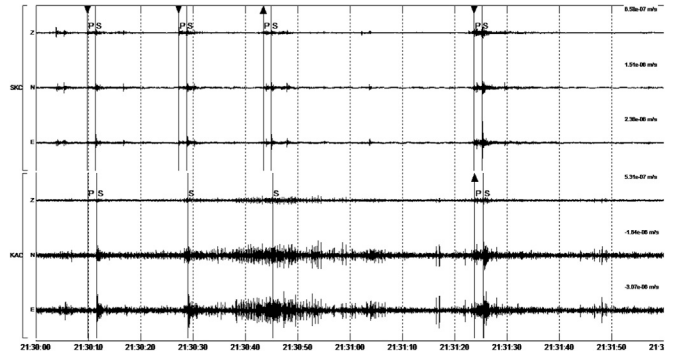
Fig. 18. Example of detection performance in the disturbed seismogram form at station KAC and in a seismogram with medium noise from station SKC. The seismograms include a sequence of four weak events. All the events were detected on SKC while the detection of the third event on KAC failed due to strong disturbances. The scale is the same for all traces. Note that it is not possible to find the P waves of the second and third event in the POC seismogram, even if the processing would be performed by a skilled interpreter.

Table 1
Number of detected events. At the automatic location and SLRNN network the numbers are: total number of detected events (TP+FP) and in brackets: events corresponding to manual detection (TP) and events not detected manually (FP).

Manual events	Automatic location (TP+FP)	Automatic location (FN)	SLRNN (TP+FP)	SLRNN (FN)
160	202 (145+57)	15	235 (153+82)	7

6.3. Comparison with automatic location

Here we present a comparison with automatic locations (Fischer, 2003) used for WEBNET data. We examined the automatic locations in the closely observed 5 h segment. In Table 1 we compare the number of manually detected events with the automatically detected events by location (Fischer, 2003) and the result of one of the best performing neural networks. Both automatic algorithms provide more events than manual processing which indicates that there are more events than could be seen in the full frequency range seismogram used by the interpreter. Both methods resulted in some FNs. The number of FNs is higher at the automatic location, while automatic event detection (SLRNN) has more false positives. Automatic location combines detections on more stations and automatically excludes some false positives having an excessively high residual of location while our result is one station detection and therefore some false positives might be due to disturbances.

7. Conclusions and future plans

The proposed algorithm based on SLRNN proved to be an appropriate tool for local event detection. Although the training process is time consuming and in our case required numerous trials to find an optimal or satisfactory solution, the implementation and routine use is quick and simple. We found that the *LIWE* value, which is important in creating the learning error weighting coefficients, causes the cost function to significantly affect the number of successful trials during the training process so we suggest values between 50 and 200 to obtain the best results. Training data must also be prepared with special care. Completeness of the P- and S-onset picks down to the lowest magnitudes possible for the whole training set of local events is of key importance for a proper SLRNN performance. Missing P- and S-onset picks result in an increase of both the number of FNs, and the

number of false event detections (of false positives). If the training P- and S-onset picks are not equally present on all stations, it is helpful to use joint training. If the picks are complete for the station and all events, individual training performs better.

Unfortunately, we were unable to reliably verify the method on the tested data from swarm 2011. The major problem is a large number of false detections, that should be verified. But we suggest that the sensitivity of the neural network is higher than manual detection so most of false detections are weak events below the noise level. However, the results should be evaluated correctly. That means inspecting manually and carefully spectrograms with station coincidence or use some automatic detector designed to work under the noise level.

To lower the number of undetected events the SLRNN automatic detection should be under the supervision of an experienced interpreter. Each false negative should result in renewed training of the SLRNN detector. A simple coincidence should also result in a lower number of FNs as well as undetected events.

When we verify reliably the detector performance, we prefer to use the SLRNN for other WEBNET stations which were deployed later in continual regime. We also intend to use 2013 and 2014 swarm-like activities in West Bohemia. In addition, we want to test our SLRNN detector using data from a local seismic network REYKJANET which is operated on the Reykjanes Peninsula in southwest Iceland. REYKJANET is similar in size and coverage to WEBNET but the local events from Reykjanes exhibit slightly more complicated waveforms.

Acknowledgments

References

Dietz, L., 2002. Notes on configuring binder_ew: Earthworm's phase associator, URL ⟨http://www.isti2.com/ew/ovr/binder_setup.html⟩.
Elman, J.L., 1990. Finding structure in time. Cogn. Sci. 14 (2), 179–211. http://dx.doi.org/10.1207/s15516709cog1402_1.
Fischer, T., 2003. Automatic location of swarm earthquakes from local network data. Stud. Geophys. Geodaetica 47 (1), 83–98. http://dx.doi.org/10.1023/A%3A1022251605990.
Gentili, S., Michelini, A., 2006. Automatic picking of p and s phases using a neural tree. J. Seismol. 10 (1), 39–63. http://dx.doi.org/10.1007/s10950-006-2296-6.
Hinton, G.E., 1989. Connectionist learning procedures. Artif. Intell. 40, 185–234, URL ⟨http://www.sciencedirect.com/science/article/pii/0004370289900490⟩.
Čermáková, H., Horálek, J., 2015. The 2011 West Bohemia (central europe) earthquake swarm compared with the previous swarms of 2000 and 2008. J. Seismol. 1–15. http://dx.doi.org/10.1007/s10950-015-9502-3.
Horálek, J., Fischer, T., Boušková, A., Jedlička, P., 2000. The western Bohemia/Vogtland region in the light of the webnet network. Stud. Geophys. Geodaetica 44 (2), 107–125. http://dx.doi.org/10.1023/A%3A1022198406514.
Institute of Geophysics, A. S. C. R., 1991. West Bohemia local seismic network, URL ⟨http://www.fdsn.org/networks/detail/WB/⟩.
Jordan, M.I., 1986. Attractor dynamics and parallelism in a connectionist sequential machine. In: Proceedings of the Eighth Annual Conference of the Cognitive Science Society, Elbraum, Hillsdale, NJ, pp. 531–546.
Kao, H., Shan, S.-J., 2004. The source-scanning algorithm: mapping the distribution of seismic sources in time and space. Geophys. J. Int. 157 (2), 589–594, URL ⟨http://gji.oxfordjournals.org/content/157/2/589.abstract⟩.
Le Bras, R., Swanger, H., Sereno, T., Beall, G., Jenkins, R., 1994. Global association. design document and user's manual. Technical report, DTIC Document.
Madureira, G., Ruano, A.E., 2009. A neural network seismic detector. Acta Technica Jaurinensis 2 (2), 159–170.
Michálek, J., Fischer, T., 2013. Source parameters of the swarm earthquakes in West Bohemia/Vogtland. Geophys. J. Int. 195 (2), 1196–1210, URL ⟨http://gji.oxfordjournals.org/content/195/2/1196.abstract⟩.
Narendra, K., Parthasarathy, K., 1991. Gradient methods for the optimization of dynamical systems containing neural networks. IEEE Trans. Neural Netw. 2 (March (2)), 252–262.
Sleeman, R., van Eck, T., 1999. Robust automatic p-phase picking: an on-line implementation in the analysis of broadband seismogram recordings. Phys. Earth Planet. Inter. 113 (1–4), 265–275, URL ⟨http://www.sciencedirect.com/science/article/pii/S0031920199000072⟩.
Swets, J., 1996. Signal Detection Theory and ROC Analysis in Psychology and Diagnostics: Collected Papers. Scientific Psychology Series. Lawrence Erlbaum Associates, Mahwah, New Jersey, URL ⟨https://books.google.cz/books?id=1vkMAQAAMAAJ⟩.
Tiira, T., 1999. Detecting teleseismic events using artificial neural networks. Comput. Geosci. 25 (8), 929–938, URL ⟨http://www.sciencedirect.com/science/article/pii/S0098300499000564⟩.
Wang, J., Teng, T.-L., 1995. Artificial neural network-based seismic detector. Bull. Seismol. Soc. Am. 85 (1), 308–319, URL ⟨http://www.bssaonline.org/content/85/1/308.abstract⟩.
Wang, J., Teng, T.-l., 1997. Identification and picking of s phase using an artificial neural network. Bull. Seismol. Soc. Am. 87 (5), 1140–1149, URL ⟨http://www.bssaonline.org/content/87/5/1140.abstract⟩.
Werbos, P., Oct 1990. Backpropagation through time: what it does and how to do it. Proc. IEEE 78 (10), 1550–1560.
Williams, R.J., Zipser, D., 1989. A learning algorithm for continually running fully recurrent neural networks. Neural Comput. 1 (June (2)), 270–280. http://dx.doi.org/10.1162/neco.1989.1.2.270.
Wiszniowski, J., Plesiewicz, B., Trojanowski, J., 2014. Application of real time recurrent neural network for detection of small natural earthquakes in Poland. Acta Geophys. 62 (3), 469–485.
Withers, M., Aster, R., Young, C., Beiriger, J., Harris, M., Moore, S., Trujillo, J., 1998. A comparison of select trigger algorithms for automated global seismic phase and event detection. Bull. Seismol. Soc. Am. 88 (1), 95–106. ⟨http://www.bssaonline.org/content/88/1/95.abstract⟩.
Withers, M., Aster, R., Young, C., 1999. An automated local and regional seismic event detection and location system using waveform correlation. Bull. Seismol. Soc. Am. 89 (3), 657–669, URL ⟨http://www.bssaonline.org/content/89/3/657.abstract⟩.
Zweig, M.H., Campbell, G., 1993. Receiver-operating characteristic (roc) plots: a fundamental evaluation tool in clinical medicine. Clin. Chem. 39 (4), 561–577.

Geophysical Journal International

Single Layer Recurrent Neural Network for detection of local swarm-like earthquakes—the application

Jana Doubravová [ID] and Josef Horálek

Institute of Geophysics, Czech Academy of Sciences, v.v.i., Boční II 1401, *14131 Prague, Czech Republic. E-mail:* doubravka@ig.cas.cz

SUMMARY

We present results of applying a local event detector based on artificial neural networks (ANNs) to two seismically active regions. The concept of ANNs enables us to recognize earthquake-like signals in seismograms because well-trained neural networks are characterized by the ability to generalize to unseen examples. This means that once the ANN is trained, in our case by few tens to hundreds of examples of local event seismograms, the algorithm can then recognize similar features in unknown records. The detailed description of the single-station detection, design and training of the ANN has been described in our previous paper. Here we show the practical application of our ANN to the same seismoactive region we used for its training, West Bohemia/Vogtland (border area Czechia-Saxony, local seismic network WEBNET), and to different seismogenic area, Reykjanes Peninsula (South-West Iceland, local seismic network REYKJANET). The training process requires carefully prepared data set which is preferably achieved by manual processing. Such data were available for the West Bohemia/Vogtland earthquake-swarm region, so we used them to train the ANN and test its performance. Due to the absence of completely manually processed activity for the Reykjanes Peninsula, we use the trained ANN for swarm-like activity in such a different tectonic setting. The application of a coincidence of the single-station detections helps to reduce significantly the number of undetected events as well as the number of false alarms. Setting up the minimum number of stations which are required to confirm an event detection enables us to choose the balance between minimum magnitude threshold and a number of false alarms. The ANN detection results for the Reykjanes Peninsula are compared to manual readings on the stations of the REYKJANET network, manual processing from Icelandic regional network SIL (the SIL catalogues by the Icelandic Meteorological Office) and two tested automatic location algorithms. The neural network shows persuasively better detection results in terms of completeness than the SIL catalogues and automatic location algorithms. Subsequently, we show that our ANN is capable of detecting events from various focal zones in West Bohemia/Vogtland although mainly the focal zone of Nový Kostel was used for training. The performance of our detector is comparable to an expert manual processing and we can state that no important event is missed this way even in case of complicated multiple events during the earthquake swarms.

Key words: Neural networks, fuzzy logic; Time-series analysis; Earthquake source observation.

1 INTRODUCTION

Continuously recording dense seismic networks produce a huge amount of data which the majority of them are redundant when processing seismic events. Seismic events, the useful part of seismic records for the most of seismological research, occur in just a small fraction of total recorded time even in episodic periods of increased seismic activity, for example, earthquake swarms. The target seismic

events recorded on seismic stations may differ in few orders of amplitude and they may have fairly different shape and frequency content. Therefore, the classical STA/LTA (Short-Term Average over Long-Term Average) or other power-based detector detects also various disturbances and with the aim to detect even weak earthquakes it results in a high number of false detections. Well-performing detection algorithm minimizes false detections while preserving all important information, that is, all target seismic events. In our case

we want to detect only local events with completeness magnitude as low as possible. Such reduction of data enables effective processing of events either manually or automatically. Event detection can be done in the time domain, frequency domain, by using polarization analysis or pattern matching (Withers *et al.* 1998) or using a combination of these approaches. Artificial neural networks (ANNs) can be used in any of the listed methods. ANNs are machine learning algorithms inspired by the functionality of the human brain. The basic unit called artificial neuron simulates the behaviour of a natural neural cell as described by biologists, that is, the weighted sum of inputs generates logical output. An interconnection of neurons into network enables to solve complicated problems and the goal of the learning process is to find optimum weights for each neural input to get the desired result. ANN concept has been used in seismological applications mainly for classification or discrimination purposes (Dowla *et al.* 1990; Romeo 1994; Tiira 1996; Esposito *et al.* 2006; Kuyuk *et al.* 2011; Mousavi *et al.* 2016), phase picking (Dai & MacBeth 1997; Wang & Teng 1997; Gentili & Michelini 2006; Gravirov *et al.* 2010; Ross *et al.* 2018) or earthquake prediction (Panskkat & Adeli 2007; Morales-Esteban *et al.* 2013; Reyes *et al.* 2013). Several neural network concepts have been used for seismic event detection. Most of the works utilized shallow networks based on multilayer perceptron with one hidden layer (e.g. Wang & Teng 1995, 1997; Tiira 1999; Gentili & Michelini 2006; Madureira & Ruano 2009), but recently even very deep neural networks have been successfully applied, namely Mousavi *et al.* (2018) combined 2-D convolutional neural networks and bi-directional LSTM cells in a deep network with 256 000 trainable parameters. Our neural network described in Doubravová *et al.* (2016) takes into account the frequency character of the waveform by using narrow-band filter bank, as well as the time domain using STA/LTA in each frequency band. A sufficiently long time window used for distinguishing target seismic events from disturbing signals is very important for successful event detection. We achieved sufficient time history consideration by using a recurrent neural network. Our novel architecture named Single Layer Recurrent Neural Network (SLRNN) consists of only one layer of neurons whose outputs are fed back as inputs in the next time steps, but the recurrent inputs are delayed by various samples (the number of trainable parameters was 408). That enabled to feed information of the history of the time-series together with an actual value at the input of the network simultaneously.

It can happen that some weaker events are not detectable in the recording of a single station—due to different locations of events, local noise or disturbances, the radiation pattern of earthquake source or even technical issues (see examples in Doubravová *et al.* 2016). Therefore our SLRNN uses multiple station detections, that is, the event detections on more stations of the network (as the human interpreters do) which increases the detection ability significantly. Most of the event detectors employed in seismological-observation practice need a special setting of parameters matching observation conditions in a particular area (e.g. local noise, frequency content of the target events and noise) to work properly. We developed our event detection method based on SLRNN as a part of the automatic processing of data from local seismic networks WEBNET and REYKJANET that are operated in two completely different tectonic areas: West-Bohemia/Vogtland earthquake-swarm region (Czechia, Central Europe) and Reykjanes Peninsula (South-West Iceland), which are characterized by swarm-like seismicity (see Section 2). The recordings of swarm activities usually contain sequences of many events tightly spaced in time or even overlapping and interfering. But such cases pose a problem for automatic algorithms and even experienced interpreters (specialists in manual processing).

Our aim is to select pieces of signal with events without an attempt to separate correctly the individual events. Our SLRNN detector has been trained on data from network WEBNET. In this paper we present detection results of this detector when applied to continuous recordings from both WEBNET and REYKJANET networks.

2 TARGET AREAS AND LOCAL SEISMIC NETWORKS

2.1 West Bohemia/Vogtland

West Bohemia/Vogtland (latitude $\approx$49.8°N to 50.7°N, longitude $\approx$12°E to 13°E) is situated in the western part of the Bohemian Massif, geographically in the border area between Czechia and Saxony. It is a unique European intracontinental area that exhibits simultaneous activity of various geodynamic processes. Seismic activity is characterized by frequent occurrence of earthquake swarms, the main-shock–aftershock sequences also occur there but very rarely. Persistent swarm-like seismicity clusters in a number of small epicentral zones that are scattered in the area of about 40 km × 60 km. However, larger swarms ($\sim M_L > 2.5$) cluster predominantly in the focal zone Nový Kostel (NK), which dominates the recent seismicity of the whole region; a few tens of thousands of events were recorded there within the last 27 yr. The swarms usually consist of several thousands of weak earthquakes and their duration is from several days to two months. Notable earthquake swarms in the last 35 yr occurred in 1985/86 (with the strongest event of magnitude $M_{Lmax} = 4.6$), 1997 ($M_{Lmax} = 2.9$), 2000 ($M_{Lmax} = 3.3$), 2008 ($M_{Lmax} = 3.8$), 2011 ($M_{Lmax} = 3.7$), 2017 ($M_{Lmax} = 3.2$) and 2018 ($M_{Lmax} = 3.8$); an exceptional M_{Lmax}=4.4 non-swarm activity occurred in 2014. The depths of foci in the whole area range from 5 to 20 km (e.g. Horálek & Fischer 2010) but depths between 7 and 12 km are typical of earthquake swarms and main-shock–aftershock sequences (Čermáková & Horálek 2015; Jakoubková *et al.* 2018). The region is well known by its fluid activity that is probably closely connected with the local swarm-like seismicity (e.g. Horálek & Fischer 2008; Fischer *et al.* 2017). For summarizing information about the area in question we refer to Fischer *et al.* (2014). Seismicity in the West Bohemia/Vogtland region has been monitored by the WEBNET network since 1991 (Institute of Geophysics 1991; Horálek *et al.* 2000; Fischer *et al.* 2010). At present, WEBNET consists of 24 stations covering the area of about 40 km × 25 km. 15 stations are broadband (equipped with Güralp CMG3-ESP sensors and Centaur digitizers by Nanometrics) with the frequency response proportional to the ground velocity from 0.03 to 100 Hz. Nine stations are short-period (LE3-D sensors and Gaia digitizers) with a flat frequency response 1.0 to 80 Hz. All the stations are operating in continuous mode with sampling frequency of 250 Hz. All 15 broad-band stations are streaming data in real time, while the short-period stations are storing data to memory cards. The amount of data is around 1.3 GB d^{-1} considering online stations only. Waveforms from the whole network including both online and offline stations result in approx. 2 GB d^{-1}.

2.2 Reykjanes Peninsula

The Reykjanes Peninsula, SW Iceland (latitude $\approx$ 63.8°N to 64.1°N, longitude $\approx$ 21.5°W to 22.3°W), is the onshore continuation of the Reykjanes Ridge which is a part of the mid-Atlantic Ridge. The Reykjanes Ridge separates the two major lithospheric plates, the Eurasian Plate to the east and the North American Plate to the west.

On the Reykjanes Peninsula the plate boundary extends from the southwest to the east and forms a pronounced oblique rift along the whole peninsula in length of about 65 km (Sæmundsson & Einarsson 2014). The plate motion rate on the Reykjanes Peninsula is about 20 mm yr^{-1} in E–W direction and about 5 mm yr^{-1} perpendicular to it (Geirsson *et al.* 2010). The plate boundary is flanked by a deformation zone of about 30 km width where strain is built up by the plate movements (Einarsson 2008). The Reykjanes Peninsula is one of the most seismically active parts of Iceland, especially at the microearthquake level. Swarm-like sequences and solitary events scattered along the plate boundary, both with magnitudes mostly of $M_L < 3$, represent a major part of seismicity on the peninsula. Large swarms took place there in 2000 (with the strongest event of magnitude $M_{Wmax} = 5.9$), in 2003 with $M_{Wmax} = 5.3$ and in 2013 with $M_{Wmax} = 5.0$ (Jakobsdóttir *et al.* 2002; Jakobsdóttir 2008; Einarsson 2014). Recently, two medium swarms with magnitudes $M_w = 3.8$ (in 2016) and $M_w = 4.1$ (in 2017) occurred. Prevailing depths of the foci on the Reykjanes Peninsula are between 2 and 5 km which is much shallower compared to the focal depths in West Bohemia/Vogtland. The Reykjanes Peninsula is a highly complex geophysical structure with the interaction between volcanic and tectonic activity (Sæmundsson & Einarsson 2014), most of the Reykjanes Peninsula surface is covered by lava. The crustal fluid activity on the peninsula is clearly manifested by several geothermal fields and geothermal systems (Axelsson *et al.* 2015). REYKJANET network (Horálek 2013) was established on the Reykjanes Peninsula in 2013 by the Institute of Geophysics and the Institute of Rock Structure and Mechanics of the Czech Academy of Sciences with know-how, technical and material support of the University of Uppsala, Icelandic Meteorological Office (IMO) and Iceland GeoSurvey (ÍSOR). REYKJANET is aimed at monitoring interplate swarm-like seismicity in South-West Iceland. It consists of 15 broad-band stations which cover the area roughly 40 km × 20 km along the plate boundary. The stations are equipped with the Güralp CMG 40-T sensors, which are placed in special vaults, and low-power Gaia digitizers. The frequency response is proportional to the ground velocity from 0.03 to 50 or 100 Hz. All the stations operate in the continuous mode with the sampling rate of 250 Hz. The stations are supplied from batteries which are recharged from solar panels combined with wind turbines which may increase a little bit ambient noise. All the stations store the data to high capacity memory cards. Data are downloaded once in three or four months and processed afterward. The daily amount of data is some 1.3 GB, similarly to online stream of WEBNET. In addition to the REYKJANET network, seven stations of Icelandic regional network SIL (currently, a total of 68 stations spread all over Iceland), operated by IMO, have been monitored seismicity on the Reykjanes Peninsula since 1990 (Böðvarsson *et al.* 1999). The frequency response of the SIL stations is proportional to the ground velocity from 0.2 to 40 Hz. The stations operate in the continuous mode with the sampling rate of 100 Hz. The SIL recordings are processed in IMO in near-real time by a service working 24 hrs a day.

3 DATA

The training procedure of our SLRNN detector has been described including the data used in our previous paper by Doubravová *et al.* (2016). Let us remind that two WEBNET data sets, (i) events of the 2008 earthquake swarm and (ii) disturbing signals of the year 2010 without swarm-like seismicity, were used to train the SLRNN;

manual *P*- and *S*-wave picks were used to define an event during the training process. The training set contained both isolated and overlapping multiple events. The 2011 swarm was used for testing of the detection results. This way trained SLRNN detector has been applied to continuous data from 15 online stations of WEBNET employed in a near-real time data processing, and to continuous data from all 15 stations of REYKJANET processed in a batch after data collection. The REYKJANET network operates 2500 km away from WEBNET in entirely different seismogenic area than West Bohemia/Vogtland. Nevertheless, the extent of both networks is similar ($\sim$ 40 km × 20 km) as well as sampling frequency (250 Hz) and a magnitude range of events, which implies that frequency content of target events is also alike. The WEBNET network has generally lower noise than REYKJANET due to installation in deep vaults and compact bedrock (compare the waveforms in Fig. 1). A rough estimate of the background noise level is 90 nm s^{-1} for REYKJANET and 20 nm s^{-1} for WEBNET, and despite the shallower depth of SW Icelandic hypocentres there is typically higher signal-to-noise ratio for WEBNET recordings. The REYKJANET network is expected to record stronger earthquakes up to magnitude M_L 5.0+. The detection results for the WEBNET continuous data have been evaluated by using the WEBNET catalogues and bulletins created by precise manual data processing. In the case of the REYKJANET data, the SLRNN detector has been applied to all 15 stations. The primary source of information about local seismicity is the SIL catalogues provided by IMO (Dr Gunnar B. Guðmundsson, IMO, personal communication, 2017) which contain seismic events from the whole region of South-West Iceland. We evaluate the performance of the detector by comparing the results with (i) manual processing by a skilled expert and (ii) with automatic algorithms, mainly PePin (Fischer 2003) which is used routinely to process the WEBNET data in near-real time. PePin uses polarization analysis to find candidate onsets of *P*- and *S*-wave phases which are then associated together to define events. A set of parameters must be tuned in order to achieve good reliability of the resulting events. The algorithm naturally fails to correctly associate phases in case of complex waveforms (e.g. multiple events) which results in omitting some of the events which can be sometimes of not negligible magnitude. On the other hand, if an event is found and located by PePin, the location usually differs from the manual location by few hundreds of metres and the detection threshold for the WEBNET data is as low as $M_L = -1$.

4 SINGLE STATION DETECTION—METHOD

4.1 Single Layer Recurrent Neural Network (SLRNN)

For detection of seismic events on each station in the seismic network we use the detection method described in detail in Doubravová *et al.* (2016). The description of the method in teh following text is brief and in some aspects simplified. The detector is based on ANN that consists of a set of neurons (Fig. 2). Each neuron sums weighted inputs and applies activation function (a sigmoid function simulating the step function in natural neuron cell is often used). Input $v_n = 1$ of the neuron is constant and serves as a threshold adjustment of the neuron:

$$V_i = g\left(\sum_{j=1}^{n} w_{ij} v_j\right). \tag{1}$$
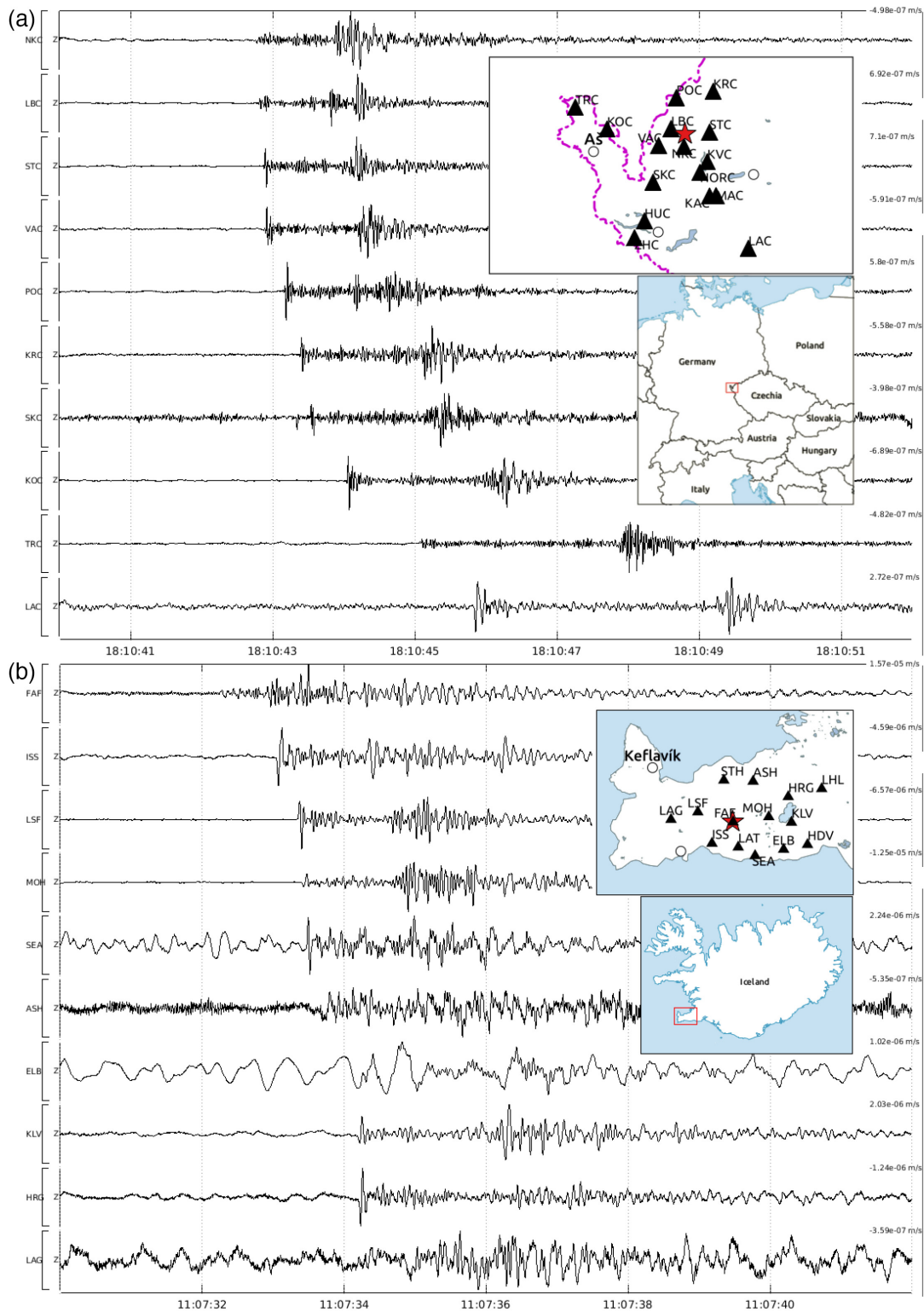
Figure 1. Waveform examples for (a) WEBNET (event of 2018 December 1) and (b) REYKJANET (event of 2017 July 26). Distribution of the WEBNET and REYKJANET stations is depicted in the insets (upper-right in panels a and b). Both events with local magnitude $M_L = 0.5$ (red asterisks in the insets) were located in the centre of the seismic networks at depths characteristic of West Bohemia/Vogtland ($d = 9.2$ km for WEBNET) and the Reykjanes Peninsula ($d = 2.5$ km for REYKJANET). Only vertical components of the ground-motion velocity filtered by bandpass (BP) of 1–40 Hz at 10 stations with the best signal-to-noise ratio are depicted. All traces are scaled according to the maximum of absolute value of displayed waveform. The maximum amplitude of each trace is on the right above the traces. It is apparent that the noise is generally lower at the WEBNET stations than at the REYKJANET ones and that the seismograms from the REYKJANET stations are more complex with longer codas which makes their interpretation more demanding.
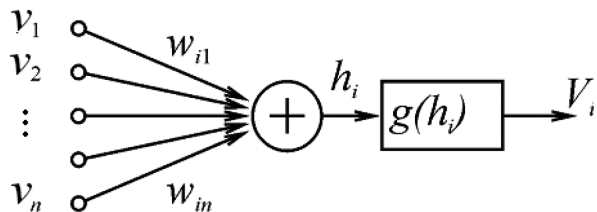
Figure 2. Single neuron scheme for ith neuron with inputs $v_1 - v_n$, weights $w_{i1} - w_{in}$, activation function $g(.)$ and output V_i.

The SLRNN consists of one neuron layer (parallel neurons) and the outputs of all neurons are fed back as inputs in the next time steps (see the scheme in Fig. 3). The outputs are applied to inputs with various delays which enables the network to get information throughout the history. After performing tests published in Doubravová *et al.*

(2016) we conclude that eight neurons' configuration with delays 1, 2, 4 and 8 samples is sufficient for event detection. Only three outputs of neurons are used as outputs of the whole network, the rest denoted as hidden neurons is used only for the feedback. We use output (V_1) as an event detection signal, output V_2 as P-wave detection and output V_3 as S-wave detection. The P- and S-wave detection outputs are auxiliary and they are used only during the training process.

The inputs of the neurons are STA/LTA ratios of seismic traces in different frequency bands. We decompose each of the three components of velocity record (Z, vertical; N, north; E, east) in narrow-band signals by a filter bank of nine half-octave filters from 0.6 to 40 Hz (frequency response of the filters is in Fig. 4), then we combine horizontal components together with computing size of horizontal resultant. The processing scheme is shown in Fig. 5. In
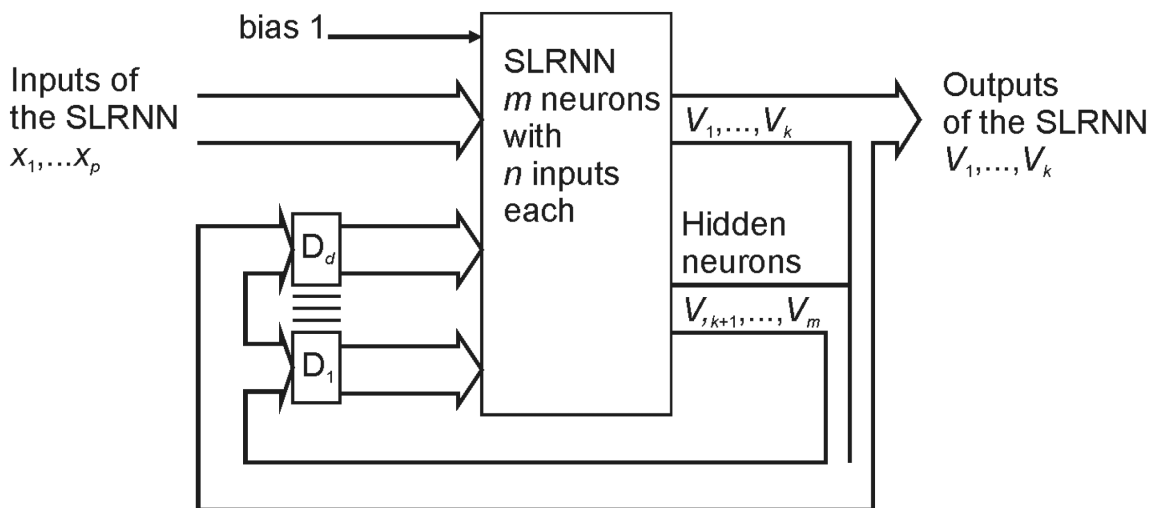
Figure 3. Single Layer Recurrent Neural Network with p inputs $x_1 \ldots x_p$, k outputs $V_1 \ldots V_k$ and $m - k$ hidden neurons with outputs $V_{k+1} \ldots V_m$. All outputs ($V_1 \ldots V_m$) are fed back as the inputs with d delays $D_1 - D_d$.

Figure 4. Frequency response of half octave filters used for preprocessing of inputs for SLRNN.

Figure 5. SLRNN inputs processing scheme.

Figure 6. Learning example for two consecutive events. First one is stronger with manual reading of both, *P*- and *S*-phase, the latter one has *S*-wave reading only; (a) seismic traces from top vertical, north, east component of the ZHC station from 2008 October 8, (b) expected outputs, (c) learning coefficient function in logarithmic scale.
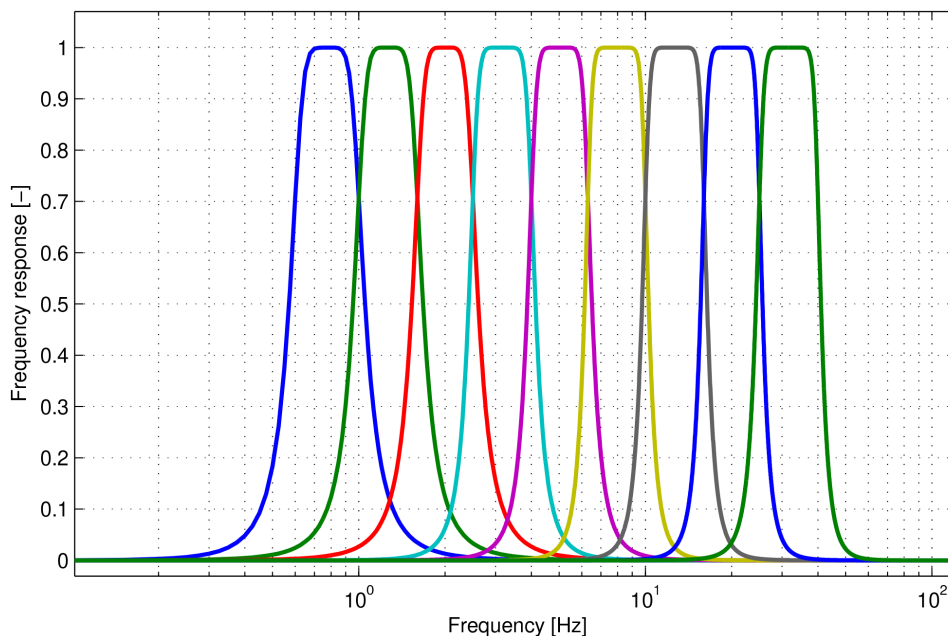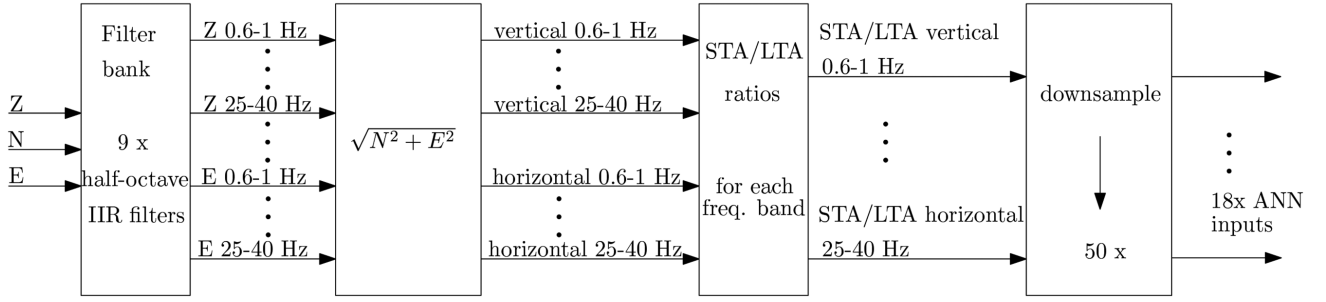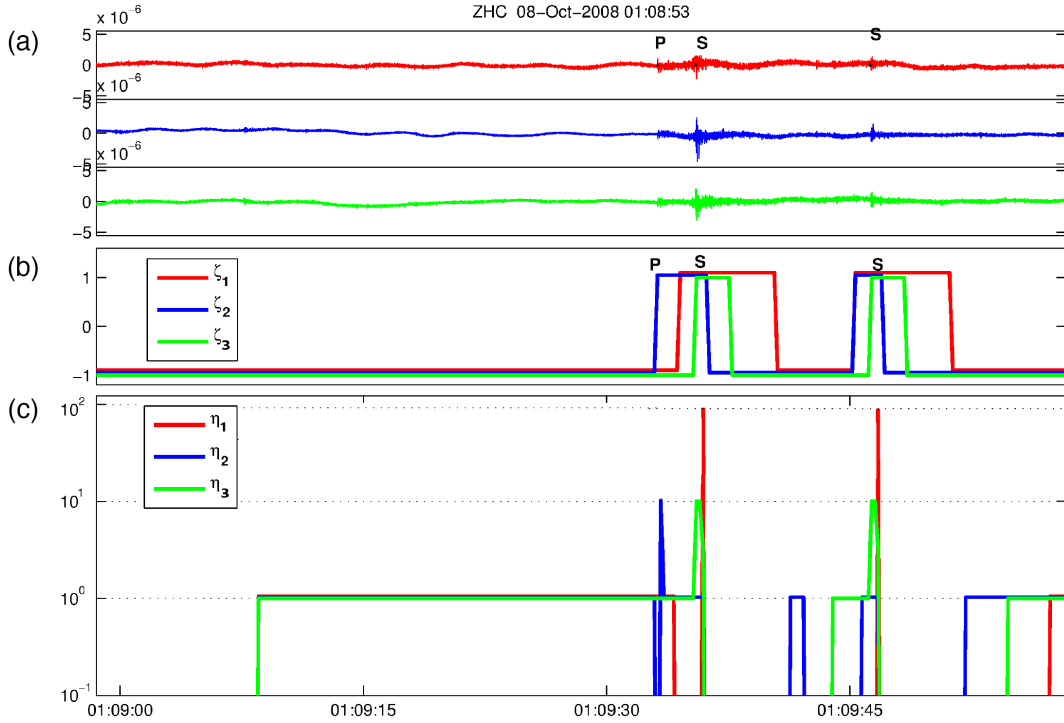
the next step we compute STA/LTA ratios and downsample the resulting signal. The original sample rate is then decimated to 5 Hz which is a compromise between the acceptable computational load and a good separation of individual waves.

4.2 Training and tests

The training process aims to find optimum neuron weights to get the desired functionality. We use supervised learning which means that we define outputs for a set of training examples and adjust the weights to get the best possible fit between desired and actual output weighted by a learning error weighting function η_i. As mentioned before, we use only three neuron outputs; that is, we define three expected outputs: $\zeta_1(t)$ - event detection; $\zeta_2(t)$ - *P*-wave detection; $\zeta_3(t)$ - *S*-wave detection. The cost function with the application of the weight decay regularization (after Hinton 1989) is defined as

$$E = \sum_t \sum_{i=1}^3 \eta_i(t)\left[\zeta_i(t) - o_i(t)\right]^2 + (1 - \gamma)\sum_{i=1}^m \sum_{j=1}^n w_{ij}^2, \qquad (2)$$

where γ is the regularization parameter, ζ_i is the *i*th expected output, o_i is the *i*th actual output and w_{ij} are weights for all *n* inputs of each of *m* neurons (in our case that means 18 direct inputs, 32 feedback inputs, 1 constant threshold input for each of the 8 neurons; in total we are searching for 408 weights). We apply the Back Propagation Through Time algorithm (Werbos 1990) which is a gradient-based cost function minimization method. That means we need to perform a number of minimization attempts to find the best set of weights (for each training setting we performed 2000 of training trials). The training data were randomly divided into an actual training set (80 per cent of data) and the validation set (20 per cent of data, not used for training). Each step of the training process reduces the cost function of the training set and in addition computes the cost function of the validation set. As long as the cost function of the training set and the cost function of the validation set decrease, the training continues. When the cost function of the validation set starts to increase, the training is stopped. This prevents the overtraining of the network - the case when the network perfectly detects the training events but fails to recognize other events well (for more information refer to Doubravová *et al.* 2016).
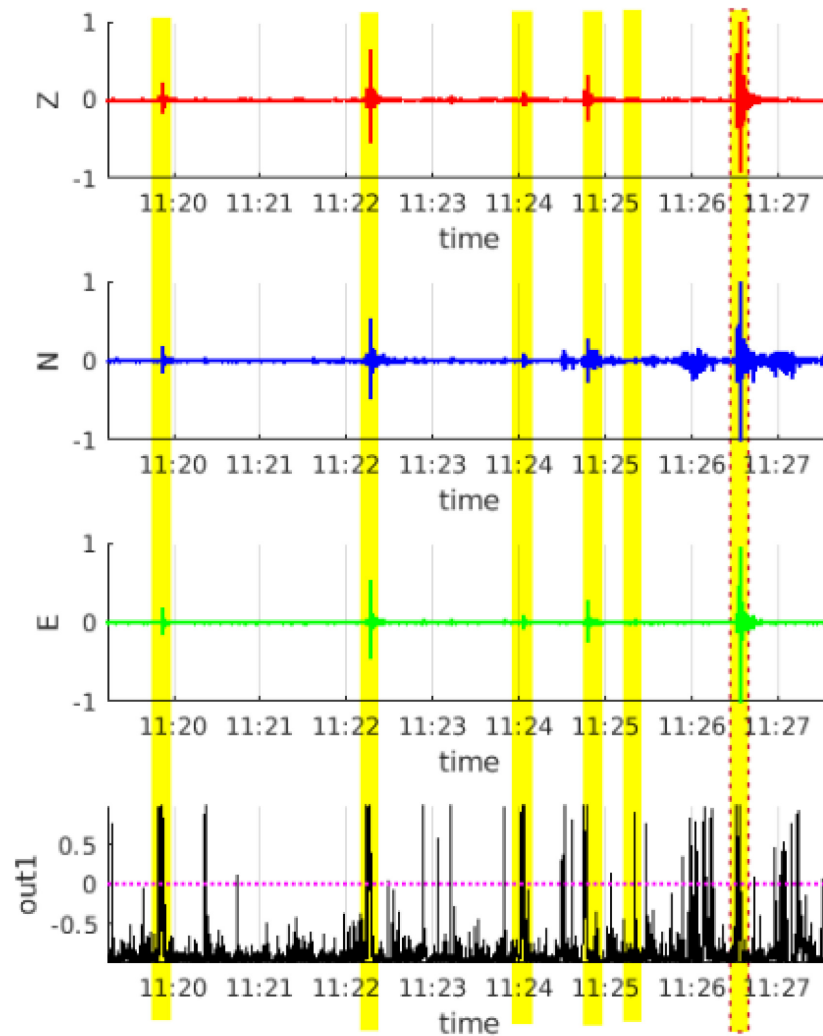
Figure 7. Example of the single-station detection. Seismogram from KLV station (2017 June 5, 11:20 to 11:27 UTC) filtered by BP of 1–40 Hz and detection output (always in range between −1 and 1). From the top: vertical, north, east component of velocity record, detection output of neural network. Yellow stripes denote seismic events (after coincidence), the strongest event marked by red dashed line is an event in SIL catalogue ($M_L = 0.9$). The detection threshold (indicated by the purple dotted line) is exceeded even in between the events.

For detection of local seismic events we need to emphasize the importance of event detection output right after *S*-wave onset. This is achieved by a much higher value of η_1 near the *S*-wave arrival (Fig. 6c). After testing (for details and test performed see Doubravová *et al.* 2016) we chose the most important point called LIWE to be 100.

During the training of the individual stations we achieved a good number of true positive rate (TPR) and true negative rate (TNR) compared to manual readings (for the best trained SLRNN TPR = 99.8 per cent and TNR = 78 per cent; that means 22 per cent false alarms). We inspected the results manually and found some false alarms to be small events omitted by manual processing. Some of the stations failed to detect events due to higher noise on the site, due to radiation pattern of a particular event, or in case of masking the waveform by the coda of the previous event. The proposed solution to this imperfection was to make use of the whole network of stations together. The coincidence of event-like waveforms on several stations in the network is crucial for successful and reliable event detection.

5 MULTIPLE STATION DETECTION—COINCIDENCE

In order to reduce the number of false detections as well as the number of undetected events due to higher signal-to-noise ratio we search for detection on other stations in the network to confirm or discard the event detection. Fig. 7 depicts three component velocity record and corresponding detection output. The detection is set whenever the detection output exceeds a certain threshold. The yellow stripes denote seismic events and one can see there are detections also in between the event stripes.

The proposed algorithm first scans all detections (detection output above zero) on all stations of the network and checks if there is a detection on a sufficient number of stations in the selected time window (we set it to 5 s with respect the size of the networks). In the next step we combine the detections together to make time intervals for events (see example in Fig. 8). As a result we define time segments containing useful information. Multiple overlapping events, especially during a swarm, lead to one time interval containing more events.
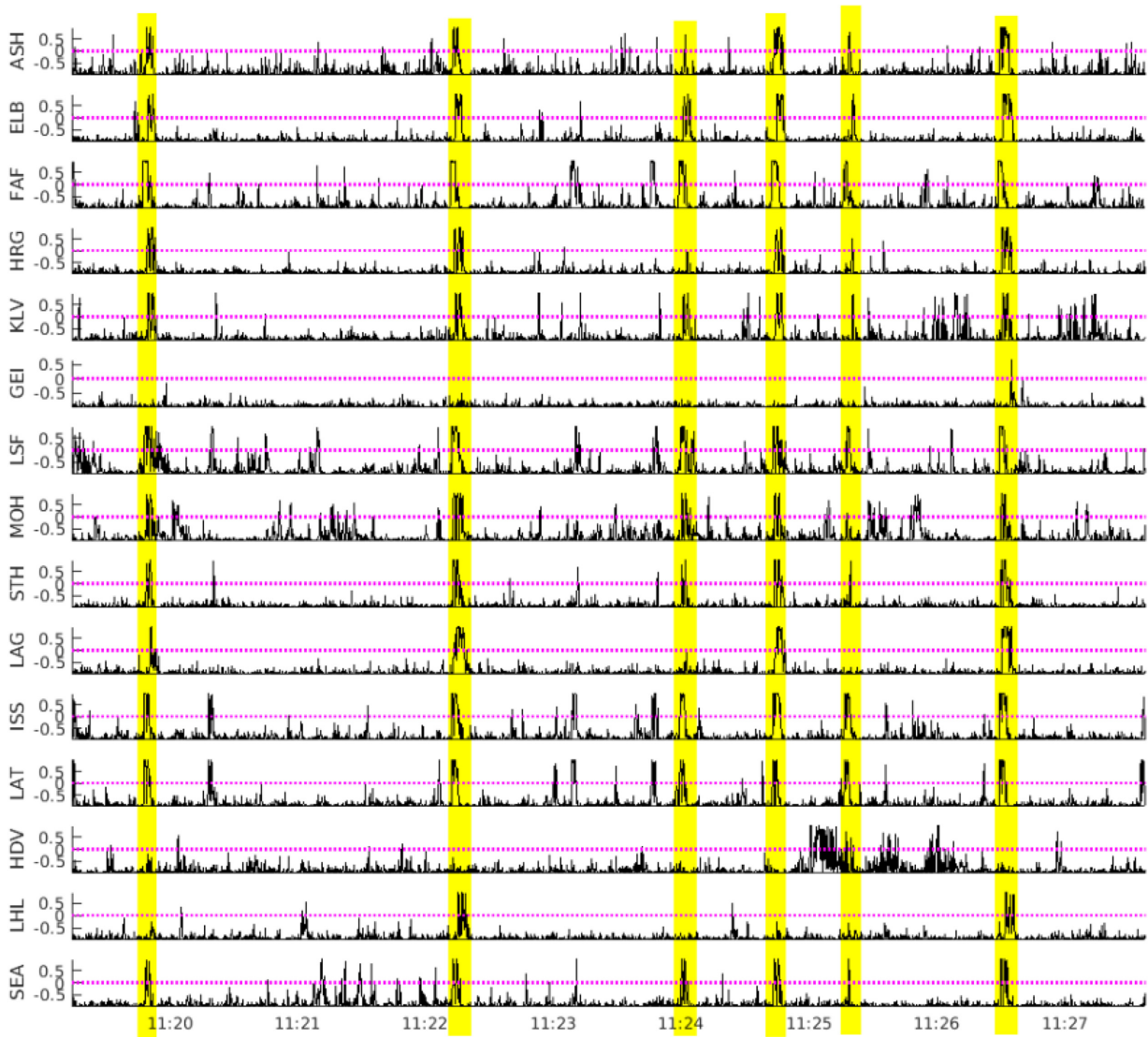
Figure 8. Example of the coincidence detection. Detection outputs of all 15 stations of REYKJANET, detection on at least six stations required. The same time segment as in Fig. 7.

The number of stations, which are needed to declare an event, is closely related to the number of false detections. Additionally, too many stations required might cause loss of weaker events. Fig. 9 shows an example of a coincidence of four and six stations and their comparison with the events detections performed manually (by the experienced interpreter). If we compare the detection results of the four- and six-station coincidence with the manual ones, it can be seen that the six-station coincidence detects all the manually identified events correctly while four-station coincidence detects also false events or events which are not interpretable (three cyan stripes which do not coincide with the yellow ones). Moreover, four station coincidence detecting more events which are merged if they overlap, produce longer time windows for events (broader stripes in Fig. 9). Two clearly separated event detections in six-station coincidence may become one longer event detection in case of four-station coincidence (note the end of the record where two yellow events become one longer cyan event). For both networks—WEBNET and REYKJANET—the coincidence of six stations seems to be the best option (see Tables 2 and 3 in Section 6.3).

6 APPLICATION TO DATA FROM LOCAL SEISMIC NETWORKS

6.1 Evaluation of results

The objective measures of a detector would be TPR (also called sensitivity or recall) and PPV (positive predictive value, also called precision). To estimate these quantities one need to calculate the number of correctly detected events (TP, true positives), undetected events (FN, false negatives) and false alarms (FP, false positives):

$$\text{TPR} = \frac{\text{TP}}{\text{TP} + \text{FN}} \tag{3}$$

$$\text{PPV} = \frac{\text{TP}}{\text{TP} + \text{FP}}. \tag{4}$$

In an attempt to automatically compare manual catalogue to detections provided by the SLRNN we faced a problem with many weak events being missing in the manual catalogue correctly

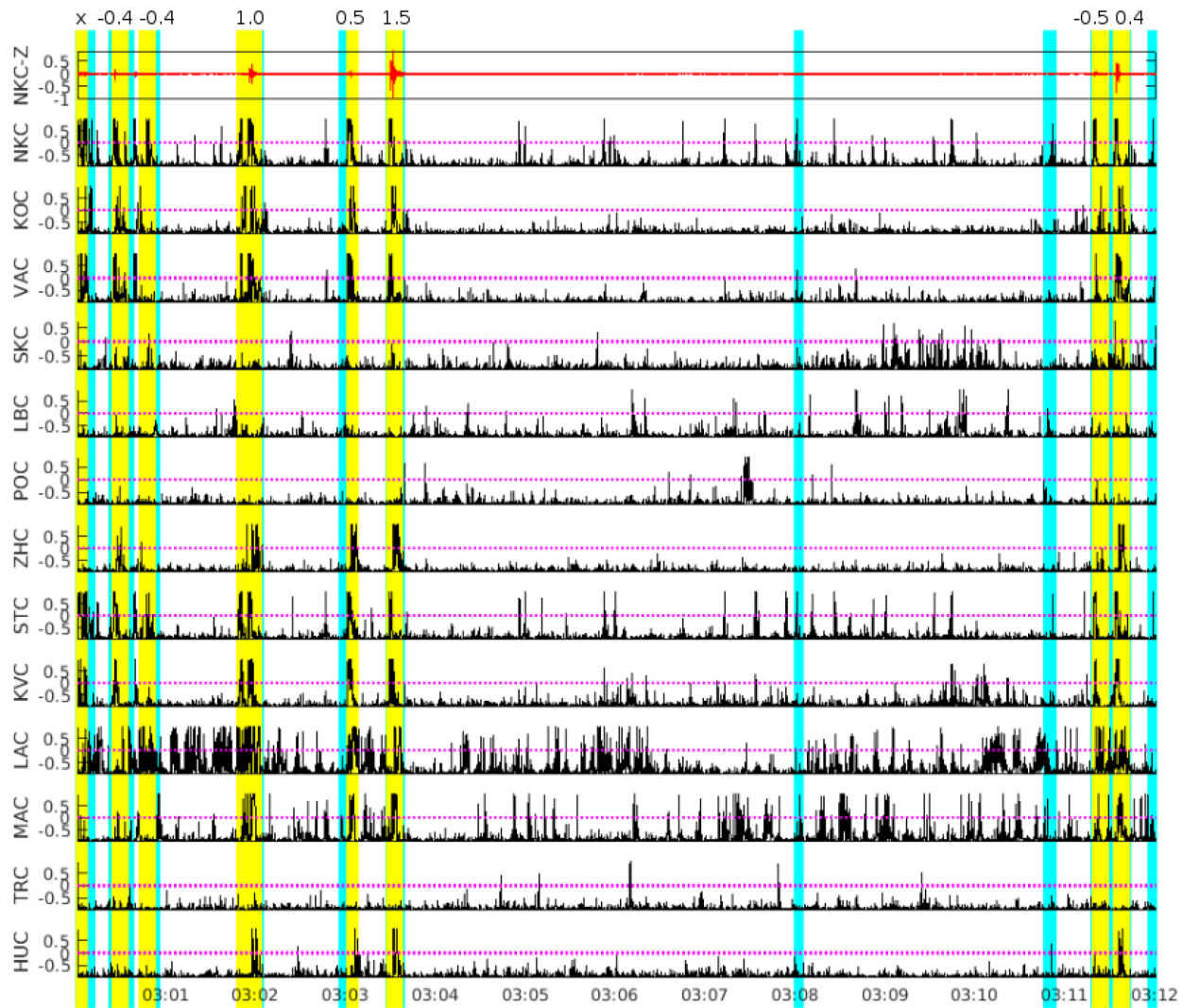**Figure 9.** Example of the detection coincidence for four (cyan) and six (yellow) WEBNET stations. Red trace above is the vertical component of seismogram from NKC station from 2018 August 24 3:00–3:12 UTC. All events in yellow were also detected manually, magnitudes M_L (from −0.5 to 1.5) are given above the yellow stripes. The first detected event in the seismogram is a multiple event consisting of several weak overlapping events, therefore the magnitude is not assigned (x sign is printed instead).

detected by the SLRNN. After all, the only reliable method to evaluate the correctness of each detection is to inspect it manually (Table 4). However, precise manual processing revealed also few weak events undetected by the SLRNN (usually with $-1 < M_L < -0.5$). Our goal is to get complete catalogue down to $M_L = 0$ for WEBNET and $M_L = 0.3$ for REYKJANET. The smaller events will never be complete due to lower signal-to-noise ratio and are often unsuitable for further processing either.

In practice, we need to reduce the amount of data for further processing as much as possible, in other words to remove redundant data from the continuous recordings. On the other hand, if the selected time segment with a seismic event is few samples longer or shorter then it does not make a difference. In case of overlapping events during the seismic swarm, we joined detections together and therefore simply counting a number of detections does not correspond to the number of detected events. In case of a very sensitive network with low threshold or little coinciding stations, many swarm events blur into long time segment. The useful information is preserved but the reduction of data is less effective.

6.2 Application to REYKJANET

A potential ANN trained on the South-West Iceland data from REYKJANET poses quite a big problem because of the absence of complete catalogues/bulletins from the REYKJANET network which would be necessary to train the ANN. It is because of the REYKJANET recordings that have not been fully processed in detail like the WEBNET ones. To create relevant bulletins from the REYKJANET stations by manual processing of continuous recording would be extremely time-consuming, requiring an experienced specialist. Consequently, we mostly use the SIL catalogues provided by IMO for the REYKJANET-data analysis. But there are more detectable local events in the REYKJANET seismograms than those given in the SIL catalogues because REYKJANET is an evidently denser network (15 stations) than a regional network SIL including seven stations in the area concerned (Fig. 10). Therefore, an application of the neural network trained for the West Bohemia/Vogtland data (WEBNET) to data from South-West Iceland (REYKJANET) has been a challenging task. We took one of the best-performing SLRNNs as tested for WEBNET and applied it to
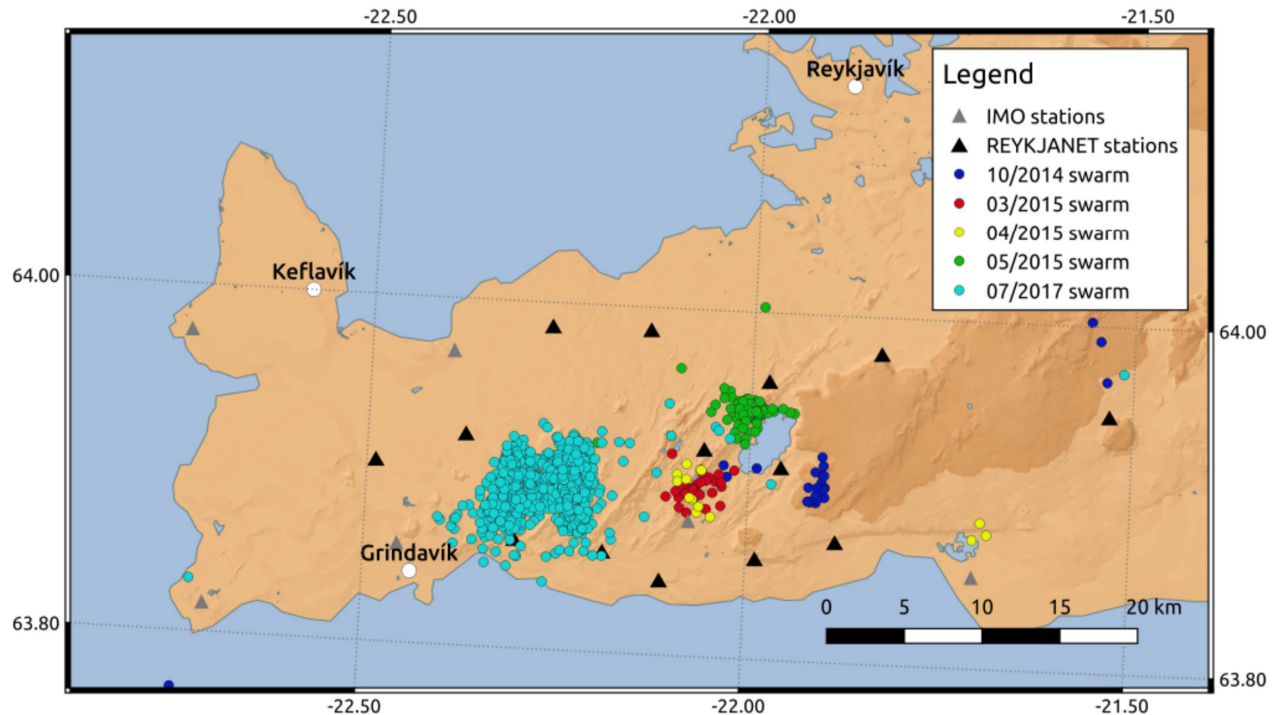
Figure 10. Map of Reykjanes Peninsula. Black triangles, REYKJANET stations; grey triangles, IMO stations; circles, epicentres of analysed earthquake activities. Blue circles, 2014 October 30–31 ($M_{Lmax} = 2.8$); red circles, 2015 March 31 ($M_{Lmax} = 2.2$); yellow circles, 2015 April 28–30 ($M_{Lmax} = 1.6$); green circles, 2015 May 29–30 ($M_{Lmax} = 3.5$); cyan circles: 2017 July 26–28 ($M_{Lmax} = 3.9$).

Table 1. Number of events for all analysed Reykjanes activities.

	ANN	SIL	Antelope	PePin	Manual (above $M_L > 0$)
(i) 30–31 Oct 2014	112	37	30	9	N/A
31 Mar 2015	216	30	37	29	N/A
28–30 Apr 2015	125	23	9	23	N/A
29–30 May 2015	937	167	34	25	N/A
(ii) 26 June 2017 11:00–12:00	124	56	N/A	N/A	281
(iii) 6–12 June 2017	184	34	N/A	N/A	64

the REYKJANET data. Since the deployment of the REYKJANET network in 2013, the seismicity on the Reykjanes Peninsula has typically been on a microearthquake level (magnitudes $M_L < 3$) except two earthquake swarms in October 2013 (immediately after putting the REYKJANET stations into operation) with $M_{Lmax} = 4.8$ and in July 2017 with $M_{Lmax} = 3.9$ ($M_{Wmax} = 4.1$), and few weaker swarm-like episodes with magnitudes up to $M_{Lmax} = 3.5$. The swarms in October 2013 occurred on the tip of the peninsula out of the REYKJANET network. We analysed in detail the detection results for (i) four weak activities from the period 2014–2015, (ii) an intensive $M_{Lmax} = 3.9$ swarm of July 2017 and (iii) scattered background seismicity on the Reykjanes Peninsula in June 2017 (for basic data and locations of the analysed activities refer to Table 1 and Figs 10 and A3). The SIL catalogue is the primary reference for evaluation of the SLRNN-detection results for both (i) and (ii). Besides, we used a catalogue of the event detections produced by PePin automatic algorithm (Section 3) and Antelope software package (by Boulder Real Time Technologies, Ltd.) that

were applied to the REYKJANET data of the activities given in (i), and a detailed bulletin of the 2017 swarm containing manual onset picks from all the REYKJANET stations.

(i) First, we compared the total number of detected events by the SIL processing, PePin algorithm, Antelope software and SLRNN (also denoted as ANN) in the individual weak activities. The Antelope automatic location procedure uses weighted STA/LTA phase detections (mainly *P*-wave phases are correctly picked). The PePin algorithm uses polarization analysis for event detection. In the first step the *S*-wave arrivals (which are often clearly polarized) are identified then they are associated with matching *P*-wave arrivals in the given time window, finally the event is localized. However, in case of a false event location (e.g. due to the incorrect association of the *P*- and *S*-wave arrivals) the event is omitted in the catalogue (for more information about the PePin detector see Fischer 2003). The comparison of the SIL, Antelope, PePin and ANN catalogues is depicted in Fig. 11. It is apparent the number of events detected by SIL, PePin and Antelope is comparable for all the activities, while the number of detected events by the SLRNN is about five times higher. We manually checked one of the activities with a reasonable number of events—the mini-swarm of the 2015 March 31. In total, 30 events have been listed in the SIL catalogue ($M_{Lmax} = 2.2$), 37 were located by Antelope and 28 by PePin.

Inspecting the events manually, we found out none of the 'catalogues' (SIL, Antelope and PePin) to have been a complete subset of another one; each catalogue contained some unique events which were missing in the other two catalogues (see Fig. A1). The SLRNN detector provided 217 events including all the detected events given in the SIL, PePin and Antelope catalogues. Fig. A1 represents the comparison of detected/undetected events from each catalogue (SIL, PePin and Antelope) with those in the other two catalogues and with the SLRNN detections. By combining the SIL,
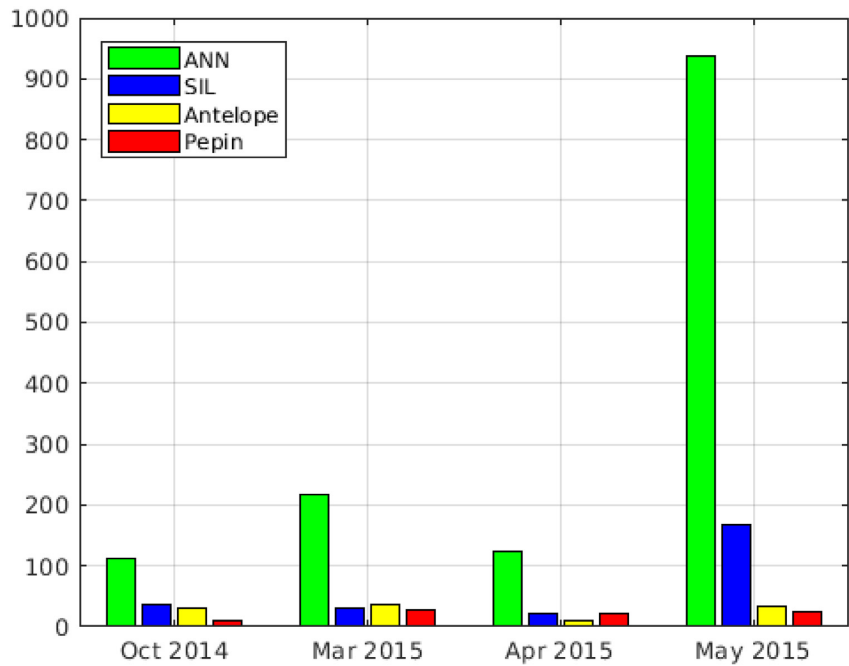
Figure 11. Number of events in analysed microswarms on the Reykjanes Peninsula.
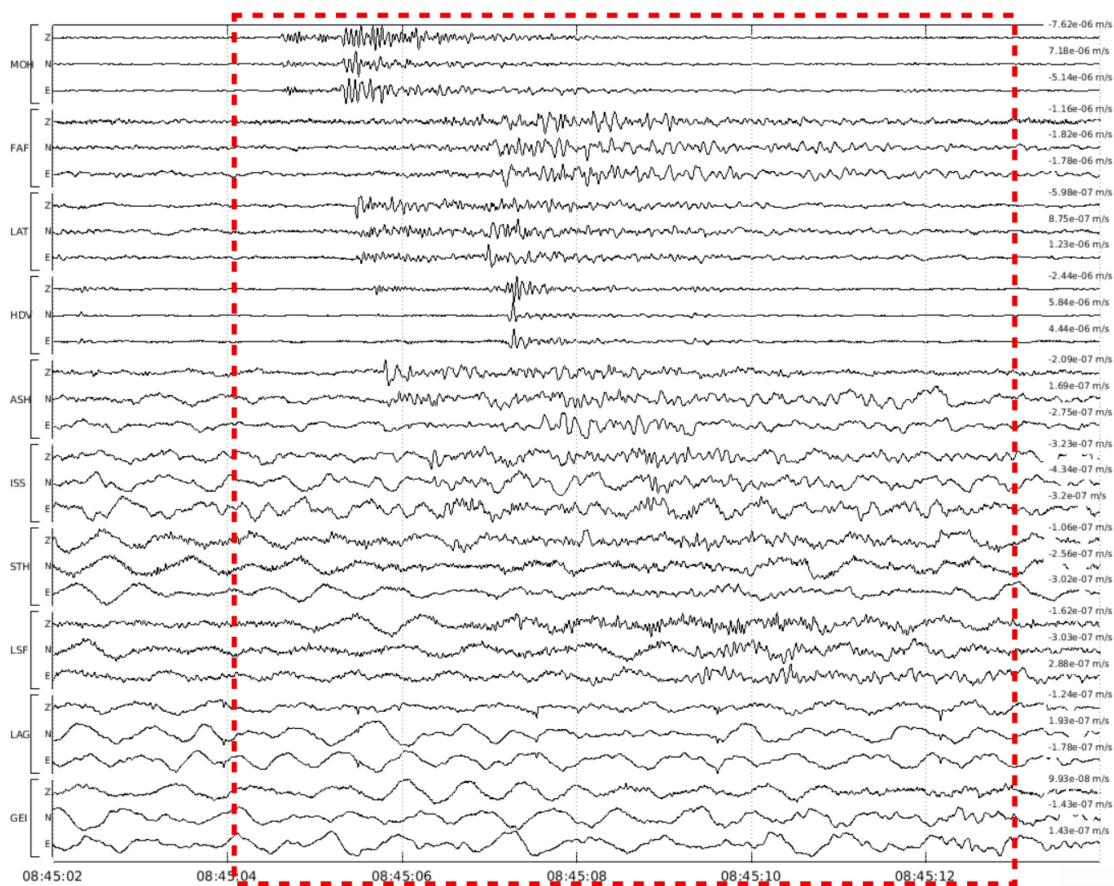
Figure 12. REYKJANET seismograms of one of the weakest events ($M_L = -0.6$, roughly estimated) of 2015 March 31 detected by the SLRNN with six-station coincidence. 10 nearest stations (sorted by the epicentral distance) are shown. It is evident that the event is recognizable on the five nearest stations only, on the remaining stations its 'useful' signal is buried in noise. The event (its detection) is characterized by the maximum amplitude over all components of all stations in the whole detection time window (marked by dashed red line). Three component ground-motion velocity seismograms are filtered by BP of 1–40 Hz. The number above each trace gives the maximum amplitude of the ground-motion velocity in the displayed period.
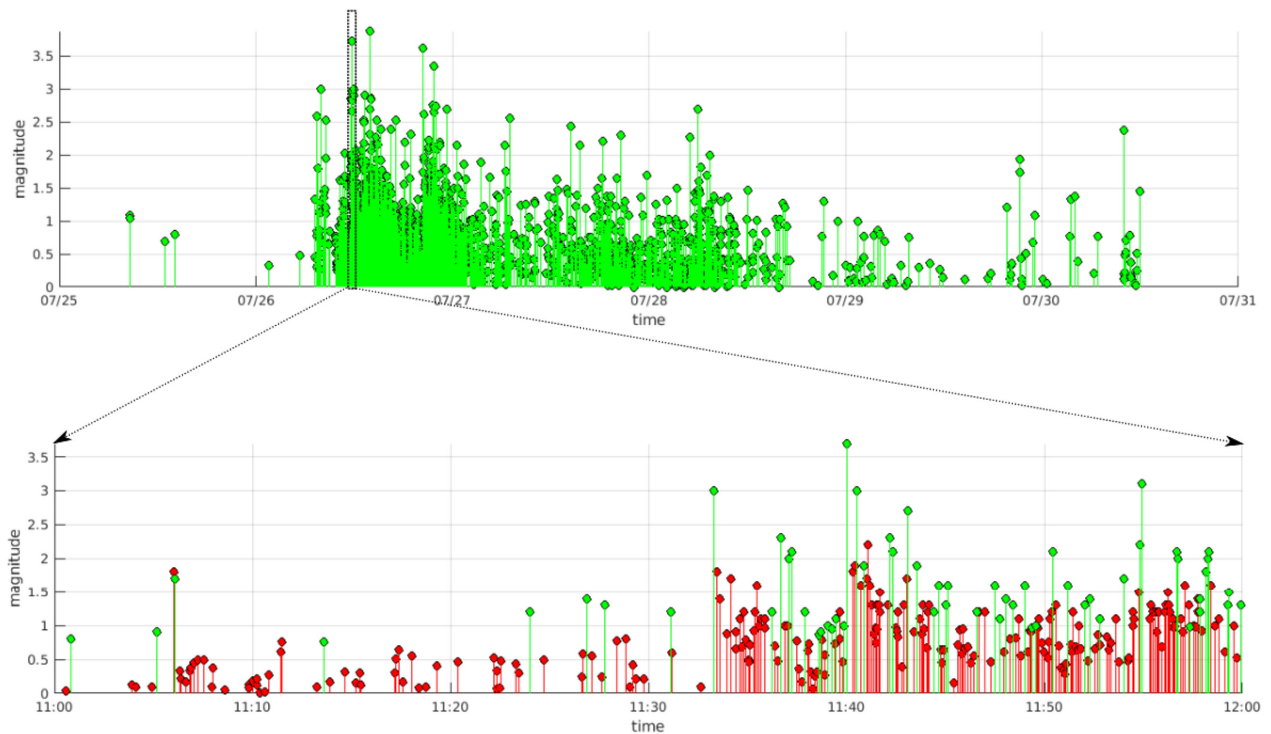
Figure 13. Magnitude-time distribution of the 2017 Reykjanes seismic swarm, only events with magnitude $M_L \geq 0$ are considered. Upper plot: the whole activity according to the SIL catalogue; lower plot: 1 hr segment around the second strongest shock of $M_L = 3.7$ (2017 June 26, 11:00 to 12:00 UTC). Red points: events of the manually created REYKJANET catalogue which were missing in the SIL catalogue.

PePin and Antelope catalogues we obtained 51 real events with minimum magnitudes $M_L \approx 0$. Our SLRNN detected all of them and in addition to that about three times more weak events. But many of the small detected events are unsuitable for further processing because locating of such events would be unreliable due to unclear *P*- and *S*-wave onsets. Nevertheless, Fig. 12 demonstrates that even the small events are true local seismic events, even they are on most of the stations buried in the noise. We believe that further automatic processing leading to a location would reject some of these event detections due to insufficient number of good quality phase readings.

Fig. A1 also point to the imperfect performance of the PePin algorithm because it missed two strongest and several other weaker events in the March 2015 activity (Fig. A1, top diagram in the figure). The PePin algorithm, which defines an event by associating the *P*- and *S*-wave phases, might have failed due to more complex waveforms resulting in the false association of the *P*- and *S*-wave phases (Section 3). Let us note that PePin has been routinely used in a near-real time processing of data from WEBNET.

(ii) A prominent earthquake swarm in July–August 2017 M_{Lmax} = 3.9 was fairly rapid. Most of the seismic moment released during 2 d from July 26 to 28 (Jakoubková 2018), more than 1500 M_L > 0 events have been listed in the SIL catalogue for these days (Fig. A2). We concentrated on 1 hr of the swarm activity on July 26, from 11:00 to 12:00 UTC, that included the second strongest earthquake of the swarm (M_{Lmax} = 3.7). This segment contains both calm and turbulent phase of the swarm (Fig. A2). We performed detailed manual processing of the continuous seismograms with the assistance of an experienced expert who found 441 events in total out of which 281 were reliably located with magnitude above M_L > 0. Then we compared the manually obtained events with detections provided by the SLRNN and with the list of events in SIL catalogue.

There were 56 events in SIL catalogue and 124 event detections indicated by SLRNN (due to the turbulent nature of the swarm the detections often included more events). The results are shown in Figs 13 and A2. All of the manually picked events were correctly detected by the SLRNN and only one false SLRNN detection was found.

(iii) In order to prove the SLRNN ability to detect various local events on the whole Reykjanes Peninsula we selected a time segment containing scattered background non-swarm seismicity only (Fig. A3). We selected one week, 2017 June 6–12, where the seismic events included in the SIL catalogue were scattered in the whole area covered by the REYKJANET network. The SLRNN detected 183 events, 34 events of which had been listed in the SIL catalogue and no event present in SIL catalogue was missed. By manual processing of the waveforms we were able to confirm reliably 37 new events which we located and for which we estimated M_L ranging from −0.5 to 1.3 (30 above M_L= 0). Remaining 112 events were mostly unfit for location due to insufficient number of clear *P*- and *S*-wave onset picks or they were false alarms (or real events hidden in ambient noise).

6.3 Application to WEBNET

The WEBNET data are routinely processed by the PePin software (Fischer 2003) which provides good automatic locations in near-real time. The events located by PePin are then re-interpreted by manual processing (adding or refining picks, location by NLLoc with more precise velocity model, and in case of more significant activities some more advanced analyses). In order to get good location residuals, the PePin software is set up to use only eight nearest stations around the NK focal zone (the central part of the network) which contains more than 90 per cent of the total seismic moment
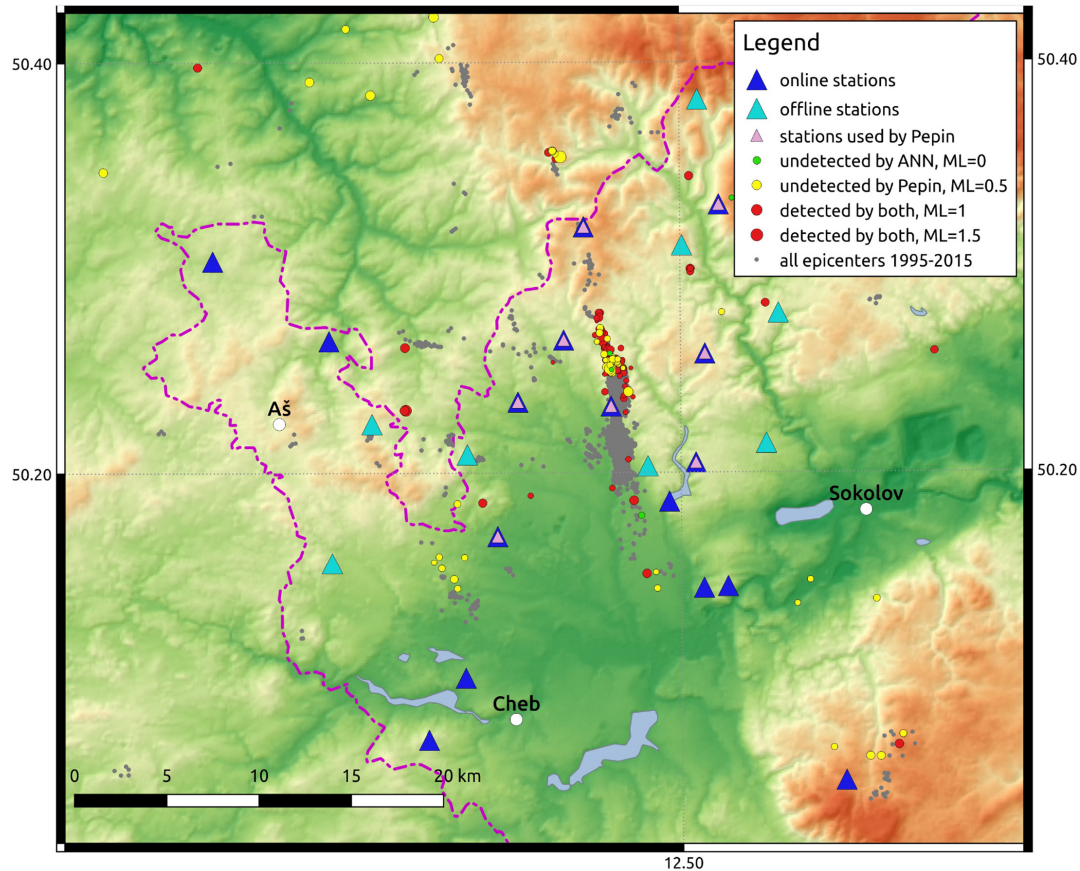
Figure 14. Detection results for local events during November and December 2018 in the map of West Bohemia/Vogtland. Blue triangles, online WEBNET stations; cyan triangles, offline WEBNET stations; pink triangles, stations used for near-real time data processing by the PePin algorithm; grey dots, epicentres of events in time period 1995–2015; red circles, events located manually and by PePin and also detected by SLRNN; yellow circles, events located manually and detected by SLRNN (not located by PePin); green circles, events located manually and by PePin (not detected by SLRNN). Diameter of circles is scaled according to local magnitude.

released in the whole seismoactive area since 1991 (Jakoubková *et al.* 2018). This unfortunately may result in omitting events outside the main focal zone. During November–December 2018 we compared in detail all events detected by the SLRNN (running in a pilot operation) with manual readings and with the PePin results. In this period the local seismicity was extremely low with maximum magnitude $M_{Lmax} = 1.3$. We took into account only events with magnitude above $M_L = -0.5$, which resulted in 183 ones. The results of our analysis are summarized in Table 2 and Table 3 and displayed in Fig. 14. There are 106 events of $M_L > -0.5$ successfully detected by both SLRNN and PePin (red circles in Fig. 14), 73 events were successfully detected by the SLRNN only (they are missing in the Pepin catalogue, yellow circles in Fig. 14), and four events missing in in the SLRNN list were successfully located by PePin (green circles in Fig. 14). It is worth mentioning that significant part of the undetected events by the PePin algorithm are located outside the main focal zone of Nový Kostel. Tables 2 and 3 provide more detailed statistics including the comparison of the detection results of the SLRNN with coincidence of six and four stations. The six-station coincidence, which we found to be an optimum for the West Bohemia/Vogtland earthquake-swarm region, results in omitting four events which were located both manually and by PePin; all four undetected events have magnitude $M_{Lmax} \approx -0.5$. If we use four-station coincidence then all manually located events are successfully detected by the SLRNN but the number of

Table 2. Number of events November–December 2018

Data set	Number of events
Manual events	317
SLRNN detections—6 stations coincidence	392
SLRNN detections—4 stations coincidence	840
PePin events	238

Table 3. Number of events compared to manual events for magnitude from $M_L > -0.5$ and $M_L > 0$, November–December 2018

	Manual events	Subset in SLRNN-6	Subset in SLRNN-4	Subset in PePin
$M_L > -0.5$	183	179	183	110
$M_L > 0$	43	43	43	27

event detections increase significantly. An example of one of the undetected events is given in Fig. A4. It is apparent that such small events may not be above noise level on sufficient number of stations.

7 DISCUSSION AND CONCLUSIONS

Processing of seismic records is a demanding task even for experts and interpreting continuous data from dense seismic networks is

Table 4. Precision and recall calculated for analysed activities (only for those with manually processed events). The number of false positives (FP) is calculated with respect to a given magnitude threshold ($M_L > 0$ or $M_L > -0.5$) of reference manual events. For a lower magnitude threshold the number of FP decreases and the numbers of both TP and FN increase (compare line 4 and 6). REYKJANET (ii) activity is a piece of an intense swarm period, that is why there are no FPs and more detected events are often joined in one detection (as can be seen in Table 1). Denotation of data sets (i), (ii) and (iii) corresponds with that in Table 1. Abbreviation '6 sta' or '4 sta' denotes 6 or 4 station coincidence.

Data set	TP	FP	FN	TPR (recall)	PPV (precision)
REYKJANET (i): 2015 Mar 31, $M_L > 0$	51	165	0	1	0.236
REYKJANET (ii), $M_L > 0$	281	0	0	1	1
REYKJANET (iii), $M_L > 0$	184	120	0	1	0.605
WEBNET 6 sta, $M_L > -0.5$	179	213	4	0.978	0.457
WEBNET 4 sta, $M_L > -0.5$	183	657	0	1	0.206
WEBNET 6 sta, $M_L > 0$	43	349	0	1	0.11
WEBNET 4 sta, $M_L > 0$	43	797	0	1	0.051

exhaustive and time-consuming. Therefore, it is desirable to hand over this job to machines. Automatic algorithms have served to replace manpower since many decades ago from triggered recording to automatic moment tensor solutions in near-real time. Studying earthquakes with low signal-to-noise ratio or overlapping events is still beyond the limits of automatic procedures although not negligible for many studies. We propose a seismic event detector based on ANNs to reduce the amount of data for further processing. The detector must be sensitive enough to recognize all the weak events with a manageable number of false alarms. The advantage of our neural network is the ability to recognize new events based on training examples (generalization capability) and very fast computation of the trained network. The weak point is the necessity to have very good manually prepared training data set. We showed that well-trained neural network can overcome this shortcoming and that a neural network trained on manually processed seismograms from WEBNET could be successfully applied to different local seismic network.

Following the approach of the interpreters, more stations in the network must be considered. This is an algorithm we call coincidence and setting up the parameters for coincidence we can lower the detection threshold at the cost of potentially more false alarms; or lower the number of false alarms at the cost of omitting weaker events. The result of such a process is a list of time periods containing a useful signal, irrespective to the complexity of seismograms. This way all the multiple and overlapping events remain in consideration for further processing.

The proposed neural network architecture—SLRNN with eight neurons—proved to be capable to detect local seismic events. Compared to automatic location algorithms based on searching for phase onsets the completeness achieved by detection is much higher. The reason is that the location algorithms must find sufficient number of correctly recognized onsets of seismic phases which is sometimes a challenging task even for trained experts. Additionally, the most effective detectors of S waves (as used among others in PePin) are based on polarization analysis, which tends to fail for weak events due to the high frequency content of the waveforms. If the number of phases found is not enough or they are incorrectly assigned, the event is usually irretrievably discarded. In case of detection we only try to recognize earthquake-like signals. This offers advantage for manual processing in terms there is no important event missing and the amount of data is reasonably reduced. For automatic location algorithms the reduction of data could be also beneficial and might increase their efficiency.

A coincidence of six stations for both networks—WEBNET and REYKJANET—seems to be optimal. Such configuration ensures detection of all important events and low completeness magnitude still preserving the number of false detections reasonable even for manual processing (Table 4). For further processing of detected events we recommend to use some amplitude- or power-based criteria to sort the events. We used simply the largest amplitude in the event period which is obviously not the best criteria. On the other hand even such an easy operation gives some guidelines. A weak event can have large amplitudes (for example if there is some disturbing signal present on some stations), but the strong local event will never be of small amplitude. This way we can exclude unimportant or negligible events from further processing by setting a suitable amplitude threshold.

Application to the REYKJANET data showed very good generalization ability of the neural network. Thanks to the generalization property of well-trained neural network we can use the same neural network for different region, or in case of West Bohemia for detection of events from different epicentral zones outside the main focal zone. We expect our trained neural network to perform similarly when being applied to any seismic activity with the frequency content similar to that used for training. The only difference in sensitivity is given by the background noise level, so we can expect lower completeness magnitude for the WEBNET data showing generally higher signal-to-noise ratio compared to the REYKJANET data. On the other hand, the proposed architecture could be possibly suitable for detection of regional or teleseismic events after new training and change of the input filtering.

In the near future there is a potential to use our neural network to pre-process data in project ICDP 'Drilling the Eger Rift' [more on https://www.icdp-online.org/projects/world/europe/eger/ or Dahm *et al.* (2013)]. An integral part of this project is the monitoring of seismic activity in West Bohemia using shallow boreholes equipped with broad-band seismometers supplemented with 3-D seismic arrays. The expected significantly larger amount of high-frequency microevents (with local magnitudes as low as $M_L \approx -2$) might be successfully detected by our SLRNN.

are due to our colleague Alena Boušková for precise manual processing of the REYKJANET and WEBNET seismograms. We also thank the WEBNET team for technical care of the REYKJANET and WEBNET networks, particularly Jakub Klicpera. We are grateful to Dr Tomas Plenefisch and one anonymous reviewer for their thorough reviews and valuable suggestions that helped us to improve the paper substantially. We also thank the anonymous reviewer for corrections of English. Editor Prof. Huajian Yao devoted careful attention to this paper, we appreciate it. The work was accomplished within the Grant Project 18-05053S of the Grant Agency of the Czech Republic, 'Physical processes related to swarm-like seismicity on the plate boundary in South Iceland and intraplate earthquake swarms in W-Bohemia/Vogtland' and the project CzechGeo/EPOS-Sci (CZ.02.1.01/0.0/0.0/16_013/0001800, OP RDE) financed from the Operational Programme Research. The monitoring systems WEBNET and REYKJANET providing earthquake data received considerable support from the project LM2015079 CzechGeo/EPOS.

REFERENCES

Axelsson, G. *et al.*, 2015. Renewability assessment of the Reykjanes geothermal system, SW-Iceland, in *Proceedings World Geothermal Congress 2015,* Melbourne, Australia.

Böðvarsson, R., Rögnvaldsson, S.T., Slunga, R. & Kjartansson, E., 1999. The SIL data acquisition system at present and beyond year 2000, *Phys. Earth planet. Inter.,* **113**(1), 89–101.

Čermáková, H. & Horálek, J., 2015. The 2011 West Bohemia (Central Europe) earthquake swarm compared with the previous swarms of 2000 and 2008, *J. Seismol.,* **19**, 899–913.

Dahm, T., Hrubcová, P., Fischer, T., Horálek, J., Korn, M., Buske, S. & Wagner, D., 2013. Eger Rift ICDP: an observatory for study of non-volcanic, mid-crustal earthquake swarms and accompanying phenomena, *Sci. Drill.,* **16**, 93–99.

Dai, H. & MacBeth, C., 1997. The application of back-propagation neural network to automatic picking seismic arrivals from single-component recordings, *J. geophys. Res.,* **102**(B7), 15 105–15 113.

Doubravová, J., Wiszniowski, J. & Horálek, J., 2016. Single layer recurrent neural network for detection of swarm-like earthquakes in W-Bohemia/Vogtland—the method, *Comput. Geosci.,* **93**, 138–149.

Dowla, F.U., Taylor, S.R. & Anderson, R.W., 1990. Seismic discrimination with artificial neural networks: preliminary results with regional spectral data, *Bull. seism. Soc. Am.,* **80**(5), 1346–1373.

Einarsson, P., 2008. Plate boundaries, rifts and transforms in Iceland, *Jökul,* **58**, 35–58.

Einarsson, P., 2014. Mechanisms of earthquakes in Iceland, in *Encyclopedia of Earthquake Engineering,* pp. 1–15, eds Beer, M., Kougioumtzoglou, I.A., Patelli, E. & Au, S.-K, Springer-Verlag.

Esposito, A., Giudicepietro, F., Scarpetta, S., D'Auria, L., Marinaro, M. & Martini, M., 2006. Automatic discrimination among landslide, explosion-quake, and microtremor seismic signals at Stromboli volcano using neural networks, *Bull. seism. Soc. Am.,* **96**(4A), 1230–1240.

Fischer, T., 2003. Automatic location of swarm earthquakes from local network data, *Stud. Geophys. Geod.,* **47**(1), 83–98.

Fischer, T., Horálek, J., Michálek, J. & Boušková, A., 2010. The 2008 West Bohemia earthquake swarm in the light of the WEBNET network, *J. Seismol.,* **14**(4), 665–682.

Fischer, T., Horálek, J., Hrubcová, P., Vavryčuk, V., Bräuer, K. & Kämpf, H., 2014. Intra-continental earthquake swarms in West-Bohemia and Vogtland: a review, *Tectonophysics,* **611**, 1–27.

Fischer, T., Matyska, C. & Heinicke, J., 2017. Earthquake-enhanced permeability—evidence from carbon dioxide release following the M_L 3.5 earthquake in West Bohemia, *Earth planet. Sci. Lett.,* **460**, 60–67.

Geirsson, H. *et al.* 2010. Overview of results from continuous GPS observations in Iceland from 1995 to 2010, *Jökul,* **60**, 3–22.

Gentili, S. & Michelini, A., 2006. Automatic picking of *P* and *S* phases using a neural tree, *J. Seismol.,* **10**(1), 39–63.

Gravirov, V., Kislov, K. & Ovchinnikova, T., 2010. Neural network method for identification of earthquake phases in increased noise level conditions, in *Geophysical Research Abstracts,* Vol. **12,** EGU2010, p. 2434.

Hinton, G.E., 1989. Connectionist learning procedures, *Artif. Intell.,* **40,** 185–234.

Horálek, J., 2013. *Reykjanet,* International Federation of Digital Seismograph Networks, 10.7914/SN/7E_2013, www.fdsn.org/networks/detail/7E_2013/.

Horálek, J. & Fischer, T., 2008. Role of crustal fluids in triggering the West Bohemia/Vogtland earthquake swarms: just what we know (a review), *Stud. Geophys. Geod.,* **52**(4), 455.

Horálek, J. & Fischer, T., 2010. Intraplate earthquake swarms in West Bohemia/Vogtland (Central Europe), *Jökull,* **60,** 67–88.

Horálek, J., Fischer, T., Boušková, A. & Jedlička, P., 2000. The western Bohemia/Vogtland region in the light of the WEBNET network, *Stud. Geophys. Geod.,* **44**(2), 107–125.

Institute of Geophysics, Academy of Sciences of the Czech Republic, 1991. *West Bohemia Local Seismic Network,* International Federation of Digital Seismograph Networks.

Jakobsdóttir, S.S., 2008. Seismicity in Iceland: 1994-2007, *Jökul,* **58,** 75–100.

Jakobsdóttir, S.S. Guðmundsson, G.B. & Stefánsson, R., 2002. Seismicity in Iceland 1991-2000 monitored by the SIL seismic system, *Jökull,* **51,** 87–94.

Jakoubková, H., 2018. Earthquake swarms in diverse tectonic environments, *Ph.D. thesis*, Charles University in Prague.

Jakoubková, H., Horálek, J. & Fischer, T., 2018. 2014 mainshock-aftershock activity versus earthquake swarms in West Bohemia, Czech Republic, *Pure appl. Geophys.,* **175**(1), 109–131.

Kuyuk, H., Yildirim, E., Dogan, E. & Horasan, G., 2011. An unsupervised learning algorithm: application to the discrimination of seismic events and quarry blasts in the vicinity of Istanbul, *Nat. Hazards Earth Syst. Sci.,* **11**(1), 93–100.

Madureira, G. & Ruano, A.E., 2009. A neural network seismic detector, *Acta Technica Jaurinensis,* **2**(2), 159–170.

Morales-Esteban, A., Martínez-Álvarez, F. & Reyes, J., 2013. Earthquake prediction in seismogenic areas of the Iberian peninsula based on computational intelligence, *Tectonophysics,* **593,** 121–134.

Mousavi, S.M., Horton, S.P., Langston, C.A. & Samei, B., 2016. Seismic features and automatic discrimination of deep and shallow induced-microearthquakes using neural network and logistic regression, *J. geophys. Int.,* **207**(1), 29–46.

Mousavi, S.M., Zhu, W., Sheng, Y. & Beroza, G.C., 2018, CRED: a deep residual network of convolutional and recurrent units for earthquake signal detection, *Sci. Rep.,* **9,** doi:10.1038/s41598-019-45748-1.

Panskkat, A. & Adeli, H., 2007. Neural network models for earthquake magnitude prediction using multiple seismicity indicators, *Int. J. Neural Syst.,* **17**(01), 13–33.

Reyes, J., Morales-Esteban, A. & Martínez-Álvarez, F., 2013. Neural networks to predict earthquakes in Chile, *Appl. Soft Comput.,* **13**(2), 1314–1328.

Romeo, G., 1994. Seismic signals detection and classification using artificial neural networks, *Ann. Geophys.,* **37**(3).

Ross, Z.E., Meier, M.-A., Hauksson, E. & Heaton, T.H., 2018. Generalized seismic phase detection with deep learning, *Bull. seism. Soc. Am.,* **108**(5A), 2894–2901.

Sæmundsson, K. & Einarsson, P., 2014, Notes on the tectonics of Reykjanes, *Iceland GeoSurvey, Report ÍSOR-2014/003* .

Tiira, T., 1996. Discrimination of nuclear explosions and earthquakes from teleseismic distances with a local network of short period seismic stations using artificial neural networks, *Phys. Earth planet. Inter.,* **97**(1-4), 247–268.

Tiira, T., 1999. Detecting teleseismic events using artificial neural networks, *Comput. Geosci.,* **25**(8), 929–938.

Wang, J. & Teng, T., 1995. Artificial neural network-based seismic detector, *Bull. seism. Soc. Am.,* **85**(1), 308–319.

Wang, J. & Teng, T., 1997. Identification and picking of s phase using an artificial neural network, *Bull. seism. Soc. Am.,* **87**(5), 1140–1149.

Werbos, P., 1990. Backpropagation through time: what it does and how to do it, *Proc. IEEE,* **78**(10), 1550–1560.

Withers, M., Aster, R., Young, C., Beiriger, J., Harris, M., Moore, S. & Trujillo, J., 1998. A comparison of select trigger algorithms for automated global seismic phase and event detection, *Bull. seism. Soc. Am.,* **88**(1), 95–106.

APPENDIX: ADDITIONAL FIGURES

Some more figures demonstrating (i) additional comparisons of events detected for selected activities that were recorded by REYKJANET (Figs A1 and A2), (ii) the distribution of the background seismicity on the Reykjanes peninsula (Fig. A3) and (iii) an example of one of four events undetected by the six-station coincidence for WEBNET (Fig. A4).
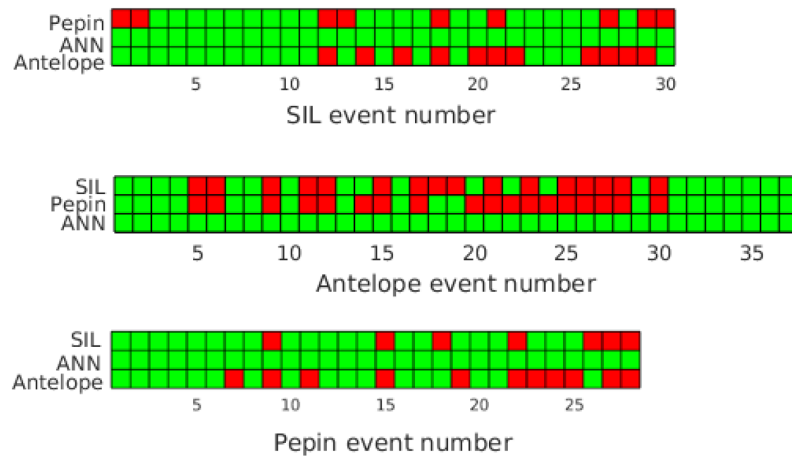
Figure A1. Detailed examination of the SLRNN detection results and the SIL, Antelope and PePin catalogues for mini-swarm of 2015 on the Reykjanes Peninsula. The diagrams represent the individual catalogues except SLRNN; from top to bottom: SIL, Antelope and PePin. Each column in the individual diagrams denotes a particular event in the respective catalogue (thus the number of columns in each diagram equals to the number of events in the catalogue). The events in the SIL and PePin diagrams are ordered according to magnitudes M_L given in the SIL and PePin catalogues from the strongest (on the left) to the weakest one (on the right); the events in the Antelope diagram are sorted according to the origin time. The rows in the diagrams denote events which are included (green cells)/missing (red cells) in the remaining three catalogues (indicated on the right). The SLRNN diagram is not presented because a total of 217 events are detected by our SLRNN including all the events given in the SIL, Antelope and PePin catalogues. Note that the each catalogue (SIL, Antelope and PePin) contains some events detected only by ANN and missed in the other two catalogues.
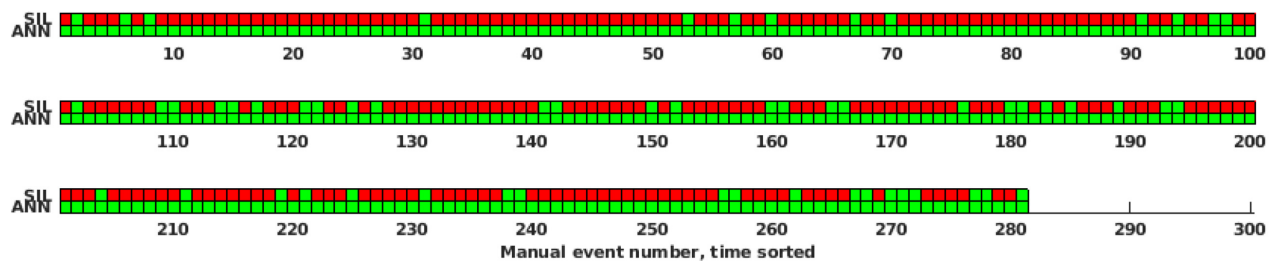

Figure A2. Comparison of the SLRNN detection results with the SIL and manual REYKJANET catalogue for 1 hr period of a larger 2017 swarm on the Reykjanes Peninsula. High rate seismicity in the time window of 2017 June 26, 11:00 to 12:00 UT, is examined. The diagram represents a comparison of the SLRNN results and SIL catalogue with the REYKJANET catalogue (281 $M_L > 0$ events) created manually by an experienced interpreter. For more information on the diagram structure refer to the caption of Fig. A1. The events are sorted according to the origin time.
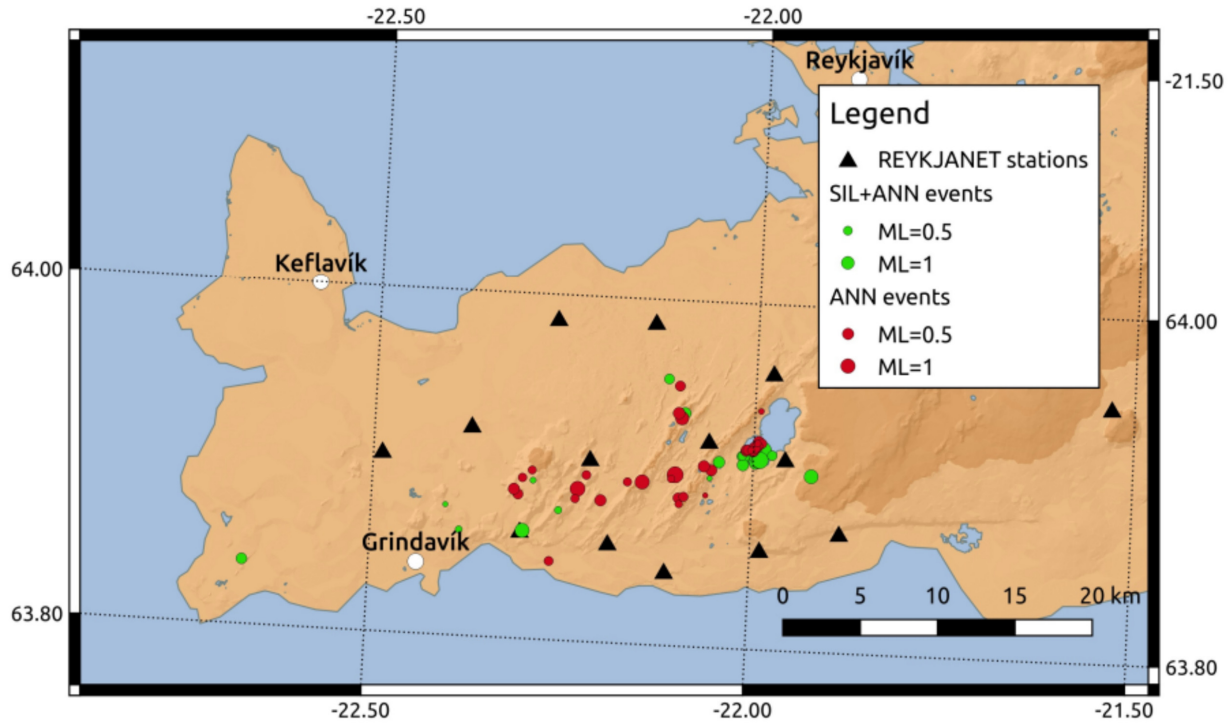
Figure A3. Examination of the SLRNN detections of background seismicity on the Reykjanes Peninsula in the period 2017 June 6–12. All 34 events listed in the SIL catalogue (green circles) are successfully detected by the SLRNN. Another 37 events (red circles) detected by the SLRNN are located using manual picks of the *P*- and *S*-wave onsets. 112 more event detections indicated by the SLRNN are the events unfit for location due to lack of reliable *P*- and *S*-wave arrival times or false alarms in some cases.
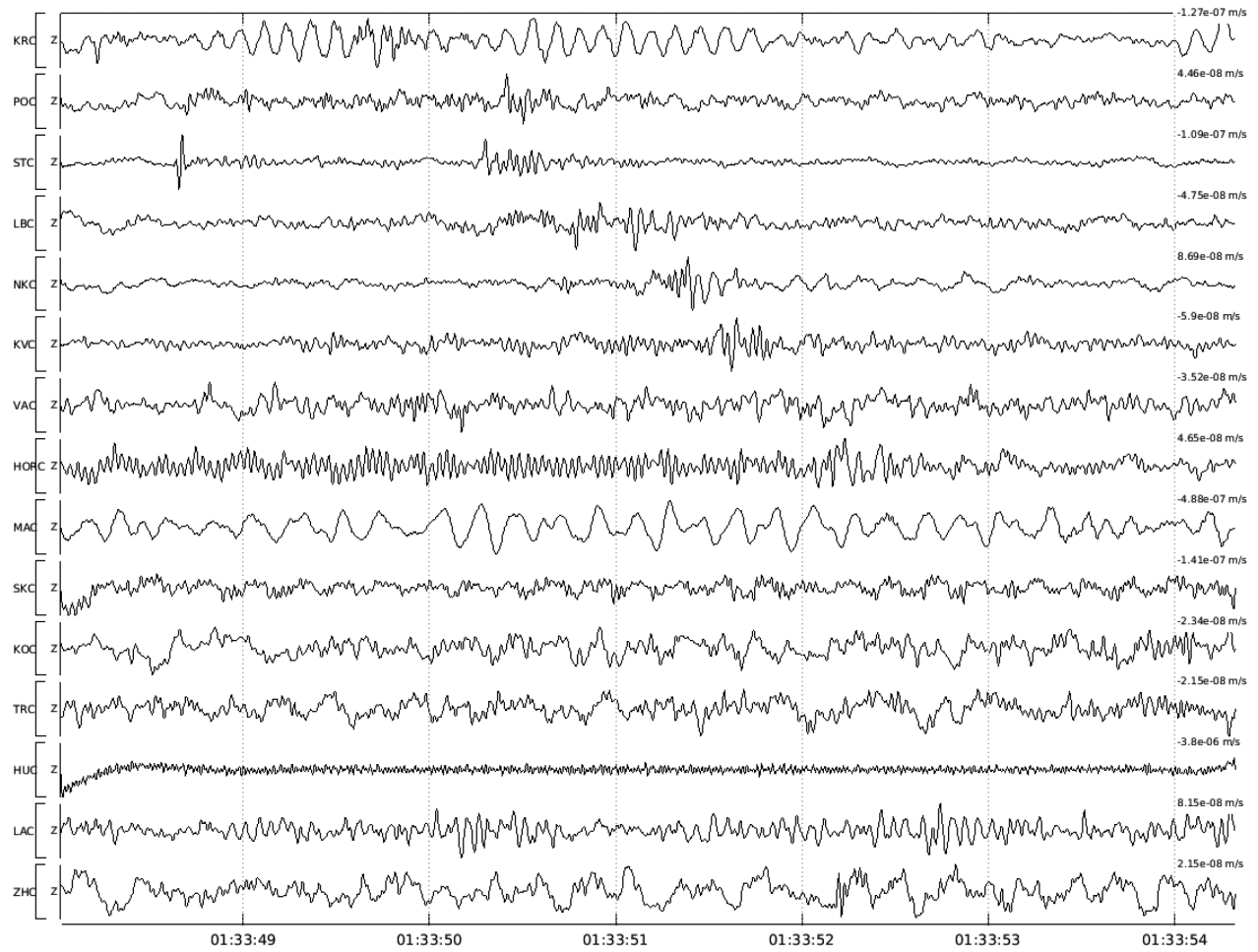
Figure A4. WEBNET seismograms of the local event (2008 November 14) undetected by SLRNN with the six-station coincidence. Manually estimated magnitude $M_L = -0.5$. Only vertical components of the ground-motion velocity (BP 1–40 Hz applied) are displayed. Stations are sorted by epicentral distance (top trace corresponds to the nearest station).